

Spring 1995

Thermocline Circulation Driven at Surface Outcrops of Isopycnal Surfaces

Gudavalli V. R. K. Vittal
Old Dominion University

Follow this and additional works at: https://digitalcommons.odu.edu/oeas_etds



Part of the [Oceanography Commons](#)

Recommended Citation

Vittal, Gudavalli V.. "Thermocline Circulation Driven at Surface Outcrops of Isopycnal Surfaces" (1995).
Doctor of Philosophy (PhD), Dissertation, Ocean & Earth Sciences, Old Dominion University, DOI:
10.25777/fkst-8n33
https://digitalcommons.odu.edu/oeas_etds/76

This Dissertation is brought to you for free and open access by the Ocean & Earth Sciences at ODU Digital Commons. It has been accepted for inclusion in OES Theses and Dissertations by an authorized administrator of ODU Digital Commons. For more information, please contact digitalcommons@odu.edu.

THERMOCLINE CIRCULATION DRIVEN AT SURFACE OUTCROPS OF
ISOPYCNAL SURFACES

by

Gudavalli V. R. K. Vittal

Bachelor of Engineering, Mechanical Engineering, 1988
Osmania University, Hyderabad, A.P., India.

Master of Engineering, Mechanical Engineering, 1990
Indian Institute of Science, Bangalore, India.

A Dissertation submitted to the Faculty of
Old Dominion University in Partial Fulfillment of the
Requirements for the Degree of

Doctor of Philosophy

Physical Oceanography

Old Dominion University
March, 1995

Approved by:

Dr. G. T. Csanady (chairman)

Dr. C. E. Grosch

Dr. J. M. Klinck

Dr. J. C. Marshall

ABSTRACT

THERMOCLINE CIRCULATION DRIVEN AT SURFACE OUTCROPS OF ISOPYCNAL SURFACES

G. V. R. K. Vittal

Old Dominion University, 1995

Advisor: Prof. Gabriel T. Csanady

Potential vorticity (PV) defined as:

$$q = \nabla\theta \cdot (f\hat{k} + \Omega)$$

where θ is density anomaly, Ω ($\nabla \times \mathbf{u}$) is relative vorticity, \hat{k} is unit vertical vector and f the coriolis parameter, is used as an dynamical tracer to study the interior thermocline circulation. Using the generalized flux form of PV equation (Haynes and McIntyre, 1987), wind stress and buoyancy fluxes at surface outcrops of isopycnal surface are translated into PV fluxes. The PV flux condition so derived considers seasonal movement of the isopycnal outcrops and geostrophic turbulence. After some transformations, mean PV transport into an isopycnic layer (PV flux times the separation distance between adjacent isopycnals, averaged over a period longer than the eddy time scales), is:

$$\frac{\partial \bar{\Pi}}{\partial s} = (f + \bar{\zeta})\bar{v}_n + \overline{v'_n \zeta'}$$

where $\partial \bar{\Pi} / \partial s$ is "total" pressure gradient along the surface outcrop of the isopycnal, ζ is the vertical component of the relative vorticity, $\overline{v'_n \zeta'}$ is Reynolds flux of vorticity and v_n is the quasi-horizontal velocity component normal to the outcrop (almost northward) within an isopycnic layer below mixed layer base. The influence of thermodynamic variables are hidden in the pressure gradient term, while seasonal migration of isopycnals does not affect the PV transport. It is argued that the Reynolds flux arising from geostrophic turbulence, dominates the transfer of PV within the isopycnic layer.

A constant layer depth model, forced by the above flux condition, is used to study its influence on the interior circulation. The impermeability theorem of Haynes and McIntyre (1987), justifies treatment of a single isopycnic layer in isolation. Non-linear, quasi-geostrophic equations are used to study the dynamics on a rectangular basin model. The model is forced by PV at the northern boundary of the domain, which represents the location where the PV flux enters the thermocline interior.

PV input at the northern boundary allows the circulation to build up until opposite PV input at some other boundaries limits the process. The model simulation shows active northern, eastern and western boundary layers, and an interior circulation pattern with properties similar those inferred by the homogenization theory of Rhines and Young (1982a). However, in the present study, the boundary layers control the key features of the circulation unlike in the classical models driven by Ekman pumping. The results show that the anticyclonic gyre forming in response to negative PV input on the northern boundary, has a strength depending on the intensity of the forcing, lateral diffusivity and the eastern boundary condition. In the case of an upwelled isopycnal (free slip eastern wall), the eastern boundary layer is stable and penetrates to a considerable distance south. On the contrary, for isopycnal intersecting the eastern boundary (no-slip wall), the eastern boundary layer separates at a short distance from the northeast corner, injecting massive amounts of positive vorticity into the basin. Cyclonic eddies are shed at a constant frequency near the eastern boundary, in the no-slip case, propagate towards the west and dissipate near the western boundary. Experiments with realistic subduction rates show that the PV transport due to the total pressure gradient along the isopycnal outcrop dwarfs the transport due to subduction. The results obtained mimic a certain extent features of subtropical gyre circulation near eastern boundaries, notably in the Azores frontal area.

*To my parents and grandparents who gave me the
strength to accomplish a dream ...*

Acknowledgments

No amount of appreciation is sufficient to thank my *Guru* Prof. G. T. Csanady who guided me through these four years with immense interest and patience. He gave me the opportunity to come to ODU and then guided me, with full meaning of this word. I am thankful for the encouragement and motivation he has provided throughout my association with him. I also want to thank sincerely Joyce Csanady, for all the love and affection she has shown to me. Gabe and Joyce have always been very kind to me and they have made me feel that I am not only their student, but also part of their family.

I thank the members of my committee, Drs. John Klinck, Chet Grosch and John Marshall for their help and suggestions. Dr. Klinck and Dr. Grosch helped me at various stages of my model development. Special thanks goes to Dr. Grosch, for his thought provoking discussions, and also for sharing his perspectives and experiences in life. Dr. Marshall was very helpful with his critical comments on the problem of thermocline circulation. I would like to thank him for all his suggestions. I also would like to thank our director, Dr. Atkinson, for his unending support and encouragement. I would take this opportunity to thank Dr. Kirwan and his wife Dede, and Dr. Hoffman for their support and kindness. I am obliged to the staff at CCPO, Carole Blett, Beverly Scott, Boyd Fletcher and Dana Oblak at the Oceanography Department for their continuous help.

Life in Norfolk is mainly associated with my friend, Dr. Venkat Maroju whose encouragement gave me strength during the pursuit of this degree. I am always indebted for him for his moral support and patience in putting up with my idiosyncrasies. I am very grateful to my friend Ana Martins who always supported me in good and bad times. I am grateful to her for teaching me things I would never even imagined.

I would like to acknowledge her help during the completion of my dissertation. I also would like to thank Ajoy Kumar, Sangki, Lisa, Andry, Surya for all those wonderful times I shared with them during the last four years. I am mainly indebted to Sangki who helped me at various stages of my work by suggesting and providing me with a lot of scientific information. His patience in listening to my confusing explanations is also greatly appreciated. I am thankful to all my friends who made my stay at Norfolk, most memorable. In particular, Thiru, Sudheer, Nadima, Madhu, Sridevi, KP, Madhumita, Ratikant, Vamsi, Talla, Andras, Pandya, Archita who took care of me in my most difficult days. I am also thankful to my friends Baba, Amar, Venu, Raghu, Gowrinath, Pratap for their financial help during my difficult times. Finally, I am thankful to my grandparents, parents, sisters, aunts, uncles and my teachers Yesupadam and Kamala Kumari for encouraging and supporting me to pursue this study.

The work described in this dissertation has been funded by NOAA under a grant titled "Air-Sea Coupling of the North Atlantic", and by the Department of Oceanography. Computer resources and facilities were provided by the Commonwealth Center for Coastal Physical Oceanography.

Contents

List of Tables	vii
List of Figures	x
1 Introduction	1
2 Background	5
2.1 Theories of thermocline circulation	5
2.1.1 Ventilated thermocline theory	6
2.1.2 Homogenization theory	7
2.1.3 The J -vector approach	13
2.2 Subduction	15
2.3 Numerical models of thermocline circulation	21
2.4 Observational studies in the subtropical North Atlantic	25
2.4.1 Circulation	26
2.4.2 Estimated ventilation rates	31
2.4.3 Eddies	31
3 Physics of vorticity input	34
3.1 Migration of surface isopycnals	35
3.2 PV flux at surface outcrop	36
3.3 Handover of PV transport	38
3.4 Geostrophic turbulence	42
3.5 Application to the eastern North Atlantic	43
4 Constant layer depth model	45
4.1 Model physics	45
4.2 Governing equations	47

4.3	Numerical methods	49
4.3.1	Numerical boundary conditions	50
4.3.2	Choice of parameters	52
5	Results	54
6	Discussion	85
7	Conclusions	93
	References	95
	Curriculum Vitae	100

List of Tables

1	List of model runs	55
---	------------------------------	----

List of Figures

1	Potential vorticity between the $\sigma_\theta = 26.5$ and 27.0 surfaces in North Atlantic (in units of $10^{-11} \text{ m s}^{-1}$). From McDowell <i>et al.</i> (1982). . . .	9
2	Potential vorticity between the $\sigma_\theta = 26.5$ and 27.0 surfaces (in units of $10^{-11} \text{ m s}^{-1}$). From Keffer (1985).	10
3	Five year mean streamfunction at the top, third and fifth levels (at the mean depths of 150, 850 and 1750 m, respectively) of an eight-level eddy-resolving numerical simulation of the wind-driven circulation. (b) The mean potential vorticity on the same surfaces. (c) The mean depth in meters of the third layer. (d) The instantaneous potential vorticity of the third layer. From Holland <i>et al.</i> (1984).	11
4	A schematic diagram showing PV flux lines on an isopycnal surface. From Marshall and Nurser (1992).	16
5	A schematic diagram showing isopycnals in the thermocline outcropping into a vertically homogenous mixed layer. From Nurser and Marshall (1991).	17
6	Annual subduction rate S_{ann} (m yr^{-1}) into the main thermocline. From Marshall <i>et al.</i> (1993).	20
7	The heat flux H_{net} (W m^{-2}) into the ocean that drives the subduction of fluid into the main thermocline. From Marshall <i>et al.</i> (1993). . . .	22
8	Tracer concentration and potential vorticity evaluated on the $\sigma = 26.0$ surface for a coarse and fine grid. From Cox (1985).	24
9	Dynamic topography relative to the 1500 dbar. From Käse <i>et al.</i> (1985). 27	
10	Annual integrated volume transport (200 to 800 m) from mean density profiles. From Stramma and Siedler (1988).	28
11	Large-scale temperature distribution at 560 m depth. From Käse <i>et al.</i> (1986).	29

12	Sketch of an isopycnal layer outcropping at the sea surface with the “handover section”	40
13	The basin averaged kinetic energy and the enstrophy against time for Case 1.	57
14	The distribution of streamfunction (ψ) and relative vorticity (ζ) after a period of four years for Case 1.	58
15	The distribution of potential vorticity (PV) for Case 1.	59
16	The distribution of streamfunction with the model domain doubled meridionally (2000 km \times 2000 km) for Case 2.	61
17	The relative vorticity distribution corresponding to streamfunction distribution (Fig. 16) for Case 2.	62
18	Case 3: The distribution of streamfunction for a prescribed vorticity gradient of (a) $5 \times 10^{-7} \text{ m}^{-1} \text{ s}^{-1}$ and (b) $3 \times 10^{-7} \text{ m}^{-1} \text{ s}^{-1}$ on the northern boundary.	63
19	The basin averaged kinetic energy and the enstrophy against time for Case 4.	65
20	Case 4: Time averaged streamfunction and relative vorticity distribution.	66
21	Case 4: Instantaneous fields of streamfunction and relative vorticity distribution at the end of four years.	67
22	Eddy fields of streamfunction and relative vorticity distribution in Case 4.	68
23	The distribution of transient and beta terms contributing to the relative vorticity in Fig. 21.	70
24	The distribution of nonlinear and viscosity terms contributing to the relative vorticity in Fig. 21.	71
25	Case 5: The distribution of streamfunction (ψ) and relative vorticity (ζ), when the forcing is only due to subduction.	73

26	Case 6: Instantaneous fields of streamfunction and relative vorticity distribution at the end of four years.	74
27	Case 6: Time averaged distribution of streamfunction (ψ) and relative vorticity (ζ), when the forcing is due to along-isopycnal pressure gradient and the subduction.	75
28	The basin averaged kinetic energy and the enstrophy against time for Case 6.	77
29	Case 7: The distribution of streamfunction (ψ) and relative vorticity (ζ), when model forcing is by positive vorticity input.	78
30	The distribution of kinetic energy and enstrophy for Case 8.	80
31	The distribution of streamfunction (ψ) and relative vorticity (ζ) after six months, for Case 8.	81
32	The distribution of streamfunction (ψ) and relative vorticity (ζ) after one year, for Case 8.	82
33	The distribution of kinetic energy and enstrophy for Case 9 with 4km grid. Conditions similar to Case 4.	83
34	The distribution of kinetic energy and enstrophy for Case 9 with 4km grid. Conditions similar to Case 6.	84
35	Variation of the meridional extent of the gyre (Y) with the non dimensional number $(\partial\Pi/\partial x/\beta^2)^{1/3}$	88
36	Variation of potential vorticity near the eastern boundary for Case 1.	90
37	Variation of potential vorticity near the eastern boundary for Case 4.	91

1 Introduction

The vertical structure of oceans shows a strong vertical density gradient in relatively shallow water (200 – 800 m), commonly known as the main thermocline. The surfaces of constant potential density (isopycnals) of the main oceanic thermocline terminate in surface “outcrops” at mid to high latitudes. Early studies by Rossby (1936) and Montgomery (1938) have shown that the flow at thermocline depths is along isopycnal surfaces. Iselin (1939) pointed out that the temperature and salinity characteristics in the interior (*i.e.*, below the mixed layer depth) can be traced back to the surface along isopycnals. The T-S properties at the surface are determined by the surface processes of heating or cooling, freshening and mixing. Such observations justify layer models for the study of circulation on isopycnic layers of the thermocline. But what forces the interior circulation is still a debatable issue in thermocline studies.

Recent analytical models force the interior either by eddy stresses (Rhines and Young, 1982a,b) or by prescribing inflow at positions where the isopycnic layers terminate (Luyten *et al.*, 1983). The scalar-like behaviour of potential vorticity (PV) has been exploited by Rhines and Young (1982a,b) to analyze the dynamics of interior circulation in isopycnic layers, using quasi-geostrophic equations but neglecting the relative vorticity. PV defined as:

$$q = \nabla\theta \cdot (f\hat{k} + \Omega)$$

where θ is density anomaly, Ω ($\nabla \times \mathbf{u}$) is relative vorticity, \hat{k} is unit vertical vector, f the coriolis parameter is a conserved quantity in the ocean interior. They argued

that eddy flux of PV, represented as the down-gradient flux of PV, leads to PV “homogenization” in isopycnic layers. PV maps for several isopycnic layers of the North Atlantic (McDowell *et al.*, 1982) support the ideas developed by Rhines and Young, but they also draw attention to boundary effects at the continental margins and near the surface outcrop of the layers.

By a completely different approach, focussing on the subduction of the surface water into the thermocline layers, Luyten *et al.* (1983) formulated the theory of ventilated thermocline. The active layers in their multi-layer model are driven by Ekman pumping when they are at the surface but are forced by layer-to-layer interactions when submerged, constrained by PV conservation. This theory aims only at the interior circulation (away from any boundary layers) and also neglects relative vorticity, as well as eddy flux of PV.

Recently, there has been renewed interest in using PV dynamics to study the thermocline problem. Our present ideas on PV dynamics originate from Ertel’s classical theorem on the conservation of PV. Based on this, and later extensions of it, Haynes and McIntyre (1987, hereafter HM; 1990) discussed the flux form of PV balances and interpreted it in an “impermeability theorem” for isopycnal surfaces. According to this theorem, the isopycnal surfaces are impermeable to PV and the total stock of PV within isopycnic layers remains constant. Input or output of PV can only occur at the isopycnic outcrop positions or at the boundaries where they terminate. This makes it possible to treat a single isopycnic layer independently of other layers. PV flux input at boundaries occurs either from friction force or from density change due to heating, freshening or mixing.

Marshall and Nurser (1992; hereafter MN92) applied the impermeability theorem to study a continuously stratified thermocline model, in which the interior isopycnic layers are forced by the PV flux vectors calculated at the mixed layer base. They showed that the PV flux vectors, consisting of advective and non-advective fluxes,

could generate circulation of significant amplitude. Their approach supposes, however, stationary isopycnal surfaces and surface outcrops, while observations show that the isopycnal outcrops move over distances of the order of 1000 km in a period of 3 to 4 months *i.e.*, at a speed of the order of 0.1 ms^{-1} , much faster than the mean meridional surface velocity. On a shorter time scale, where outcrops of adjacent isopycnals come close together, hydrodynamic instability of a frontal current (such as the Azores Current) causes completely disordered displacements of outcrop lines. An important point emphasized by HM and MN92 is that when isopycnals move relative to the fluid (because of density change), PV moves with them.

Another physical process pertinent to thermocline circulation is the transfer of surface water into the interior, known as “subduction”. It is generally believed that subduction influences the interior circulation to a significant extent. Using thermodynamic arguments, Nurser and Marshall (1991) obtained a simple relationship for the subduction rate at the base of the mixed layer in terms of a “net heat gain” and PV at the mixed layer base. The net heat gain here refers to the net surface buoyancy flux less that due to cold water advection by Ekman drift. According to this result, the subduction rate is directly proportional to the net heat gain and inversely to PV at mixed layer base. Their relation emphasizes the role of buoyancy in controlling the subduction and setting the PV of the thermocline.

The aim of the present study is twofold. First, it reviews what determines PV input into isopycnic layers at their outcrop position and then discusses the physical processes that transfer PV into the interior. The flux form of the PV equation (MN92) is used to determine PV input by wind and buoyancy flux. The derivation takes into account the seasonal migration of isopycnals, as well as shorter term motions due to geostrophic turbulence. The approach is similar to that used by Csanady and Pegleri (1995) in deriving the PV input at the intersection of isopycnals with the continental slope. The study also investigates the validity of Nurser and Marshall’s

(1991) formula for subduction velocity, connecting it to surface buoyancy flux and PV. This theory is mainly applicable to the eastern subtropical North Atlantic, where the isopycnic surfaces of the upper thermocline outcrop. This is also the region of water mass subduction where the water is forced from the surface layer into the interior (Sarmiento *et al.*, 1982; Jenkins, 1987). Detailed discussion of this region is presented in second chapter.

Second, this study develops a simple model of boundary driven flow through PV input, within an isopycnic layer. The model retains the simplicity of other conceptual models, such as those of Rhines and Young (1982a,b), or Luyten *et al.* (1983), but also takes into account the relative vorticity and eddy flux of PV. Assuming a constant layer depth (a necessary overidealization), a non-linear, quasi-geostrophic model is developed here, driven by PV gradient flux at the northern boundary. The PV flux forced at the outcrop position is assumed to be transferred to a “handover” section, which lies a short distance from the outcrop position. This handover section is the northern boundary of the model. It will be argued that Reynolds flux of vorticity is the main vehicle by which PV entering at the surface is transferred into the interior domain. The model uses a fine grid so as to resolve the boundary layers, important in this boundary forced problem. Some of the model parameters are chosen to represent the eastern subtropical North Atlantic.

The thesis is organized in the following manner. In the second chapter, the literature of thermocline circulation is reviewed. The derivation of the forcing function is explained in chapter three, showing how the combined effect of wind and buoyancy flux defines the PV flux at the outcrop. Chapter four describes the model physics and the single layer quasi-geostrophic model of circulation in an isopycnic layer. The results of various simulations carried out are presented in chapter five. The results obtained are discussed in chapter six and the conclusions are presented in chapter seven.

2 Background

2.1 Theories of thermocline circulation

The idea that the subsurface layers of the main oceanic thermocline are forced by surface processes originates with the studies of Iselin (1936, 1939) and Montgomery (1938). Early diagnostic studies from Rossby (1936) and Montgomery (1938) have shown that the flow in the thermocline layers is along surfaces of constant potential density (isopycnals). Montgomery (1938) analyzed temperature and salinity distributions along isopycnal surfaces and gave a descriptive account of the circulation, assuming that flow is confined to “isentropic” layers.

The depth of the isopycnals decreases as one moves to higher latitudes in the subtropical gyre. They eventually intersect the sea surface along ‘outcrop’ curves. From these outcropping positions, the water affected by atmospheric interactions can reach depths of the order of 1 km along the isopycnals. From an analysis of T-S diagrams, Iselin (1939) concluded that the water mass characteristics in the permanent thermocline are determined by surface processes. Accordingly, the sea surface is a key site where thermodynamic and mechanical interactions with the atmosphere take place and from where the “memory” of these interactions is carried with the fluid down into the ocean interior (Holland *et al.*, 1984).

Similarly to temperature and salinity, PV is also a conserved property in the ocean interior, while at the surface its value is set by surface processes. The importance of PV in oceanic general circulation studies rests on Ertel’s theorem and has been emphasized by several authors, see for example Rhines (1986a,b) and Bryan (1987). The usefulness of the isentropic PV concept in atmospheric and oceanic circulation

studies is due to the invertibility of the PV field into three-dimensional velocity and density fields (Hoskins *et al.*, 1985). In the absence of diabatic heating and frictional or other forces, PV is simply advected like a materially conserved chemical tracer (Rossby, 1940; Ertel, 1942).

Initial theoretical studies of the thermocline circulation (Robinson and Stommel, 1959; Needler 1967; Welander, 1971) concentrated on finding similarity solutions to the planetary-scale equations for PV and density. Because of the constraint to maintain the same form of the solution through the domain of the solutions had many unrealistic features. One such feature was that the solutions required all isopycnals to rise to the surface at the eastern boundary. The solutions were unable to satisfy realistic surface conditions and ignored the role of dissipation in the dynamics. The complexity of the nonlinear equations stalled further efforts in this direction.

Later studies considered the ocean a stack of layers of constant potential density, an approach simplifying the nonlinear equations. In the early eighties, two thermocline theories came into prominence, the theory of potential vorticity “homogenization” by Rhines and Young (1982a,b, hereafter RY82) and the theory of the ventilated thermocline of Luyten *et al.* (1983). The former involves the redistribution of the PV by lateral eddy mixing in a recirculating gyre. In the latter, surface Ekman pumping forces fluid into the interior at the surface outcrop, with Sverdrup dynamics governing the interior circulation.

2.1.1 Ventilated thermocline theory

Luyten *et al.* (1983, hereafter LPS) developed the ventilated thermocline theory, with the subsurface isopycnal layers forced at their outcrop positions. Their multi-layer model study is based on the Iselin’s (1939) concept of flow in the subsurface layers. Here “ventilation” refers to subduction of mass into or extraction from the subsurface layers. In the LPS model, the surface density distribution and Ekman

pumping prescribed at the outcrop position defines the structure of the thermocline and its associated motion. The water pushed down into the thermocline at the outcrop position downwells along the isopycnals as it moves southward, the motion governed by Sverdrup balance. The no-zonal flow condition imposed at the eastern boundary requires the thickness of the isopycnal layer to be constant. At the same time it also requires that potential vorticity ($\sim f/h$, in linearized form) must be conserved. To satisfy both the constraints the flow has to pull away from the eastern boundary as the flow moves southward.

Consequently, three distinct regions form in the ocean interior: a *pool region* where the PV is homogenized by turbulent eddy mixing (as in the RY82 theory), a *ventilated region* forced at the upper surface by Ekman pumping, and a *shadow zone* on the eastern boundary which cannot be reached by fluid intruding from the outcrop line. Pedlosky (1990) attributes shadow zone formation to inexact conservation of PV in the ventilation theory. While this theory successfully extends classical concepts of wind-driven circulation to interior layers, it ignores PV input at the surface due to buoyancy forcing. Furthermore, its treatment of eastern boundary conditions is unrealistic. Contrary to the observations in the North Atlantic, the no-zonal flux condition at the eastern boundary used in LPS model assumes that all unventilated isopycnals are flat along the eastern wall. Further, it also requires all isopycnals of the ventilated thermocline to rise to the surface.

2.1.2 Homogenization theory

The fully submerged isopycnal layers of the thermocline which are not directly forced, either by wind or by buoyancy, are said to be unventilated. RY82 analysed the circulation of such unventilated layers and formulated the theory of PV homogenization. Here “homogenization” refers to the erosion of horizontal gradients. According to their theory, PV gets homogenized across geostrophic contours by the lateral diffu-

sion of PV. Geostrophic contours are isolines of constant PV on surfaces of constant density.

The theory of homogenization postulates advection to be dominant over diffusion (large Peclet number, UL/K , where K is the lateral diffusivity, U and L are the velocity and length scales, respectively) so that PV is nearly uniform *along* the streamlines. As the fluid recirculates along these closed contours indefinitely, the weak diffusivity has sufficient time to make PV uniform *across* the streamlines. However, if diffusion is strong, then gradients of PV will diffuse in from the boundaries.

Evidence for homogenized regions, postulated in the RY82 theory are observed in the PV maps of McDowell *et al.* (1982) and Keffer (1985), derived from hydrographic data (Fig. 1 and Fig. 2). Numerical model studies of Holland *et al.* (1984) also show homogenized regions (Fig. 3) within the subtropical gyres, with gradients at the boundaries. McDowell *et al.* (1982) and Keffer (1985) used a linearized form of PV ($f d\rho/dz$) to calculate the PV from the hydrographic measurements of ρ alone. Figures 1 and 2 show homogenized region of PV in the subtropical region with strong PV gradients at the gyre boundary. The mean PV in the second layer of the Holland *et al.* (1984) study also show similar characteristics. However, the homogenized region in their study is the result of eddy diffusion.

The homogenized thermocline theory uses a standard β -plane quasi-geostrophic approximation which allows only small overall departures of isopycnal depths from their rest values. The theory assumes that eddies are weak everywhere along streamlines and that in spite of this, the lateral diffusion of PV is the largest dissipative process along it (Young, 1986). The time dependent study of Rhines and Young (1983) showed that the homogenization of a passive tracer occurs in two stages. Initially, rapid shear-enhanced diffusion averages out the initial values of the tracer along the streamline, followed by a slower phase in which the diffusion homogenizes the tracer across the isopleths, held to streamlines by the strong advection. For a nonlinear,

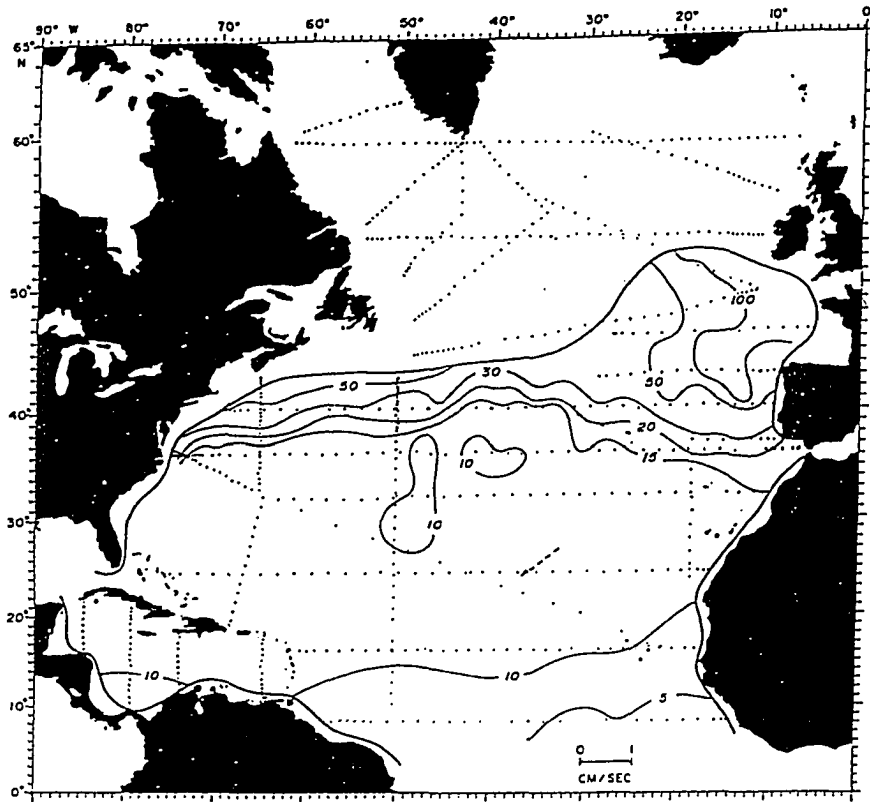


Figure 1: Potential vorticity between the $\sigma_\theta = 26.5$ and 27.0 surfaces in North Atlantic (in units of $10^{-11} \text{ m s}^{-1}$). A plateau of uniform potential vorticity appears at its rim. From McDowell *et al.* (1982).

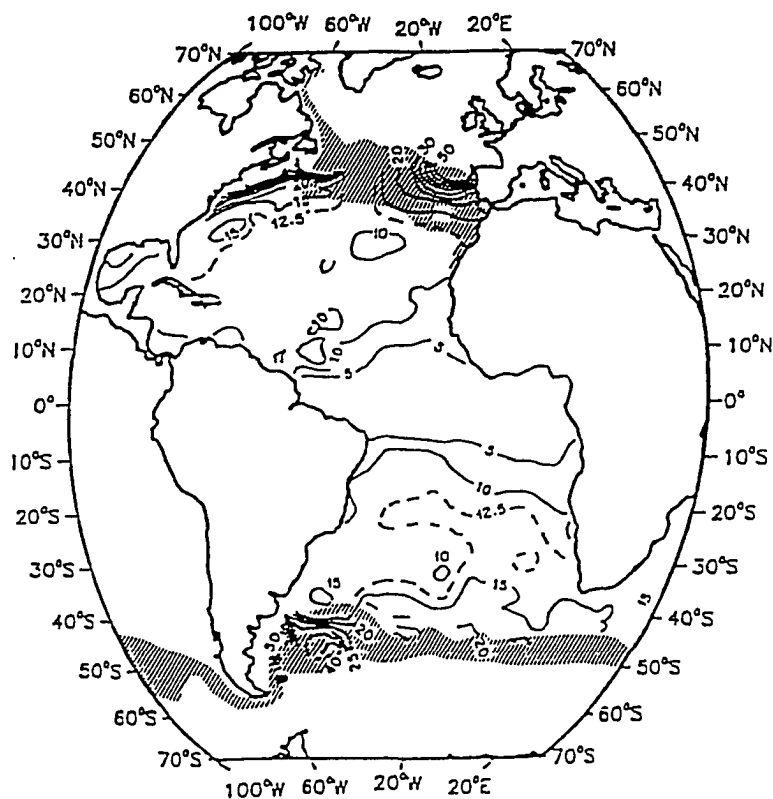


Figure 2: Potential vorticity between the $\sigma_\theta = 26.5$ and 27.0 surfaces (in units of $10^{-11} \text{ m s}^{-1}$). Note regions of homogenized potential vorticity in the North and South Atlantic. From Keffer (1985).

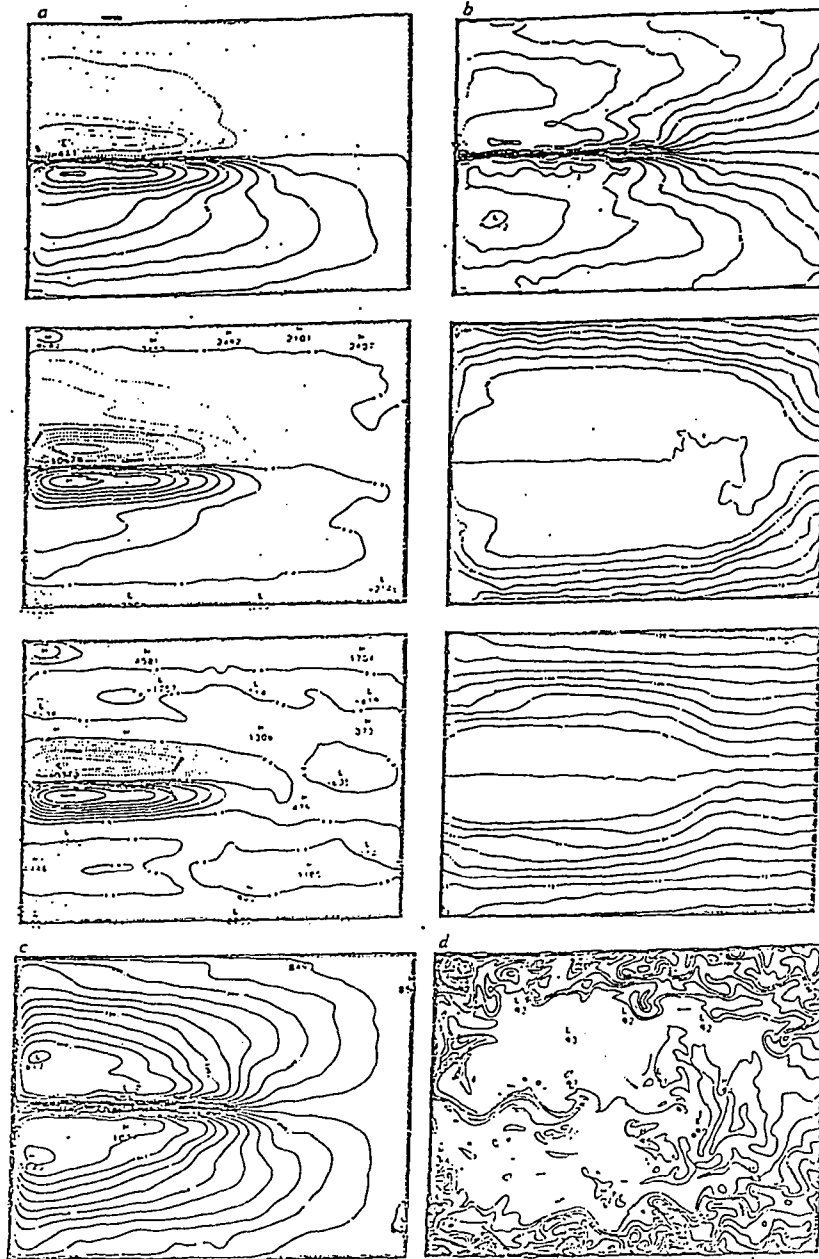


Figure 3: Five year mean streamfunction at the top, third and fifth levels (at the mean depths of 150, 850 and 1750 m, respectively) of an eight-level eddy-resolving numerical simulation of the wind-driven circulation. (b) The mean potential vorticity on the same surfaces. (c) The mean depth in meters of the third layer. (d) The instantaneous potential vorticity of the third layer. From Holland *et al.* (1984).

dissipative model, Dewar *et al.* (1984), showed that the time taken to establish the circulation is the diffusion time scale rather than the time taken by the planetary waves to cross the basin.

RY82 theory does not allow isopycnal surfaces to deform strongly or to intersect the sea surface thus exposing deeper layers to wind forcing. Hence, it is not applicable where outcropping and ventilation affect PV distribution. Furthermore, the non-linear interaction of any boundary layers with the interior flow is ignored.

Pedlosky and Young (1983) superimposed ventilated and unventilated layers in such a way that the sum of the meridional transports satisfied the Sverdrup relation. They noted that the size of the homogenized PV pools shrinks in the unventilated layers and also that the strength of the circulation diminishes in the ventilated layers if the subsurface layers carry a portion of the Sverdrup transport. They also emphasized the importance of dissipation in obtaining a unique solution. In the unventilated region, they hypothesized that PV homogenization depends on PV mixing at mesoscale levels and on the interaction of the mid-ocean gyre with the western boundary current regions.

Western boundary layers were generally neglected in the theories of RY82 and LPS. Initially, these layers were treated as passive conduits to move the fluid from the south to the north (Young and Rhines, 1982). Later, Ierley and Young (1983), showed that the theory of homogenization is not applicable when strong western boundary currents are present. The homogenization theory of RY82 requires PV to be functionally related to the streamfunction everywhere on the closed streamline as the PV is not uniform inside a closed geostrophic contour. Ierley and Young (1983) demonstrated that when all the streamlines pass through the frictional boundary layer the PV in the lower layer (not homogenized) is no longer functionally related to its streamfunction but it is determined by the dynamics of the frictional boundary layer. The inclusion of a strong frictional western boundary layer into their two layer, quasi-

geostrophic model resulted in the occurrence of PV gradients enhancing cross-stream mixing.

While RY82 stress the importance of weak, nonconservative eddy mixing, the LPS model derives flow structure from the conservation of PV. The observational evidence shows that both lateral mixing (as in RY82) and downstream advection at the isopycnic outcrop (as in LPS model) are important to the actual ocean circulation (Jenkins, 1987). Both the homogeneous and the ventilated models neglect relative vorticity in comparison with the planetary vorticity for the scales of motion considered.

2.1.3 The \mathbf{J} -vector approach

Another approach to the study of circulation in thermocline layers (Marshall and Nurser, 1991; MN92) which also based on PV conservation, concentrates on surface input of PV. This approach builds upon the earlier work of Truesdell (1951), Obukhov (1962) and Haynes and McIntyre (1987; 1990). The generalized flux form of the PV equation that expresses Haynes and McIntyre's ideas are:

$$\begin{aligned}\frac{\partial q}{\partial t} + \nabla \cdot \mathbf{J} &= 0 & (2.1) \\ \mathbf{J} &= \mathbf{u}q + \nabla\theta \times \mathbf{F} + (f\hat{\mathbf{k}} + \boldsymbol{\Omega})\frac{d\theta}{dt} \\ \boldsymbol{\Omega} &= \nabla \times \mathbf{u} \\ q &= \nabla\theta \cdot (f\hat{\mathbf{k}} + \boldsymbol{\Omega})\end{aligned}$$

where q is PV and \mathbf{J} is the PV flux vector. Advective and non-advective fluxes together constitute the \mathbf{J} vector. HM summarized the results in two theorems which govern PV budgets between isopycnals: the following two statements hold exactly whether or not diabatic heating and frictional or other forces are acting:

1. There can be no net transport of PV across any isentropic surface.
2. PV can be neither created nor destroyed, within a layer bounded by two isentropic surfaces.

Isentropic surfaces are the surfaces of constant potential temperature. HM demonstrated that buoyancy and mechanical forcing can only dilute or concentrate PV content between isentropic surfaces but can neither create it or destroy it. The isentropic surfaces behave as if they are exactly impermeable to the PV-substance defined as ρq even when diabatic heating or cooling, including that associated with turbulent mixing, makes them permeable to mass and chemical substances (cf. Haynes and McIntyre, 1990). PV-substance is a globally conserved substance of which ρq is the density or q is the amount per unit mass. Global conservation of PV-substance is the result of the fact that the quantity ρq can be written in the divergence form (Eq. 2.1). It is closely related to Kelvin's circulation. Consider a control volume (dV) bounded by two isopycnals, plus a perimeter lying parallel to $(f\hat{k} + \Omega)$. The PV-substance integrated over the control volume is then:

$$\iiint \rho q \, dV = \iint \rho(f\hat{k} + \Omega) \cdot \hat{n} dA$$

taken over the bounding surface with the outward normal \hat{n} . Substituting for Ω yields:

$$[\rho(\int \mathbf{u} \cdot d\mathbf{l} + fA)]_{\rho_2}^{\rho_1} = 0.$$

where A is the area projected normal to f , $d\mathbf{l}$ is a vector line segment defining the perimeter. fA is the planetary vorticity contribution. The robust conservation of absolute circulation thus accounts for the conservation of integrated PV (Rhines, 1993). HM argued that if a region of low PV is created in the middle of a fluid by mixing its mass density, (for example), this will be compensated for by an increase in PV at the edges of the region due to enhanced stratification. In a similar way, any twisting force on the fluid results in producing regions of positive and negative vorticity which cancel when integrated over the entire domain of isopycnals (Rhines, 1993).

Isopycnal surfaces in the oceans are equivalent to the isentropic surfaces of the atmosphere. MN92 used \mathbf{J} vectors to quantify the amount of PV that enters the

isopycnals and then to portray subsequent PV transport. The impermeability of isopycnal surfaces to PV only allows PV flux between two such surfaces to originate from either the free surface or a solid boundary. MN92 illustrated this idea schematically (Fig. 4). Open PV flux lines emanating from the sea surface (where there is net buoyancy forcing) end either on the oceanic boundaries (where frictional forces come into play) or at the ocean surface (where the mixed layer cools). Closed flux line ([1] in Fig. 4) recirculates through the western boundary. Fig. 5 shows the same in a vertical section.

The idealized thermocline model of MN92 did not include the Western Boundary Current. However, the western boundaries can be a source or sink of PV, so that some of the flux lines may terminate there. Csanady and Pelegri (1995) elucidated the mechanism by which PV entering through the sea floor gets into the interior. They postulated that mean PV transport is continuous along isopycnals between the bottom boundary layer (where mechanical turbulence transports PV) and a boundary current in statistically steady state (where geostrophic turbulence transports PV). Within the boundary current Reynolds flux of PV is the \mathbf{J} vector. Hence, in the boundary current the divergence of Reynolds fluxes balances planetary vorticity advection and other terms in the vorticity equation.

2.2 Subduction

The phenomenon of the transfer of near-surface fluid from the turbulent mixed-layer down into the adiabatic and geostrophic interior is known as *subduction*. Its opposite (upwelling of fluid into the mixed layer) is sometimes called *obduction* (Huang, 1994). The mechanism of subduction or obduction is closely related to and controlled by mixed layer dynamics which in turn depends on the mechanical and buoyancy forcing acting at the sea surface. Hence, the surface boundary conditions influence the interior circulation indirectly by determining the amount of mass (and the associated

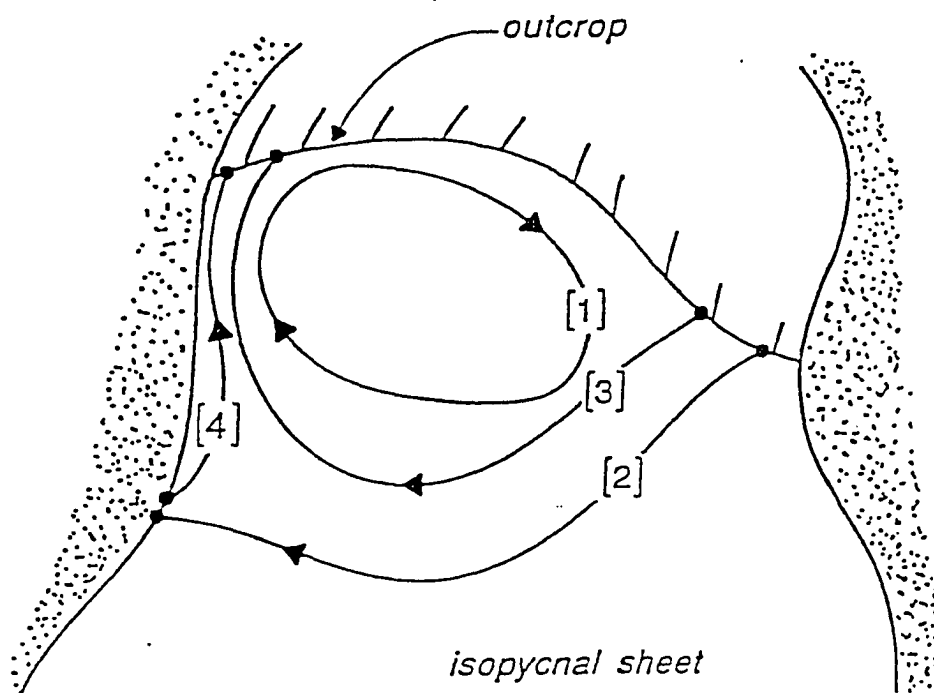


Figure 4: A schematic diagram showing PV flux lines on an isopycnal surface. Closed flux lines [1] recirculate through the western boundary current. Open flux lines [2] and [3] emanate from the sea surface and can either attach themselves onto the coast [2] or return to the ocean surface [3]. Flux line [4] emanates from the coast and terminates from the sea surface. From Marshall and Nurser (1992).

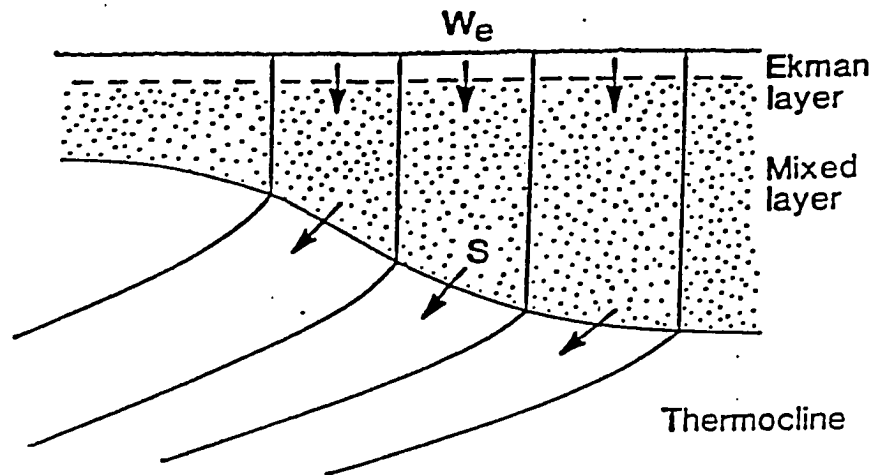


Figure 5: A schematic diagram showing isopycnals in the thermocline outcropping into a vertically homogenous mixed layer. Ekman pumping at the surface W_e drives horizontal flow in the mixed layer, which slides to and from the thermocline through the sloping base of the mixed layer. The mass flux per unit surface area through the mixed-layer base is S ; it is the field of S that drives flow in the thermocline. From Nurser and Marshall (1991).

PV) that is subducted into or extracted from an isopycnal layer. The fluid can be subducted into the interior due to either the lateral convergence of isopycnals as a result of convergent Ekman drift or non-uniform buoyancy flux forcing the fluid across isopycnals at variable rates. The sum of these two determines the amount of fluid that is taken into the subsurface layers (Rhines, 1993).

Earlier ventilated thermocline models (LPS; Huang and Bryan, 1987) assumed that the fluid is pumped into the thermocline layers at a rate equal to Ekman pumping defined as $(\rho f)^{-1}$ times the curl of the wind stress. However, Ekman pumping alone could not account for the high ventilation rates inferred from tracer studies of Sarmiento (1983) and Jenkins (1987). The currently prevailing view is that fluid is pumped down from a shallow surface Ekman layer into a deeper mixed layer. It is from the base of that mixed layer (the depth of which varies spatially and temporally) that the thermocline is ventilated. Mixed-layer dynamics was neglected for simplicity in the earlier development of the thermocline theory, but later models (Woods, 1985; Huang, 1990) emphasized its role in thermocline circulation. Woods (1985) pointed out that the lateral induction of fluid across the sloping base of the mixed layer makes a significant contribution to the ventilation of the thermocline layers. Ekman layer is considered as the depth over which the wind influences the interior. Hence, recent thermocline models include a shallow Ekman layer embedded in a mixed layer which overlays an adiabatic stratified interior (Huang, 1990; Nurser and Marshall, 1991; MN92), as in Fig. 5. In this usual model, the outcropping isopycnals are vertical in the mixed layer because the vertical density gradients are supposed to be eliminated by wind and surface cooling.

In the above general approach, the instantaneous subduction rate S , is defined as the downward velocity of a parcel of fluid relative to the base of the mixed layer (Cushman-Roisin, 1987b; Nurser and Marshall, 1991; Williams, 1991):

$$S = -\frac{\partial h}{\partial t} - \vec{u}_b \cdot \nabla h - w_b \quad (2.2)$$

where h is the mixed layer depth, \vec{u}_b is the horizontal velocity vector of the particle at the base of the mixed layer, w_b is its vertical velocity and t is the time. The quantity S is the volume flux of the fluid per unit horizontal area per unit time that enters the thermocline from the mixed layer *across* the mixed-layer base (Marshall *et al.*, 1993). Seasonal deepening or shoaling of the mixed layer does not result in the permanent transfer of the fluid from the mixed layer into the adiabatic interior (Woods, 1985). Hence, over the course of a year, the vertical velocity and the lateral induction (though an order of magnitude smaller than $\partial h/\partial t$) result in long-term transfer of fluid from the mixed layer into the permanent thermocline (Marshall *et al.*, 1993).

Based on the above kinematic relation (Eq. 2.2), Marshall *et al.* (1993) evaluated the subduction rate from the Ekman pumping field of Isemer and Hasse (1987) and from the climatological hydrographic dataset of Levitus (1982). They calculated vertical subduction rates of up to $3.0 \times 10^{-6} \text{ m s}^{-1}$ over some of the subtropical gyre (Fig. 6). In the region of the eastern North Atlantic where the isopycnals of the upper thermocline outcrop, the rates are of the order of $0.8 \times 10^{-6} \text{ m s}^{-1}$.

Using a simple mixed layer model (Fig. 5), Nurser and Marshall (1991), reformulated the subduction rate (S) in terms of the buoyancy flux and PV available at the mixed layer base. Assuming the velocity and potential density continuous across the mixed layer base, they showed that:

$$S = \frac{f H_{net}}{g h \rho Q_b} \quad (2.3)$$

where H_{net} is the heat absorption associated with the cross-isopycnal transport and $Q_b = -f \rho^{-1} \partial \rho / \partial z|_{z=-h}$ is the PV at the mixed layer base. According to the above formulation, the total PV flux between the mixed layer and the thermocline ($S Q_b$) is proportional to $f H_{net}/h$. This relation implies that subduction is physically determined by what Nurser and Marshall (1991) defined as “net” heat gain. However, the above derivation neglected the seasonal movement of the isopycnals, thus limiting

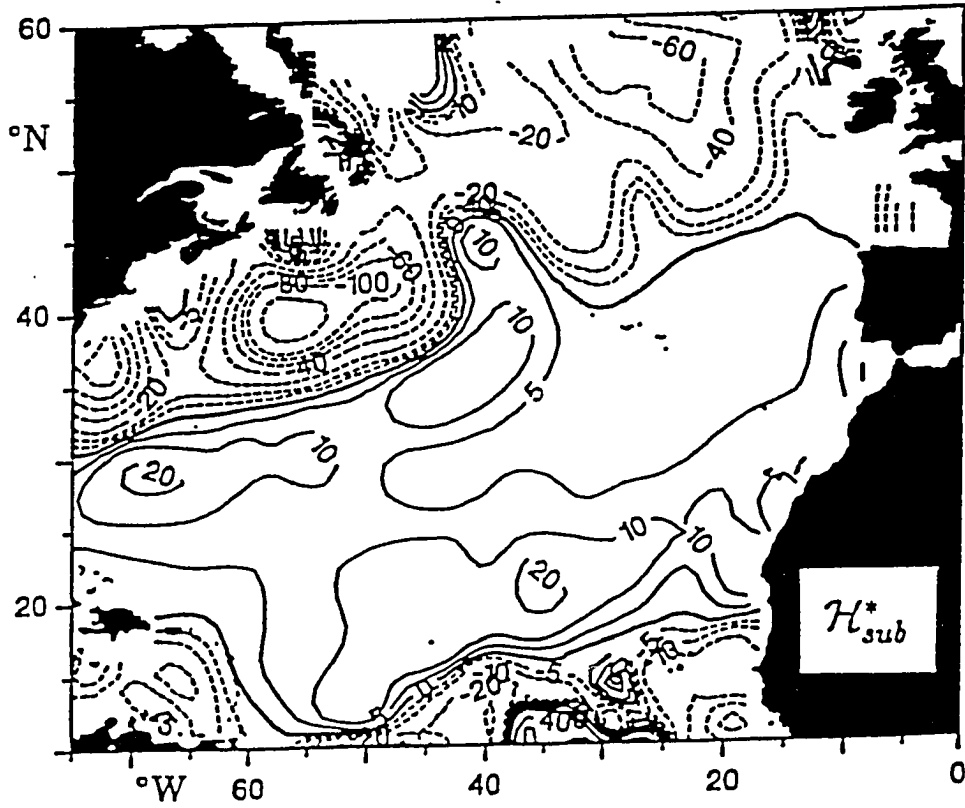


Figure 6: Annual subduction rate S_{ann} (m yr^{-1}) into the main thermocline. From Marshall *et al.* (1993).

the validity of the above formulation to the case of stationary isopycnal outcrops. Marshall *et al.* (1993) defined H_{net} as:

$$H_{net} = \frac{g\alpha}{c_p} H_{in} - H_{salt} - H_{Ek} \quad (2.4)$$

where α is the thermal expansion coefficient, c_p is the heat capacity of the water, H_{in} is the surface heat flux, H_{salt} is the buoyancy due to the surface salt flux (contributed by the evaporation and precipitation rates). H_{Ek} is the buoyancy flux acquired by the Ekman drift defined as:

$$H_{Ek} = \frac{g}{\rho f} \hat{k} \times \tau \cdot \nabla \rho_m$$

where τ is the wind stress and ρ_m is the mixed-layer density.

The H_{net} obtained from the climatology data of Levitus (1982) and Isemer and Hasse (1987), is of the order of 5 to 10 W m⁻² over the subtropical gyre favouring subduction, except along the Gulf Stream where the net heat flux is negative (~ -50 to -100 W m⁻²) supporting entrainment (Fig. 7). A heat flux of 10 W m⁻² acting on a mixed layer of 100 m depth with a PV of 3.0×10^{-10} m⁻¹ s⁻¹ at the mixed layer base, gives a subduction rate of the order of 1.5×10^{-6} m s⁻¹.

2.3 Numerical models of thermocline circulation

Though analytical models provide some insight into the underlying physics, they cannot take into account many non-linear processes and they also neglect important processes in lateral boundary layers. In the PV maps of McDowell *et al.* (1982) derived from observations, boundary currents and mesoscale fields are poorly represented because relative vorticity was neglected in comparison to the planetary vorticity. Numerical models remain the only tools to explore such complicated features of circulation as the interplay of boundary layers with interior dynamics, a process in which relative vorticity is important.

Eddy resolving, multi-layer numerical models, using either the quasi-geostrophic approximation (Holland *et al.*, 1984) or primitive equations (Cox, 1985; Böning and

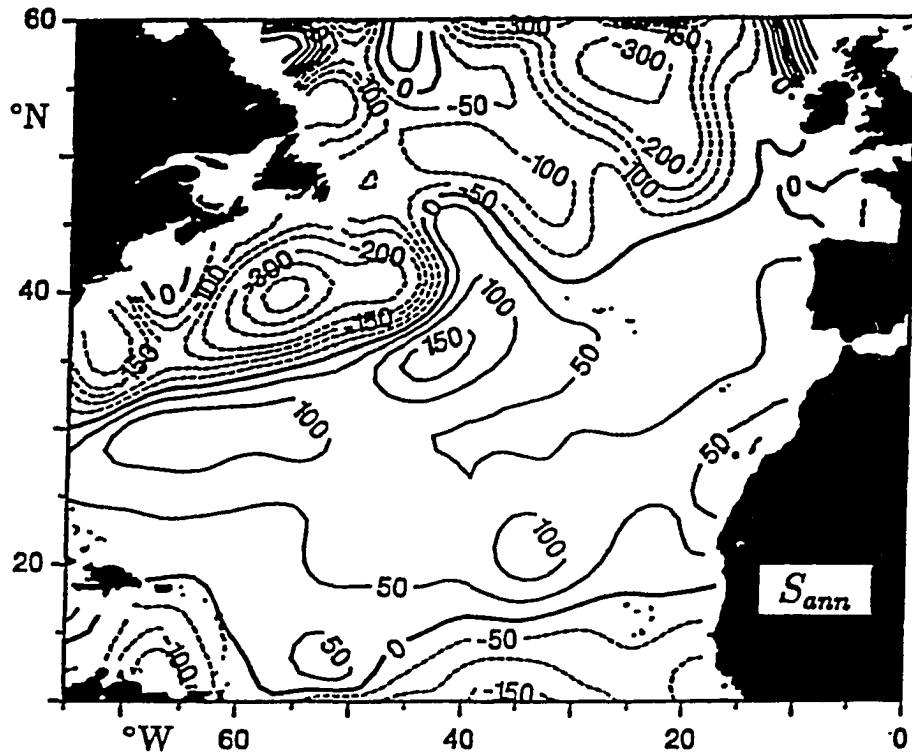


Figure 7: The heat flux H_{net} (W m^{-2}) into the ocean that drives the subduction of fluid into the main thermocline; positive values are associated with subduction and negative values with entrainment. From Marshall *et al.* (1993).

Cox, 1988), reproduced all the dynamical regions predicted by the RY82 and LPS analytical models, illustrating, in particular, the role of mesoscale eddies in diffusing PV. Unventilated subsurface layers in these models are forced by eddy processes. The eddy field arises from the combined baroclinic/barotropic instability of an eastward jet formed at the subtropical/subpolar gyre boundary and also due to the baroclinic instability of the westward return flow (Holland *et al.*, 1984; Cox, 1985). The reversal of the north-south PV gradient in the latter region, the southeastern part of the subtropical gyre provides the necessary conditions for baroclinic instability according to the Charney–Stern criteria (Cox, 1985). Eddies arising in this region have energy an order of magnitude smaller than in the jet formed at the subtropical/subpolar gyre boundary, but they are important in a broader region.

Cox (1985) used an eddy-resolving, primitive equation model to study the influence of mesoscale eddies within the subtropical thermocline. Patterns of tracer and PV along the 26.0σ surface are shown in Fig. 8. Figs. 8a and 8c correspond to coarse grid case where eddies are not resolved. The tracer age is estimated from the decay of the value specified at the surface, and in the absence of mixing measures the time elapsed since a parcel of water was in contact with the surface. Fig. 8c shows the low PV water masses formed at the isopycnal outcrop are advected along the eastward jet to be carried southward and westward by the interior flow of the subtropical gyre. These ventilated waters stand in marked contrast to the unventilated (recirculating) waters, their high PV due to lateral mixing and bottom friction (Huang, 1988). In a high resolution experiment (fine grid case), the distinction between these water masses was effectively eliminated by strong lateral mixing, forming a homogeneous PV mass in the interior of the thermocline layer (Fig. 8d).

In the numerical models, the process of PV homogenization differs from the RY82 theory in two ways. Firstly, eddies present near the boundaries are found to be quite effective in homogenizing the PV on a much shorter time scale than in the RY82

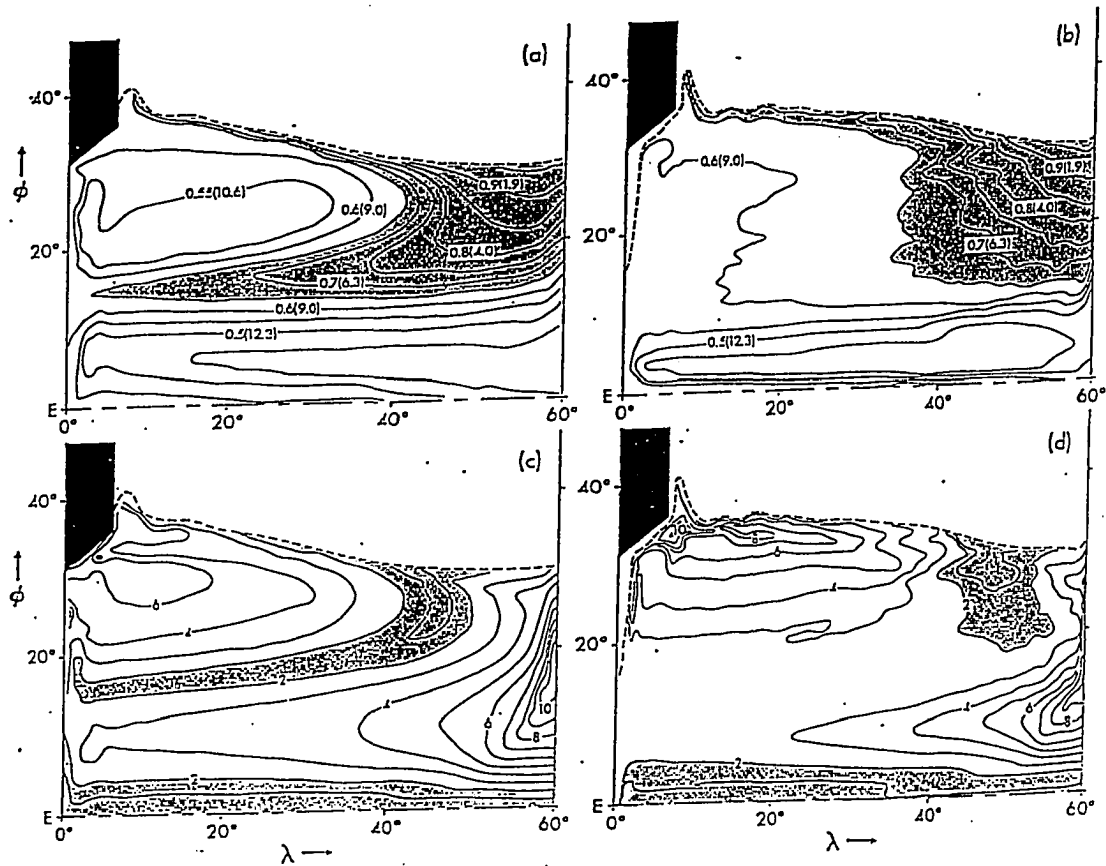


Figure 8: Tracer concentration and potential vorticity evaluated on the $\sigma = 26.0$ surface. Tracer (time-since-ventilation in years, in parentheses) for (a) the coarse grid case, (b) the fine grid case. Potential vorticity in units of $10^{-9} \text{ m}^{-1} \text{ s}^{-1}$ for (c) the coarse grid case, (d) the fine grid case. From Cox (1985).

theory. Secondly, low PV (homogenized) waters (McCartney, 1982) formed at the isopycnal outcrops produce local meridional maxima and minima in PV, giving rise to eddies. These eddies vigorously mix the subducted low PV waters with the higher PV thermocline waters. Such numerical models expose the limitations of the analytical theories in including non-linear processes that influences the interior circulation.

Moderate Peclet numbers (3 to 5) found in the north-east North Atlantic (in ventilated layers), in Rhines and Schopp's (1991) model study make mesoscale eddy mixing dominant, able to homogenize quasi-conserved properties over 300 to 1000 km. This study showed that the ratio of eddy-to-mean kinetic energy increases as one moves to quieter regions of the midocean, demonstrating that eddy mixing cannot be neglected there. Similar conclusions follow from the work by Cox (1985) and Böning and Cox (1988). These model studies suggest that the non-diffusive approach taken in the LPS class of models must be augmented by recognizing potent eddy mixing. All numerical modeling efforts on thermocline ventilation suggest that the ocean is strongly laterally diffusive, even in regions far from boundary currents (Rhines, 1993; Böning and Cox, 1988). The idea of vigorous eddy mixing is also supported by the observed distribution of transient tracers entering from the sea surface (Jenkins, 1987).

2.4 Observational studies in the subtropical North Atlantic

The northeastern part of the subtropical North Atlantic has early been thought to be the seat of water mass subduction (Montgomery, 1938; Iselin, 1939). Ekman pumping calculations (Leetmaa and Bunker, 1978) and the pattern of winter outcropping of the isopycnals (Levitus, 1982) also suggest ventilation in this region. Ventilation occurs principally in the northwestern portion (*i.e.*, around 40°N, 40° W) of the eastern subtropical gyre which is strongly influenced by wintertime convection (Jenkins, 1987; Sarmiento *et al.*, 1982). In this region, colder, fresher oxygen-rich waters are

subducted and advected from the northern flank of the Azores Current into the thermocline layers (Käse *et al.*, 1986). Hence, it is essential to understand the circulation and dynamics of this region to better model the thermocline problem.

2.4.1 Circulation

Observations reveal that the eastern North Atlantic region, earlier considered to be part of the quiescent interior of the wind driven subtropical gyre, also contains jet-like flows (Gould, 1985; Käse *et al.*, 1986; Stramma and Siedler, 1988). The circulation in this region is affected by three named currents: the Azores Current, the Portugal Current and the North Equatorial Current. The three dynamical scales important in this region are: the scale of mean circulation (1000 km), the scale of meandering flow (500 km) and the scale of mesoscale eddy field (100 km) (Käse *et al.*, 1985) (Fig. 9). The circulation pattern in the upper thermocline (200-800 m) of the eastern subtropical North Atlantic starts with strong eastward flow west of 35° W and north of 29° N, turns southward within 1000 km of the coast, then separates from the coast north of 20° N (Stramma and Siedler, 1988) (Fig. 10). Drifter studies (Krauss and Käse, 1984) suggest that the westward return flow along the 33° W meridian starts at 33° N, somewhat further north than in Fig. 10. In the subsurface layers, westward outflow occurs at a higher latitude than in the surface layer (0-200 m) (Stramma, 1984). Käse *et al.* (1986) documented the recirculation of the subtropical gyre east of the Madeira Islands, at 560 m *i.e.*, within the thermocline (Fig. 11). The turning part of the gyre near the coast is found to have a larger east-west and a smaller north-south extension in summer than in winter and its center shifts by 2° latitude to the south in summer (Stramma and Siedler, 1988). In the northern part of this region, Käse *et al.* (1986), described a convoluted current system dominated by the time-dependent meandering of the eastward flowing Azores Current (AC) and the formation of mesoscale eddies in the recirculating region.

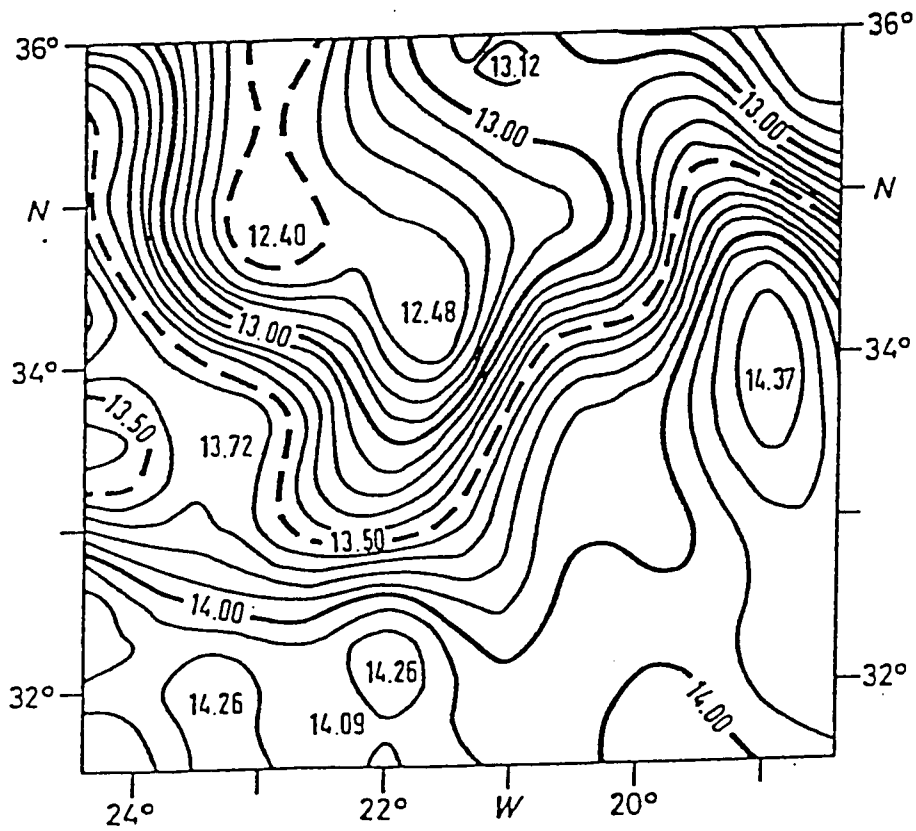


Figure 9: Dynamic topography relative to the 1500 dbar. From Käse *et al.* (1985).

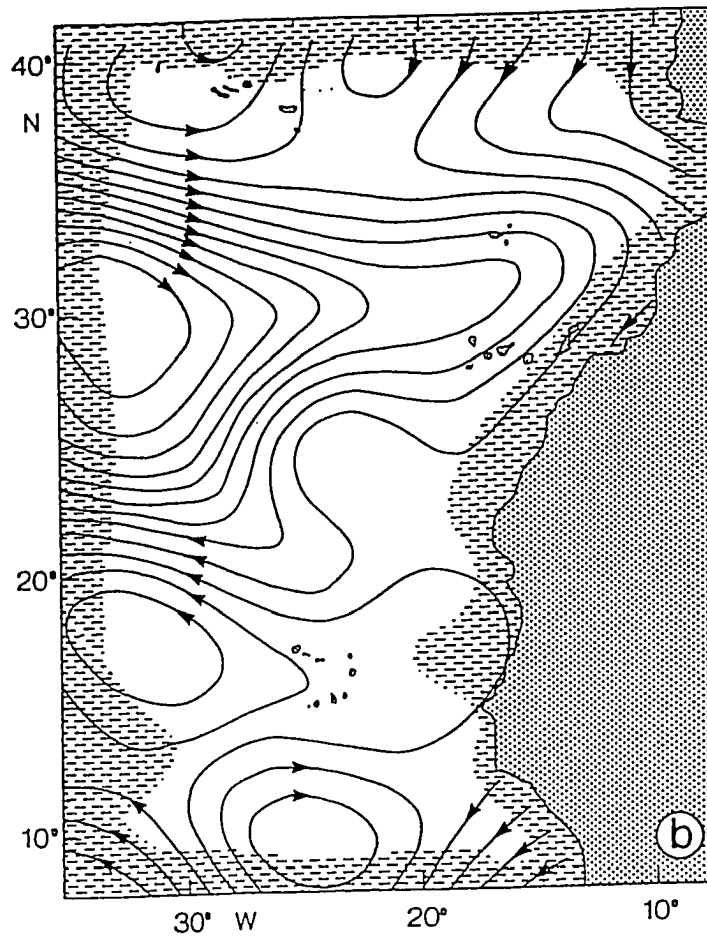


Figure 10: Annual integrated volume transport (200 to 800 m) from mean density profiles. Contour intervals represent $0.5 \times 10^6 \text{ m}^3 \text{ s}^{-1}$. From Stramma and Siedler (1988).

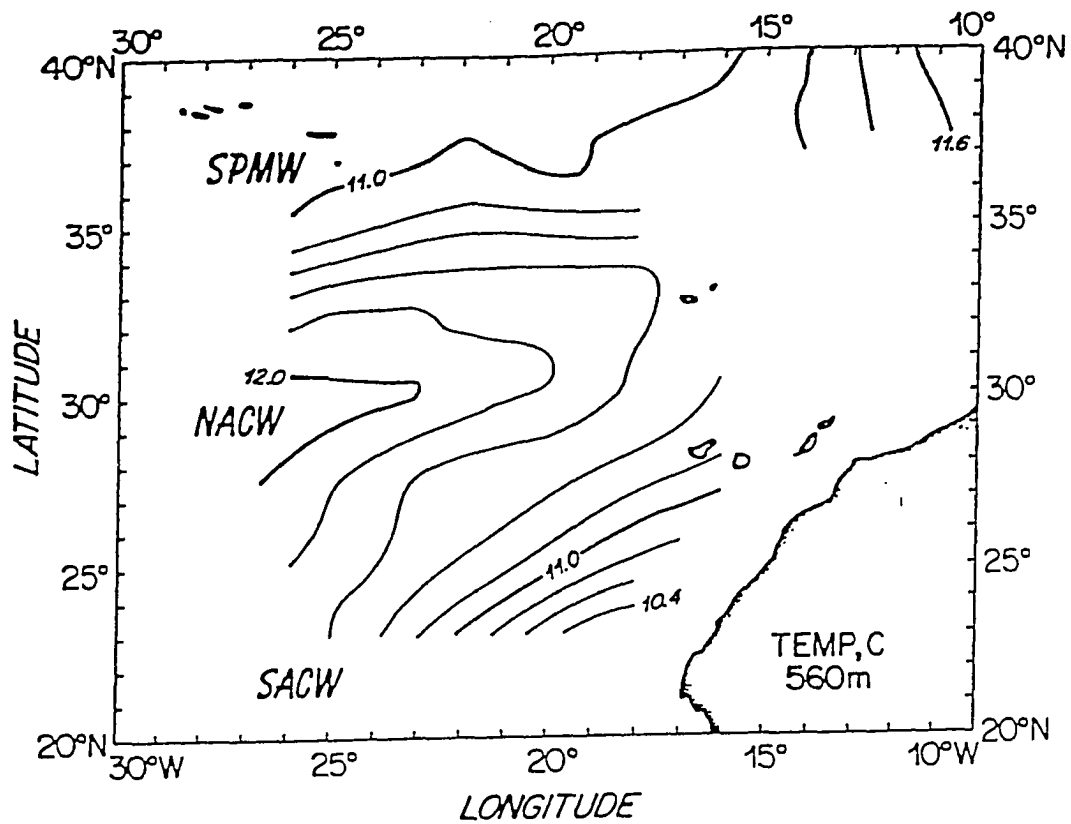


Figure 11: Large-scale temperature distribution at 560 m depth. NACW and SACW denote North Atlantic Central Water and South Atlantic Central Water, respectively. From Käse *et al.* (1986).

In the literature, the AC is generally considered to be the southeastward branch of the Gulf Stream continuation, east of the splitting region near 40°N, 40°W (Käse *et al.*, 1986; Krauss, 1986). After crossing the Mid-Atlantic Ridge AC is looked upon as the northern boundary of the subtropical gyre (Gould, 1985; Käse *et al.*, 1985). This strong narrow current, enters the region south of the Azores between 33°20' and 35° N, and flows southeastward past the Azores (Stramma, 1984). Käse and Siedler (1982) found this current at the depth of 1000 m. Evidence for strong eastward flow in this region is also found in some early papers (e.g., Jacobsen, 1929; Stommel *et al.*, 1978). The AC transports approximately 10 Sv (1 Sv = $10^6 \text{ m}^3 \text{ s}^{-1}$) eastward across 35°W, between 30°N and 40°N (Käse and Siedler, 1982; Gould, 1985; Käse *et al.*, 1986). This estimated total volume transport in the Azores front is half of that reported by Mann (1972) for the southern branch of the Gulf Stream extension and by Joyce (1981) for the circulation around the Azores plateau.

Gould (1985) reported the existence of a permanent front southwest of the Azores associated with the AC. Käse and Siedler (1982) considered this jet or front to be an integral part of the North Atlantic gyre circulation. The wind stress curl, surface heat flux changes and volume transport changes in this region provide conditions that are favourable to the formation of the oceanic fronts (Siedler *et al.*, 1985). They reported near surface velocities in the front of the order of 0.2 ms^{-1} . Surface speeds measured (from buoy data) by Gould (1985) in this frontal area are around 0.4 ms^{-1} (in early June), whereas Schmitz *et al.* (1988) measured 0.15 m s^{-1} from the current meter and float data in the upper thermocline at 32°N and 24°W. The geostrophic velocities are of the order 0.1 m s^{-1} in the eastward and westward return flow, increasing to 0.25 m s^{-1} in the meandering region (Käse *et al.*, 1985). The frontal width observed is of the order of 60 km increasing to 100 km in some regions (Käse *et al.*, 1985). The northern boundary of the front is the surface outcrop of the $26.5 \sigma_\theta$ contour in late winter. The orientation of the front is NW-SE, meandering predominantly in the

north-south direction (Gould, 1985). A synoptic survey by Käse *et al.*, (1985) in this region indicates (Fig. 9) that there are two dominant wavelengths, one at 570 km associated with the meandering of the AC and the other at 200 km associated with the mesoscale eddy field superimposed on the meandering jet.

2.4.2 Estimated ventilation rates

In the β triangle area centered around 27° N, $32^\circ 30'$ W, Jenkins (1987) estimated the along-isopycnal subduction velocity of $1.6 \times 10^{-3} \text{ m s}^{-1}$. This area in the eastern subtropical Atlantic is a region of low eddy activity with a mean meridional flow (Behringer and Stommel, 1980). It was studied earlier (Armi and Stommel, 1983) to apply the beta spiral as a diagnostic tool to determine absolute geostrophic velocity. The estimated along-isopycnal velocities in this region are comparable to the mean geostrophic velocities. The Ekman pumping estimates from Leetmaa and Bunker (1978) data give along-isopycnal velocities of the order $1.0 \times 10^{-3} \text{ m s}^{-1}$ here. But at $40^\circ - 43^\circ$ N, Saunders (1982) estimated a southward velocity of $3.0 \times 10^{-3} \text{ m s}^{-1}$ to $5.0 \times 10^{-3} \text{ m s}^{-1}$. From the numerical model studies, Spall (1990) estimated vertical subduction velocity to be of the order of $1.25 \times 10^{-6} \text{ m s}^{-1}$ over most of the eastern North Atlantic except along the AC and the meandering Portugal current where it is as large as $3.0 \times 10^{-6} \text{ m s}^{-1}$ compared to the downward Ekman pumping rate of $0.85 \times 10^{-6} \text{ m s}^{-1}$.

2.4.3 Eddies

The eastern North Atlantic is a region of low eddy activity (Dantzler, 1977; Wyrтки *et al.*, 1976; Emery, 1983). The eddies and meanders often dominate the hydrographic structure in this region (Krauss and Käse, 1984). In Central Atlantic eddies, vertical displacements of the isotherms are of the order of $\pm 150 \text{ m}$ (Krauss and Meincke, 1982). Compared to the mean slopes of the isopycnals, related to mean currents,

fluctuating slopes with scales around 100-200 km are much stronger signals in this region (Krauss and Käse, 1984).

The average eddy kinetic energy in the eastern North Atlantic (for fluctuations with periods of more than two days), calculated from the hydrographic data of Käse *et al.* (1985) is around $0.15 \text{ m}^2 \text{ s}^{-2}$. From drifter studies, however, Krauss and Käse (1984) estimated eddy kinetic energy to be between 0.01 to $0.02 \text{ m}^2 \text{ s}^{-2}$. Although eddy kinetic energy in this region is a order of magnitude smaller than in the Gulf Stream (Emery, 1983), it is much larger than the mean flow kinetic energy. The eddies are derived from the large-scale circulation, and are not due to fluctuating winds or to the influence of the Mid-Atlantic Ridge (Krauss and Meincke, 1982; Käse *et al.*, 1986). The area southwest of the Azores is high in mesoscale activity and it is a likely source of eddies propagating to the western basin of the North Atlantic (Gould, 1985). The mesoscale eddy field in this region is dominated by the AC which undergoes large amplitude North-South meandering (Käse *et al.*, 1985) with occasional eddy detachment (Käse *et al.*, 1986). The eddy kinetic energy is largest in the region where the AC turns south and in the westward flowing recirculation region (Krauss and Käse, 1984).

Cyclonic, cold core eddies form in the Azores frontal area adjacent to the meanders of the AC (Gould, 1985). These eddies, originally 100-115 km in diameter, propagate to the west at a rate close to 2.2 km day^{-1} over a 200 day period. However, they do not cross the mid-Atlantic ridge. The core of the eddies retain the properties of the northern water mass and propagate westward into the 18° water mass. Käse *et al.*, (1985), found the dominant scale for mesoscale eddies to be 100 km, whereas salinity, oxygen, helium-tritium age maps of Joyce and Jenkins (1993), show scales around 160 km. The eddies are to be generated where surface flows interact with complex bottom topography (Stramma, 1984) or shear flows are strong (Wyrтки *et al.*, 1976). The transfer of energy is from the mean field to the eddy field. Two

dominant periods of 138 days and 60 days found by Käse *et al.* (1985), are associated with period of the meandering patterns and with the mesoscale eddies. From eddy kinetic energy and potential energy calculations, they estimated a time scale of 19 days for the fluctuations to grow from zero to their average energy level.

3 Physics of vorticity input

As mentioned in the background chapter, isopycnal layers of the main oceanic thermocline outcrop at mid to high latitudes. Outcropping of isopycnals here refers to the location where the isopycnal intersects the base of the mixed layer. Surface processes are known to be influential in setting the temperature and salinity structure of the interior layers (Iselin, 1939). Analogous to temperature and salinity, PV is also a conserved quantity in the interior, while at the surface, friction and density change play the role of PV “sources or sinks”. Thus, surface heating or cooling, evaporation or precipitation, mixing near the surface determine the PV distribution in outcropping isopycnal layers. Because PV is a dynamical quantity, its distribution is a clue to circulation within the isopycnal layers. One may then surmise, that surface processes at the layer outcrops drive a system of thermocline circulation, in addition to determining TS characteristics.

Conventional modelling either forces the subsurface layers indirectly with the wind stress curl applied to the surface layer (Holland *et al.*, 1984; Cox, 1985) or prescribe diapycnal (cross-isopycnal mass) fluxes supposedly by representing heating or cooling (Pedlosky, 1986; Luyten and Stommel, 1986; Cushman-Roisin, 1987a). Differing from conventional theory, Marshall and Nurser (1992) treated in some detail the problem of thermocline circulation forced by surface PV input. Their approach supposes stationary isopycnal surfaces and surface outcrops. Here, with some idealizations, a mathematical expression for the surface PV flux is derived for the unsteady problem, allowing for the seasonal migration of isopycnals as well as their meanders and other expressions of geostrophic turbulence, following Csanady and Vittal (1995).

3.1 Migration of surface isopycnals

At their surface outcrop in the northern North Atlantic, isopycnal surfaces are nearly vertical in the mixed layer. Although there is significant positive or negative heat flux (depending on the season), mixing is vigorous enough to keep vertical density gradients small. Surface heating and cooling gives rise to large meridional displacements of isopycnal outcrops. In the northern hemisphere they are northward in the spring and southward in the fall. Observations show that, on average, the isopycnals move some 1000 km over a period of three to four months, thus advecting at a mean speed of the order of 0.1 m s^{-1} .

The surface density will be represented here by density anomaly, $\theta = 1 - \rho/\rho_0$ (ρ_0 is a reference density). It is a function of x, y and t where x is the zonal coordinate, y is the meridional coordinate and t is the time. In the eastern North Atlantic, a prototype location for the present study, the outcrop positions make a smaller angle with the zonal direction than with the meridional direction. To focus on isopycnic layers, we introduce isopycnic coordinates at the sea surface, replacing the y -coordinate by density anomaly θ . Thus, for a fixed θ , the surface outcrop of an isopycnal surface is the locus $y = Y(x, \theta, t)$. Hence, $\theta(x, y, t) = \theta(x, Y[x, \theta, t], t)$. In the transformed coordinates the following identities for the derivatives hold (Csanady, 1990):

$$\begin{aligned}\frac{\partial \theta}{\partial x} + \frac{\partial \theta}{\partial y} \frac{\partial Y}{\partial x} &= 0 \\ \frac{\partial \theta}{\partial t} + \frac{\partial \theta}{\partial y} \frac{\partial Y}{\partial t} &= 0 \\ \frac{\partial \theta}{\partial y} \frac{\partial Y}{\partial \theta} &= 1\end{aligned}$$

The total derivative of the density anomaly now becomes:

$$\dot{\theta} = \frac{d\theta}{dt} = \frac{\partial \theta}{\partial t} + u \frac{\partial \theta}{\partial x} + v \frac{\partial \theta}{\partial y} = \frac{\partial \theta}{\partial y} \left(v - \frac{dY}{dt} \right) \quad (3.1)$$

where $dY/dt = \partial Y/\partial t + u\partial Y/\partial x$. The bracketed term $(v - dY/dt)$ is the surface diapycnal velocity, or the velocity relative to a (possibly moving) isopycnal, similar to

entrainment velocity. The time derivative (dY/dt) accounts for seasonal changes as well as the effects of geostrophic turbulence. Mechanical and convective turbulence gives rise to Reynolds fluxes of heat and salt. The divergence of these fluxes and of the radiant heat flux determines the density tendency $\dot{\theta}$.

3.2 PV flux at surface outcrop

Conservation of potential vorticity can be expressed in the following “flux” form (Haynes and McIntyre, 1987; Marshall and Nurser, 1992):

$$\frac{\partial q}{\partial t} + \nabla \cdot \mathbf{J} = 0 \quad (3.2)$$

with the definitions:

$$q = \nabla \theta \cdot (f \hat{k} + \mathbf{\Omega})$$

$$\mathbf{\Omega} = \nabla \times \mathbf{u}$$

$$\mathbf{J} = \mathbf{u}q + \nabla \theta \times \mathbf{F} + (f \hat{k} + \mathbf{\Omega}) \frac{d\theta}{dt}$$

where q is PV, f Coriolis parameter, \mathbf{u} velocity vector, \hat{k} vertical unit vector and $\mathbf{\Omega}$ is the relative vorticity. \mathbf{J} is PV flux vector, containing the advective flux $\mathbf{u}q$ and contributions from the non-conservative force vector \mathbf{F} (in kinematic units, *i.e.* divided by reference density) and from the density tendency $\dot{\theta}$. The following discussion concentrates on the magnitude and properties of the PV flux vector on an isopycnal surface, at and near the intersection of such a surface with the free surface. The PV flux out of the ocean is given by the vertical component of \mathbf{J} at the free surface. There, advective flux vanishing, only friction and density tendency fluxes contribute to the \mathbf{J} vector at the surface. The force vector \mathbf{F} is taken to be the vertical wind shear stress at the surface:

$$\mathbf{F} = \hat{i} \frac{\partial \tau_x}{\partial z} + \hat{j} \frac{\partial \tau_y}{\partial z}$$

where τ_x, τ_y are Reynolds stress components in the horizontal plane and \hat{i} and \hat{j} are unit vectors along x and y . The vertical component of the PV flux is then, from

equation 3.2:

$$\mathbf{J} \cdot \hat{\mathbf{k}} = -\dot{\theta}(f + \zeta) + \frac{\partial \theta}{\partial x} \frac{\partial \tau_y}{\partial z} - \frac{\partial \theta}{\partial y} \frac{\partial \tau_x}{\partial z}$$

where $\zeta = \partial v / \partial x - \partial u / \partial y$. Transforming to horizontal isopycnal coordinates using equation 3.1, this becomes:

$$\mathbf{J} \cdot \hat{\mathbf{k}} = -(f + \zeta) \frac{\partial \theta}{\partial y} \left(v - \frac{dY}{dt} \right) - \frac{\partial \theta}{\partial y} \frac{\partial Y}{\partial x} \frac{\partial \tau_y}{\partial z} - \frac{\partial \theta}{\partial y} \frac{\partial \tau_x}{\partial z} \quad (3.3)$$

Considering the first order balance terms, the equations of motion in the surface layer are:

$$\begin{aligned} -v(f + \zeta) &= -\left(\frac{\partial \Pi}{\partial x} + \frac{\partial u}{\partial t} \right) + \frac{\partial \tau_x}{\partial z} \\ u(f + \zeta) &= -\left(\frac{\partial \Pi}{\partial y} + \frac{\partial v}{\partial t} \right) + \frac{\partial \tau_y}{\partial z} \end{aligned} \quad (3.4)$$

where $\Pi = p + (u^2 + v^2)/2$, is the “total” pressure. The momentum diffusion in the surface layer is neglected as it is a process of second order importance, at the scales of the present study. Substituting the above expressions (Eq. 3.4) into equation 3.3, PV flux across the free surface is:

$$\mathbf{J} \cdot \hat{\mathbf{k}} = (f + \zeta) \frac{\partial \theta}{\partial y} \frac{\partial Y}{\partial t} - \left(\frac{\partial \Pi}{\partial y} + \frac{\partial v}{\partial t} \right) \frac{\partial \theta}{\partial y} + \left(\frac{\partial \Pi}{\partial x} + \frac{\partial u}{\partial t} \right) \frac{\partial \theta}{\partial x} \quad (3.5)$$

The last two terms make up the vector product of pressure gradient–plus–acceleration and density gradient. If one considers these terms to vanish, then PV flux across the surface is only due to the result of isopycnal movement. Under such conditions, the PV flux across the surface can be positive only if $\partial Y / \partial t$ is negative, because $\partial \theta / \partial y$ is always negative. Hence, the regions where there is cooling or evaporation (for $\partial Y / \partial t$ to be negative), the PV flux across the surface is positive *i.e.* out of the ocean. Positive $\mathbf{J} \cdot \hat{\mathbf{k}}$ means upward flux of positive PV at the surface, which is equivalent to downward flux of negative PV. However, the two terms vanish only when the two vectors are parallel *i.e.* when the local acceleration vanishes in addition to the pressure being constant along isopycnal outcrops. Such a situation of the pressure

being constant along isopycnal outcrops might arise when the surface forcing dictates the mere translation of the isopycnals.

However, the above expression (Eq. 3.5) can be further reduced if the coordinate system is turned locally into the along-isopycnal (s , nearly eastward) and cross-isopycnal (n , nearly northward) directions. The vector product becomes $-(\partial\Pi/\partial s + \partial v_s/\partial t) \partial\theta/\partial n$, where v_s is the along-isopycnal velocity component. Replacing also $\partial Y/\partial t$ by $\partial N/\partial t$, the rate of displacement of the isopycnal in the normal direction, the incoming PV flux is:

$$\mathbf{J} \cdot \hat{\mathbf{k}} = \frac{\partial\theta}{\partial n} [(f + \zeta) \frac{\partial N}{\partial t} - (\frac{\partial\Pi}{\partial s} + \frac{\partial v_s}{\partial t})] \quad (3.6)$$

The Eq. 3.6 can also be interpreted in terms of the heating or cooling caused by the thermal fluxes. In a steady state situation, the $\mathbf{J} \cdot \hat{\mathbf{k}}$ reduces to:

$$\mathbf{J} \cdot \hat{\mathbf{k}} = - \frac{\partial\theta}{\partial n} \frac{\partial\Pi}{\partial s} \quad (3.7)$$

which is equivalent to

$$\mathbf{J} \cdot \hat{\mathbf{k}} = (f + \zeta) v_g \cdot \nabla\theta \quad (3.8)$$

where v_g is the geostrophic velocity. The above expression for PV flux is similar to the MN92 relation, where $v_g \cdot \nabla\theta$ represents the geostrophic heating or cooling defined in their study. Or in other words, the total pressure gradient accounts for the geostrophic heating or cooling.

3.3 Handover of PV transport

How does an isopycnic layer cope with surface input of PV? To explain the underlying physics, the outcrop region of an isopycnic layer is idealized as illustrated in Fig. 12. The figure portrays two adjacent isopycnal surfaces in a vertical section normal to the surface outcrop, intersecting the free surface at right angles. The meridional distance between the outcropping isopycnals is relatively large, creating a broad surface “footprint” of size $\delta\theta \partial N/\partial\theta$. The mixed layer portion joins the interior portion of the

layer at a “handover section”, where density tendency and non-conservative force are negligible. Here the isopycnals are nearly horizontal and much closer together, separated by $\delta\theta \partial z/\partial\theta$. As the surface outcrop moves, the interior portion gets stretched or squashed: the cross-hatched piece of length $\delta t \partial N/\partial t$ is removed or formed in time δt .

A control volume approach elucidates the budget of PV flux. The control volume chosen here is enclosed by the two isopycnals shown in Fig. 12, the free surface and the handover section, and two vertical planes normal to the outcrop, δs apart, being the front and back “faces” of the control volume. PV fluxes in and out of the control volume are: $\mathbf{J} \cdot \hat{\mathbf{k}}$ across the free surface (Eq. 3.6), $\mathbf{J} \cdot \hat{\mathbf{n}} = v_n (f + \zeta) \partial\theta/\partial z$ across the handover section, $\mathbf{J} \cdot \hat{\mathbf{s}} = v_s q$ across the faces, with $\hat{\mathbf{s}}$ and $\hat{\mathbf{n}}$ unit vectors and the v_s and v_n velocity components along $\hat{\mathbf{s}}$ and $\hat{\mathbf{n}}$. By virtue of the impermeability theorem (Haynes and McIntyre, 1990), there is no flux across the isopycnal surfaces. According to Eq. 3.2, the integral of $\partial q/\partial t$ over the control volume equals the surface integral of the inward PV fluxes.

The definition of PV in Eq. 3.2 show that q vanishes at the surface and over the mixed layer, and so does its time derivative. This holds over most of the control volume, except in a thin portion at the base where the isopycnal $\theta + \delta\theta$ turns quasi-horizontal, setting up the stratification. However, the contribution of that portion to the integral balance of PV is a second order quantity. The primary contribution to q is from the volume change due to stretching or squashing of the isopycnic layer interior, implying PV gain or loss that must be added to the surface integral of the inward fluxes. A similar volume change contribution would have to be taken into account if the mixed layer base moved rapidly upward or downward.

PV transports (flux times surface area) out of the control volume are therefore:

$$\begin{aligned} \text{surface} &: -\mathbf{J} \cdot \hat{\mathbf{k}} \frac{\partial N}{\partial \theta} \delta\theta \delta s \\ \text{handover section} &: -\mathbf{J} \cdot \hat{\mathbf{n}} \frac{\partial z}{\partial \theta} \delta\theta \delta s \end{aligned}$$

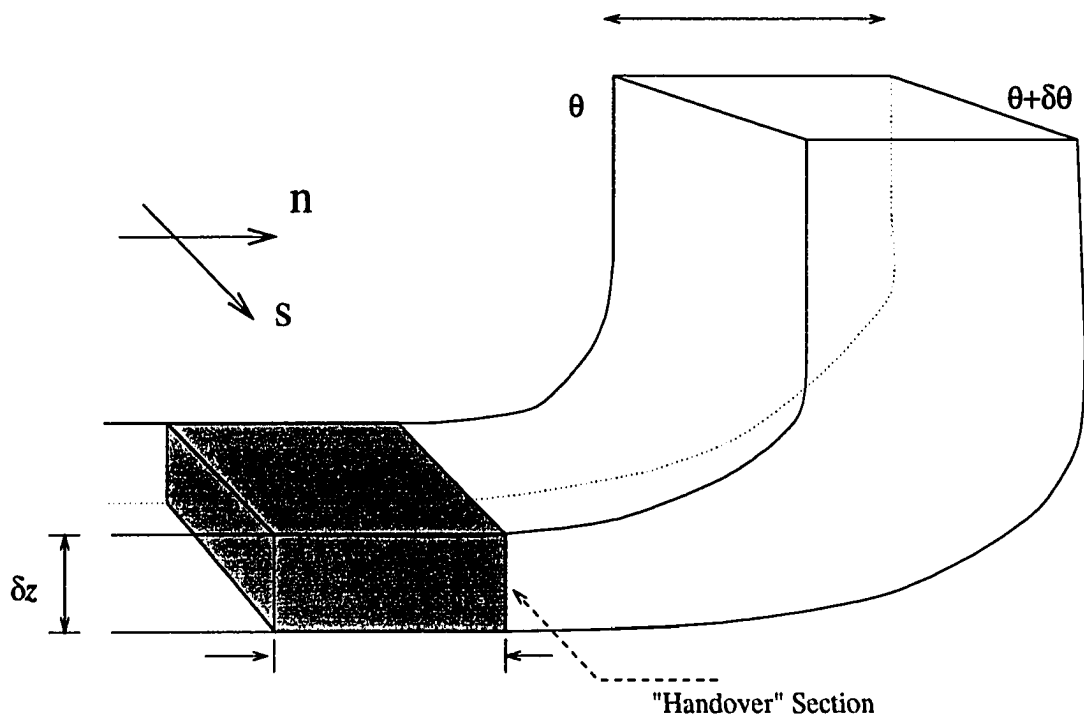


Figure 12: Sketch shows an isopycnal layer outcropping at the sea surface with the "handover section" a short distance from the outcrop position. This is where we advocate the PV flux to be injected into the ocean interior.

$$\begin{aligned}
\text{faces} &: \frac{\partial}{\partial s} \int \int \mathbf{J} \cdot \hat{s} \, dn \, dz \, \delta s \\
\text{volume change} &: (f + \zeta) \frac{\partial N}{\partial t} \delta \theta \delta s
\end{aligned}$$

The sum of these terms must add up to zero. As the handover section is assumed to be at a short distance from the outcrop position, the absolute vorticity at the handover section is, to first order, the same as at mixed layer base, *i.e.*, as at the surface. With q vanishing over the mixed layer, the divergence of PV transport across the faces can be approximated as:

$$\delta \theta \frac{\partial}{\partial s} \int (f + \zeta) v_s \, dn$$

Diagnostic estimates put this term to the order of 10^{-8} which is two orders of magnitude smaller than the other ones. Therefore, neglecting the divergence of PV transport across the faces and substituting the previous expressions for the fluxes, the terms containing $\partial N / \partial t$ cancel out. The remaining balance of PV transport, expressed in (s, n) coordinates, is:

$$\frac{\partial \Pi}{\partial s} + \frac{\partial v_s}{\partial t} = (f + \zeta) v_n \quad (3.9)$$

where v_n is the velocity component normal to the surface outcrop at the handover section. The right hand side is the PV transport per unit along-isopycnal length out of the interior of the isopycnic layer. The velocity v_n can be viewed as a quasi-horizontal version of the subduction velocity. The above relation is similar to Marshall and Nurser's (1992) relationship between subduction velocity and "net" heat gain (Eq. 2.3). On account of their steady state assumption, the local acceleration does not appear in Marshall and Nurser's formula which might play an important role in unstable meanders of a frontal current.

In the steady state, the above expression 3.9 reduces to:

$$v_n = \frac{\partial \Pi / \partial s}{(f + \zeta)} \quad (3.10)$$

The equivalent form of the Eq. 3.10, in terms of the vertical subduction velocity (S) is:

$$S = \frac{\partial \Pi / \partial s}{(f + \zeta) \frac{\partial \theta}{\partial N} \frac{\partial z}{\partial \theta}} = \frac{(f + \zeta) v_g \frac{\partial \theta}{\partial N}}{(f + \zeta) \frac{\partial z}{\partial \theta}} = \frac{(f + \zeta) v_g \cdot \nabla \theta}{\rho q} \quad (3.11)$$

which is exactly similar to the MN92 relationship for the subduction velocity, where q is the PV as defined in Eq. 2.3.

In their study, the “net” heat gain is required to support geostrophic flow across stationary isopycnal outcrops. In Eq. 3.9 however, the contribution to PV transport from the density tendency term or the density gradient is absent, making the introduction of net heat gain artificial. The pressure gradient term in Eq. 3.9, accounts for the geostrophic heating described in MN92 study. The important new point about Eq. 3.9, is that such a relationship applies regardless of the seasonal migration of isopycnals. PV input to an isopycnal layer due to surface heat fluxes reflect in the mean pressure gradient, and is not tied to a specific rate of heating required to hold an isopycnal in a fixed position: isopycnals move if the heat flux so decreases.

3.4 Geostrophic turbulence

Consider now the case of outcropping isopycnal layers under the influence of geostrophic turbulence. Statistically steady state will be assumed, except for the slow seasonal change mentioned before. The effects of any geostrophic turbulence are averaged out over a period much shorter than the slow seasonal time scale, but longer than the lifetime of any eddies. Also, velocity change on the seasonal time scale is neglected. Averaging yields the mean PV transport into an isopycnal layer: (again per unit along-outcrop length)

$$\frac{\partial \bar{\Pi}}{\partial s} = (f + \bar{\zeta}) \bar{v}_n + \overline{v'_n \zeta'} \quad (3.12)$$

The new term is the Reynolds flux of vorticity resulting from geostrophic turbulence. While the total pressure gradient along the isopycnal outcrop is PV source term, advection by mean flow (subduction, converted to flow along isopycnal surfaces) and

Reynolds flux of vorticity are the means of conveying PV into the interior of isopycnic layers.

The result here is analogous to the boundary condition derived by Csanady and Pelegri (1995) at the footprint of an isopycnic layer over a continental slope. In that study, shear stress force in the bottom boundary layer is the source of PV. PV transport by geostrophic turbulence balances the alongstream pressure gradient just outside the boundary layer where advective cross-stream transport is prevented by the solid boundary. Offshore from this handover section, cross-stream transport of PV diminishes, its divergence balancing streamwise PV change in the boundary current. A similar situation may prevail in a surface current flowing along isopycnal outcrops, such as the Azores current.

3.5 Application to the eastern North Atlantic

The above described theory is applied to the eastern North Atlantic region where the isopycnals of the upper thermocline outcrop. This coincides with the Azores frontal area where the frontal dynamics favour the ventilation of the interior layers. As described in the background chapter, the eastward flowing Azores Current moves with surface velocities of the order of 20 cm s^{-1} and transports 10 Sv. The observations show a strong meandering pattern in the eastward jet while the westward return flow is associated with eddies moving towards the western boundary. Also the current region observed in this region is characterized by geostrophic turbulence of considerable magnitude (Käse *et al.*, 1985).

The PV influx into the interior is dependent on the total pressure gradient along isopycnal outcrop (Eq. 3.12). A rough estimate of the mean pressure gradient can be obtained by calculating the variation of mixed layer depth along the outcropped isopycnal. The winter mixed layer depth varies about 100 m over a distance of 1000 km in the latitudinal direction along the isopycnal surface outcrop (Marshall *et al.*,

1993; McDowell *et al.*, 1982), setting up a mean pressure gradient of the order of 10^{-6} m s⁻².

Also the mean cross-isopycnal velocity $\overline{v_n}$ (in Eq. 3.6) observed in this area is negative (Armi and Stommel, 1983; Saunders, 1982; Pollard and Pu, 1985). Jenkins (1987) estimated the meridional mean tracer transport to be 1×10^{-3} m s⁻¹. The Ekman pumping estimates from Leetmaa and Bunker (1978) data give isopycnal velocities of the order of 1×10^{-3} m s⁻¹.

The influence of the PV source term in generating the interior circulation is tested using a constant layer depth model. The model description and the numerical techniques used are discussed in the following chapter.

4 Constant layer depth model

Equation 3.6 derived in the previous chapter, based on the principle of conservation of PV, quantifies mean PV transport into an outcropped isopycnal at the handover section. According to the impermeability theorem (HM), the distribution of PV in the interior of an isopycnic layer is subject to a conservation law accounting for its advection and diffusion. The pattern of circulation to which the PV distribution gives rise depends on the isopycnic layer depth, the distribution of which cannot be determined for a single layer in isolation. The time averaged mean distribution of potential density surfaces (Levitus, 1982) suggests, however, that the mean isopycnic layer thickness is almost uniform over the subtropical region, at least within a short distance from their outcrop position. Therefore, a simple constant layer-depth model may not give an entirely unrealistic qualitative idea of such a boundary driven circulation. PV changes in such a model appear in relative vorticity: in reality some of that change may occur as an adjustment of the layer depth. This would reduce the intensity, but increase the width of any jet-like currents. The constant layer depth model is akin to barotropic models of wind-driven circulation in a deep surface layer such as Munk (1950) or Cessi *et al.* (1987), and shares their shortcomings, but also their main advantage: simplicity.

4.1 Model physics

To analyse the consequences of surface PV input discussed in the previous chapter, a barotropic, constant layer depth model is used with rectangular basin geometry, of dimensions 2000 km by 1000 km. A β -plane is assumed, with rigid lid and floor,

impermeable to PV.

The northern boundary of the model represents the outcrop position (or rather, the handover section in Fig. 3.1), through which the PV flux enters the domain. The model is hence forced on the northern boundary by prescribing quantitatively the net PV flux at the handover section. This method of forcing is so different from Ekman pumping that its results cannot be foreseen from classical circulation theories. The PV flux condition applied at the northern boundary, derived in chapter 3 (Eq. 3.5), is:

$$\frac{\overline{\partial\Pi}}{\partial s} = (f + \bar{\zeta})\bar{v}_n + \overline{v'_n\zeta'}$$

PV being a conserved quantity in the interior, the Reynolds flux term ($\overline{v'_n\zeta'}$) can be parameterized in terms of a mean PV gradient flux, analogous to the G. I. Taylor's mixing length argument for the turbulent boundary layer (1915, cited in Goldstein, 1938). If local fluctuations of PV on an isopycnal surface occur on account of a mean PV gradient ($\overline{\partial\zeta/\partial n}$), then the Reynolds flux term is of magnitude $l' \partial\zeta/\partial n$, where l' is the random displacement of the parcel in the cross isopycnal direction. Therefore, the Reynolds flux of vorticity is:

$$\overline{v'_n\zeta'} = -A \frac{\partial\zeta}{\partial n} \quad (4.1)$$

where $A = \overline{v'_n l'}$ is an eddy mixing coefficient. In case of unrestricted motion on the isopycnal surfaces, the mixing coefficient (A) behaves more as in a free turbulent flow than in a wall layer (Csanady and Pelegri, 1995). Hence, the horizontal variation of A is neglected at the handover section and is assumed constant in the present study.

Substituting for the Reynolds flux term, the northern boundary condition then reduces to:

$$-A \frac{\partial\zeta}{\partial n} = \frac{\overline{\partial\Pi}}{\partial s} - (f + \bar{\zeta})\bar{v}_n \quad (4.2)$$

The above expression shows that the vorticity diffusion at the boundary is the net result of the along-isopycnal pressure gradient at the outcrop and the advective

flux carried down into the interior by the subducting water mass. This latter term is referred to as subduction in the present study. In the absence of subduction, the pressure gradient at the surface outcrop alone determines the PV flux.

To qualitatively represent the process of subduction occurring in the subtropical eastern North Atlantic (Sarmiento *et al.*, 1982; Pollard and Pu, 1985; Jenkins, 1987), the mass inflow is assumed and prescribed over 1200 km on the eastern portion of the northern boundary, for the model runs that account for subduction. Most of the subducted water mass upwells out of the isopycnic layer near the north-western corner. Hence, for convenience, the mass outflow is prescribed over the rest of the northern boundary so as to balance the assumed mass influx. For simplicity, the following form of the meridional velocity distribution is assumed on the northern boundary:

$$v_n(x) = v_o \sin[\pi x/a] \text{ for } x \leq a \quad (4.3)$$

$$v_n(x) = -v_i \sin[\pi(L-x)/(L-a)] \text{ for } a < x \leq L$$

where, a is the extent over which the outflow occurs (800 km) and L is the basin dimension in east-west direction. v_i and v_o are the amplitudes of the inflow and outflow sinusoidal profiles. v_i is the maximum prescribed subduction velocity and v_o is chosen so as to satisfy the mass balance.

In the rectangular domain the s and n directions are replaced by the x and y directions, the quasi-isopycnic velocities v_s and v_n by u and v velocities.

4.2 Governing equations

The isopycnic PV transport and diffusion equation is:

$$\frac{\partial q}{\partial t} + u \frac{\partial q}{\partial x} + v \frac{\partial q}{\partial y} = A \left(\frac{\partial^2 q}{\partial x^2} + \frac{\partial^2 q}{\partial y^2} \right) \quad (4.4)$$

where q is PV defined as $(f + \zeta)/h$, A is the diffusion coefficient, f is the planetary vorticity, ζ is the vertical component of the relative vorticity and $h = \partial z / \partial \theta$ is

layer depth or the Jacobian of transformation from vertical to isopycnic coordinates.

Relative vorticity

$$\zeta = \frac{\partial v}{\partial x} - \frac{\partial u}{\partial y} \quad (4.5)$$

is considered to be of the same order as the planetary vorticity and u and v are the along isopycnal velocities. The viscous diffusion term ($A\nabla^2 q$) accounts for the eddy flux of PV. Under the constant layer depth assumption and the β -plane approximation, $f = f_o + \beta y$, Eq. 4.4 reduces to:

$$\frac{\partial \zeta}{\partial t} + u \frac{\partial \zeta}{\partial x} + v \frac{\partial \zeta}{\partial y} + \beta v = A \left(\frac{\partial^2 \zeta}{\partial x^2} + \frac{\partial^2 \zeta}{\partial y^2} \right) \quad (4.6)$$

Also the equation of continuity with no diapycnal velocity is:

$$\nabla \cdot \mathbf{u} = 0 \quad (4.7)$$

The flow field can thus be represented by a streamfunction ψ , such that $v = \partial\psi/\partial x$, $u = -\partial\psi/\partial y$. Substituting for v and u in Eq. 4.6, gives

$$\frac{\partial \zeta}{\partial t} + \frac{\partial \psi}{\partial x} \frac{\partial \zeta}{\partial y} - \frac{\partial \psi}{\partial y} \frac{\partial \zeta}{\partial x} + \beta \frac{\partial \psi}{\partial x} = A \left(\frac{\partial^2 \zeta}{\partial x^2} + \frac{\partial^2 \zeta}{\partial y^2} \right) \quad (4.8)$$

When u and v are substituted in the definition of ζ , an elliptic Poisson's equation results for the streamfunction:

$$\nabla^2 \psi = \zeta \quad (4.9)$$

Solving for ψ and ζ from the last two equations, with appropriate boundary conditions, yields the flow and vorticity fields in a constant depth isopycnic layer.

Boundary conditions are: $\psi = 0$ along the eastern, southern and western boundaries, on the northern boundary either $\psi = 0$ or the integrated values from the above velocity distribution (Eq. 4.3). Vorticity flux is prescribed along the northern boundary (Eq. 4.2), free slip on the southern boundary, no slip on the western boundary, free slip or no slip (in different experiments) on the eastern boundary.

4.3 Numerical methods

The vorticity transport equation (Eq. 4.8) is integrated using centered finite differences for the spatial derivatives and leapfrog differences for time derivatives. This method is second order accurate in space and time and is a one-step, explicit, three time level scheme. It requires the values for ψ and ζ at (n) and (n-1) time levels to calculate their new values at the (n+1) time level. For numerical stability, the advective terms are evaluated at the middle (n) level and friction terms at the (n-1) time level (Roache, 1976). This means that friction lags by a time step. The stencil for the explicit form of Eq. 4.8 is:

$$\frac{\zeta_{i,j}^{n+1} - \zeta_{i,j}^{n-1}}{2\Delta t} = -J(\psi, \zeta)_{i,j}^n - \beta \frac{\psi_{i+1}^n - \psi_{i-1}^n}{2\Delta x} + A \frac{\zeta_{i+1,j}^{n-1} + \zeta_{i-1,j}^{n-1} + \zeta_{i,j+1}^{n-1} + \zeta_{i,j-1}^{n-1} - 4\zeta_{i,j}^{n-1}}{\Delta x^2} \quad (4.10)$$

where $J(\psi, \zeta)$ is the Jacobian containing non-linear terms, Δx is the grid spacing in x and y directions. Subscripts (i, j) refers to indices on numerical grid in x and y directions, whereas superscripts (n) refer to time levels. $J(\psi, \zeta)$ is defined as:

$$J(\psi, \zeta) = \frac{\partial \psi}{\partial x} \frac{\partial \zeta}{\partial y} - \frac{\partial \psi}{\partial y} \frac{\partial \zeta}{\partial x} \quad (4.11)$$

and is evaluated following Arakawa (1966), according to the formula:

$$J(p, q) = \frac{1}{3} [(p_x q_y - p_y q_x) + (\frac{\partial}{\partial y}(q p_x) - \frac{\partial}{\partial x}(q p_y)) + (\frac{\partial}{\partial x}(p q_y) - \frac{\partial}{\partial y}(p q_x))]$$

where the subscripts here denote the gradients. The above formulation of the non-linear terms eliminates non-linear instability as well as spurious transfer of energy to short waves (Kowalik and Murthy, 1993). Furthermore, it conserves both average enstrophy (half the vorticity squared) and mean kinetic energy (Arakawa, 1966).

Solution of Poisson's equation poses a boundary value problem which in the present study is solved using Dirichlet boundary conditions (ψ prescribed). The discretized form of Poisson's equation, using a second-order difference is:

$$\frac{\psi_{i+1,j} + \psi_{i-1,j} - 2\psi_{i,j}}{\Delta x^2} + \frac{\psi_{i,j+1} + \psi_{i,j-1} - 2\psi_{i,j}}{\Delta x^2} = \zeta_{i,j} \quad (4.12)$$

For a rectangular domain (the case here), the above discretized form reduces to a system of simultaneous linear algebraic equations.

Direct elliptic solver subroutines from the FISHPAK package (available in the public domain from NCAR) are used to solve Poisson's equation. The subroutines take a five point finite difference approximation to Poisson's equation in Cartesian coordinates, and incorporate the boundary data, thus forming a linear system of equations. This system of equations is then solved by a cyclic reduction algorithm.

4.3.1 Numerical boundary conditions

On the northern boundary, the PV flux condition (Eq. 4.2) is specified as:

$$A \frac{\zeta_{i,j+1} - \zeta_{i,j-1}}{2\Delta y} = \frac{\overline{\partial \Pi}}{\partial s} + \left(f + \frac{\zeta_{i,j+1} + \zeta_{i,j-1}}{2} \right) v(x) \quad (4.13)$$

The above form is reduced to an explicit expression in $\zeta_{i,j+1}$, which is outside the model domain. $\zeta_{i,j+1}$ is evaluated at each timestep using the new $\zeta_{i,j-1}$ values, so as maintain the diffusive PV flux constant across the boundary.

Along the western boundary a no-slip condition is imposed, which approximately represents the effect of contact with the continental slope (discussed in detail by Csanady and Pelegri, 1995). Along the eastern boundary both the free-slip and no-slip conditions are examined, the former representing an upwelled isopycnic layer. Along the southern boundary the free slip condition is always used.

The no-slip condition is that the tangential velocity is equal to zero on the boundary. Vorticity ζ is then produced at no-slip boundaries. From a Taylor series, the first order approximation to such a wall generated vorticity (ζ_w) is:

$$\zeta_w = \frac{2(\psi_{w+1} - \psi_w)}{\Delta x^2} \quad (4.14)$$

where $(w+1)$ is the adjacent grid point to the wall in the interior. The wall vorticity is an extremely important quantity, because the vorticity transport equation (Eq. 4.8) merely determines how ζ is advected and diffused, conserving total ζ at the interior

points. It is the diffusion and subsequent advection of this wall-produced vorticity which actually drives much of the circulation (Roache, 1976) in addition to, of course, the vorticity input at the northern boundary. In case of a free slip wall, there is no wall stress which would take momentum out of the flow. The velocity gradient normal to the wall, $\partial v/\partial n$ and the wall vorticity in this case are zero (Roache, 1976).

For solving Poisson's equation, ψ values are specified on all boundaries. No normal flow conditions on the eastern, southern, western boundaries imply a constant streamfunction on the boundary. On the northern boundary the streamfunction is either zero (no normal flow) or calculated from the velocity distribution specified in section 4.1 for cases where subduction is accounted. Integrating the velocity profile along the northern boundary yields the following distribution for ψ :

$$\psi(x) = c_1 - \frac{v_o a}{\pi} \cos\left(\frac{\pi x}{a}\right) \quad \text{for } x \leq a \quad (4.15)$$

$$\psi(x) = c_2 + \frac{v_i(L-a)}{\pi} \cos\left(\frac{\pi(L-x)}{(L-a)}\right) \quad \text{for } a < x \leq L$$

where $c_1 = v_o a/\pi$, $c_2 = 2 v_o a/\pi + v_i(L-a)/\pi$.

The flux boundary condition (Eq. 4.13) was implemented using pseudo-boundary points or ghost points (Roache, 1976). The ψ and ζ values at these ghost points do not play a role in calculating the interior quantities, and are used only in the evaluation of ψ and ζ on the boundary. These fictitious points allow the same computing algorithm to be used for the points on the boundary as for the points in the interior. At the ghost points, the values of ψ and ζ are calculated so as to satisfy the above described boundary conditions. Thus, for a free slip boundary condition the vorticity at the ghost point is equal to that of its mirror reflection counterpart inside the boundary. For a no-slip condition, the tangential velocity outside the boundary is set equal, but opposite in sign, to that inside the boundary. In this manner, the values of ψ and ζ are extrapolated from known interior values at every time step, to be used at the following time step.

4.3.2 Choice of parameters

The values used for A , v_i , $\overline{\partial\Pi/\partial x}$ are taken from the observational estimates in the subtropical North Atlantic.

Observational studies (Armi and Stommel, 1983; Jenkins, 1987) estimated isopycnic diffusivity values, in the interior regions of the eastern subtropical North Atlantic (in the beta triangle area), around $500 \text{ m}^2 \text{ s}^{-1}$ on the $26.5 \sigma_\theta$ surface. At higher latitudes, where the upper thermocline isopycnals outcrop, the values should be higher still. To also facilitate the use of a longer time step (to avoid numerical instability), we choose $1000 \text{ m}^2 \text{ s}^{-1}$ for A , a value that has been used in other model studies (*e.g.*, Musgrave, 1990).

Geostrophic velocities observed in the subtropical North Atlantic (around 40° N) show that the total pressure generally rises toward the east. Such a positive pressure gradient forces the interior with negative PV flux. As explained in section 3.5, diagnostically estimated value of 10^{-6} m s^{-2} for the pressure gradient is chosen for most of the model runs.

The choice of subduction velocity is based on some observational estimates in the eastern North Atlantic, where the ventilation of the interior thermocline occurs. Based on the along isopycnal velocity estimates of Saunders (1982), Pollard and Pu (1985) and Jenkins (1987) in this region, the inflow velocity v_i in the present study is chosen to be $5 \times 10^{-3} \text{ m s}^{-1}$. Käse *et al.* (1989) also used similar values for modeling the recirculation in the eastern North Atlantic.

Because this is a boundary forced problem, it is necessary to resolve the boundary layer. The choice of grid spacing (Δx), in general, is governed by the inertial scale $(u/\beta)^{1/2}$ or by the Munk boundary layer scale $(A/\beta)^{1/3}$, both around or greater than 40 km for realistic parameter values. Eight km grid spacing is chosen in both the x and y directions so as to cover the boundary layers with five grid points.

The choice of the time step is governed by the numerical stability of the hyperbolic

vorticity equation. The time step permissible in such a hyperbolic equation is limited by the requirement that no signal may travel faster than one grid interval per time step. In general, it is either the advection limit, $c \equiv u\Delta t/\Delta x \leq 0.5$, or the diffusion limit, $d \equiv A\Delta t/\Delta x^2 \leq 0.25$ (in a two-dimensional case; Roache, 1976) that limits the timestep Δt . For an one-dimensional problem, when both the nonlinear and diffusive terms are retained, $c^2 + 4d \leq 1$ controls the time step to a smaller value than either the c or d limits (O'Brien, 1985). For the above mentioned values of A , Δx a time step of forty minutes was chosen in most model runs to ensure numerical stability.

The solve Eqs. 4.8 and 4.9: a forward time-centered space scheme was used to calculate the vorticity at the second time step as the leapfrog scheme require values for ψ and ζ at two time levels. With ψ and ζ known at two time steps, the vorticity equation and Poisson's equation are solved by the numerical techniques explained above. The iterative process is continued until the mean of the basin averaged kinetic energy is almost constant.

The results obtained from various simulations are presented in the next chapter.

5 Results

The numerical simulations are carried out to test the physical ideas developed in Chapter 3. Different model runs are made to test the influence of different types of forcing and lateral boundary conditions on the interior flow. In all the model runs, PV gradient flux defined across the northern boundary (Eq. 4.13) is the forcing term. In Case 1, the mean pressure gradient alone is the PV source term used for the forcing. Under similar conditions, the influence of the meridional basin dimension and the strength of the forcing in determining the meridional extent of the gyre is tested in Cases 2 and 3. In these cases a free-slip condition is used on the eastern boundary, physically representing the upwelled boundary layer. In Case 4 and the following ones, no-slip condition is prescribed on the eastern boundary, treating it as the solid wall. In Case 5, PV input due to subduction alone is considered. The influence of both the physical processes in setting the mean circulation in an isopycnic layer is tested in Case 6. The effect of forcing the model with negative PV is tested in Case 7. The influence of time-dependent forcing on the interior circulation is tested in Case 8. The effect of grid size on the evolution of flow for Cases 4 and 6 is explained under Case 9.

All the simulations were started from rest. The model was run until the basin averaged kinetic energy and enstrophy reached a quasi-steady state. The evolution of vorticity and streamfunction in each case was calculated and supplemented occasionally by an analysis of the different terms in the vorticity equation. Table 1 lists the parameters used in different Cases, discussed here in order.

	Domain ($km \times km$)	A_h (m^2s)	Eastern B. C.	$\partial\Pi/\partial x$ $10^{-7}(ms^{-2})$	Subduction	Grid Size km
Case 1	2000×1000	1000	Free Slip	10	No	8
Case 2	2000×2000	1000	Free Slip	10	No	8
Case 3	2000×1000	1000	Free Slip	3	No	8
				5	No	8
Case 4	2000×1000	1000	No-Slip	10	No	8
Case 5	2000×1000	1000	No-Slip	0	Yes	8
Case 6	2000×1000	1000	No-Slip	10	Yes	8
Case 7	2000×1000	1000	No-Slip	-10	No	8
Case 8	2000×1000	1000	No-Slip	$10 \sin(\omega t)$	No	8
Case 9	2000×1000	1000	No-Slip	10	No	4
				10	yes	4

$$\omega = 2\pi/\text{year}$$

Table 1: List of model runs

Case 1: PV input without subduction, with free slip eastern boundary.

The model is forced with a constant PV flux at the northern boundary. Free slip is prescribed on the eastern and southern boundaries and no slip on the western boundary. As there is no subduction, the $\psi = 0$ on the northern boundary. The model is run until an asymptotic state is reached. The basin averaged enstrophy and kinetic energy (KE) show (Fig. 13) that the model spins up over a period of three years before reaching a steady state. The vorticity and streamfunction fields in the final state are illustrated in Fig. 14. The flow pattern is entirely steady with an anticyclonic gyre filling almost the whole basin. The gyre resembles the Fofonoff gyre (Fofonoff, 1954), which is a well known analytical solution for strongly non-linear flows.

The negative vorticity input forms a strong eastward jet along the northern boundary as a part of the anticyclonic circulation. The maximum velocities on the northern boundary layer are of the order of 2.0 m s^{-1} (*i.e.*, rather high). The injected negative vorticity is carried by the eastward jet to feed an eastern boundary layer. The value of the vorticity increases all along the northern boundary, then decreases along the eastern wall due to the planetary vorticity advection effect. In the interior, relative vorticity contour lines follow latitude lines (constant f/h), especially in the region where PV is homogeneous, but they cut across latitudes and vary rapidly across eastern and western boundary layers. The vorticity contours become detached from the eastern boundary and follow a particular latitude in the interior. The western boundary is the only source of positive vorticity in this experiment to balance the negative vorticity input from the forcing. The PV distribution shows a homogenized region in the interior with strong PV gradients at the boundaries (Fig. 15).

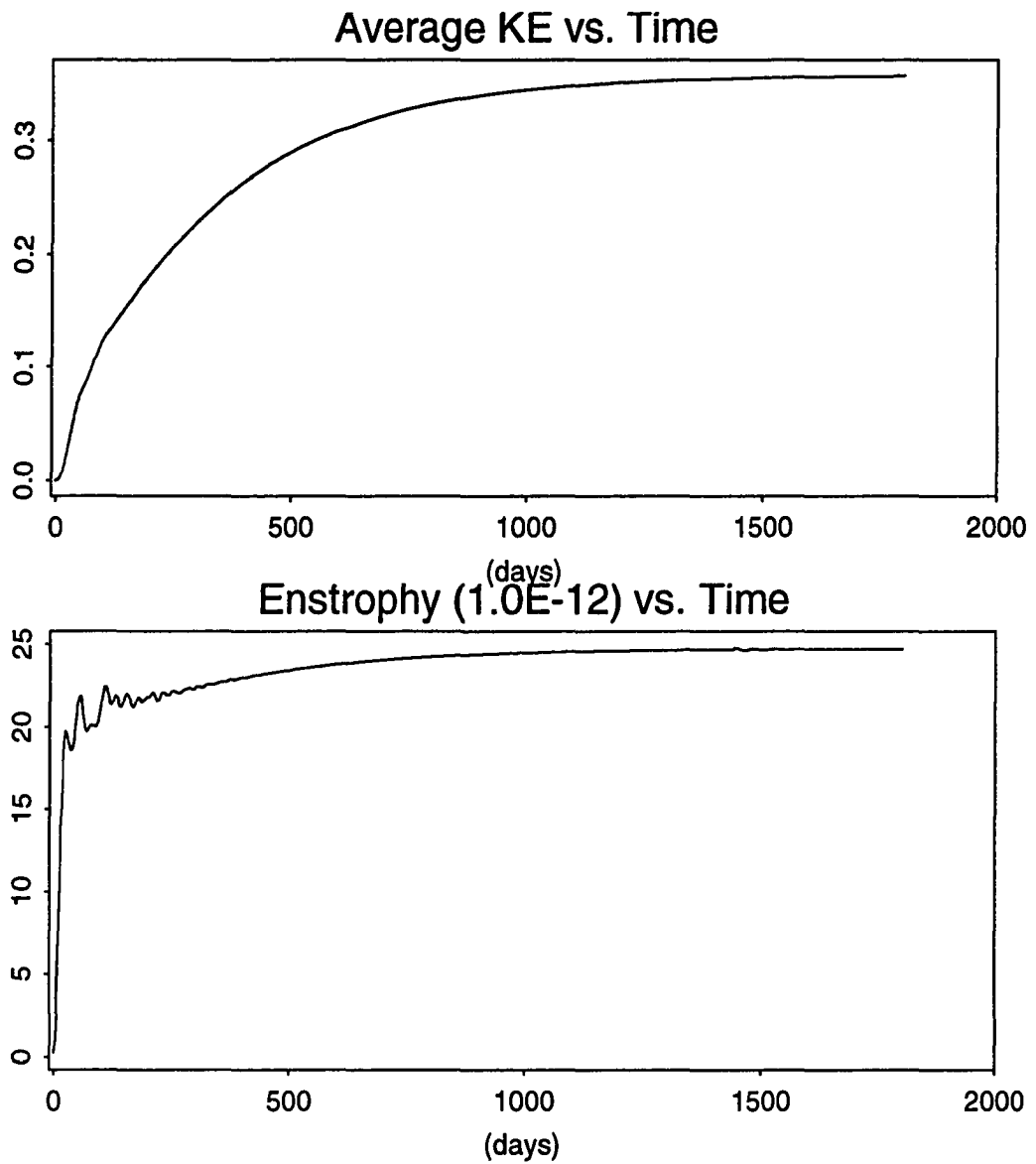


Figure 13: The basin averaged kinetic energy and the enstrophy against time for Case 1.

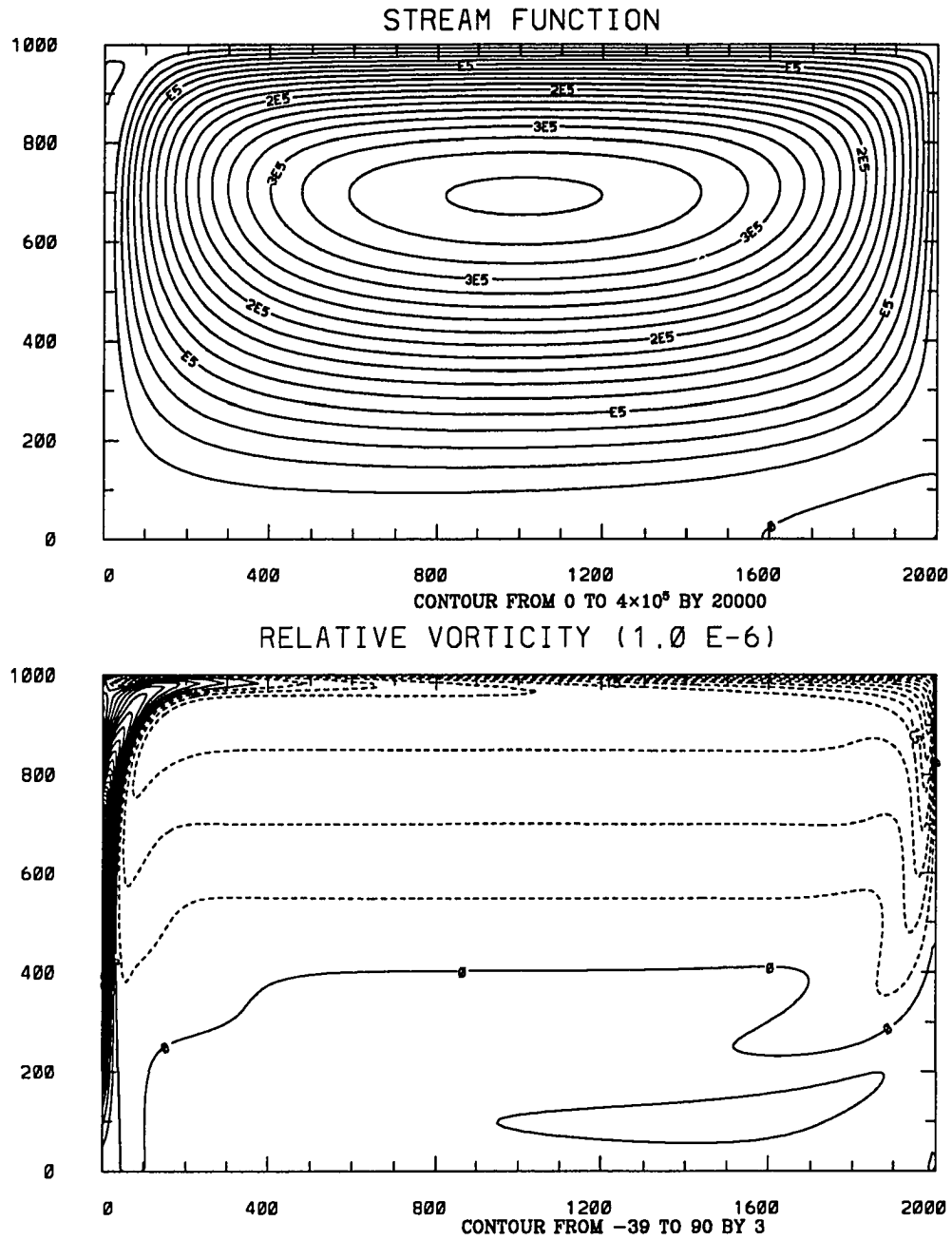


Figure 14: The distribution of streamfunction (ψ) and relative vorticity (ζ) after a period of four years for Case 1. The model is forced by a vorticity gradient of $10 \times 10^{-10} \text{ m}^{-1} \text{ s}^{-1}$ on the northern wall with a no-slip western wall and a free-slip eastern boundary. Dashed contours denote negative values.

POTENTIAL VORTICITY ($1.0E-06$)

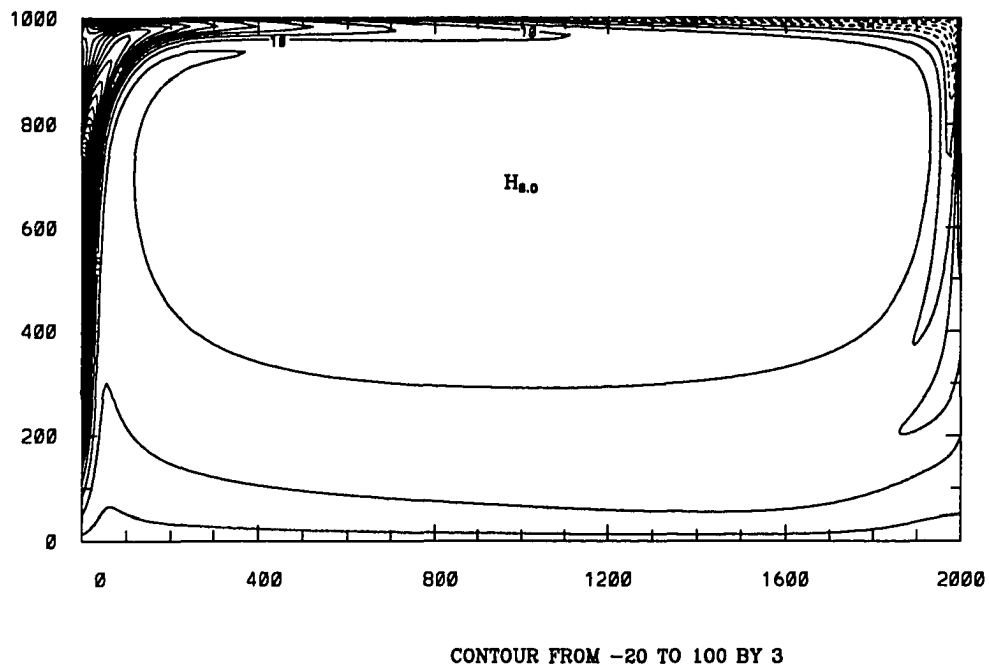


Figure 15: The distribution of potential vorticity (PV) for Case 1.

Case 2: Influence of meridional basin dimension on meridional extent of the gyre.

What determines the extent of the anticyclonic gyre observed in Case 1 is experimented with here. The variables likely to change the extent of the gyre (the meridional dimension of the model basin, Y_g) are the strength of the forcing (*i.e.*, the pressure gradient), the lateral diffusivity and the planetary vorticity gradient β . The simulation keeps conditions the same as in Case 1 except for doubling the north-south dimension of the basin. The anticyclonic gyre observed in the final state (Fig. 16) extends roughly to the same meridional distance as in Case 1 (950 km, as defined by the zero streamfunction contour). The southern portion of the domain remains quiescent as the vorticity input is insufficient to drive the circulation against the planetary vorticity gradient (Fig. 17). Decreasing the horizontal diffusivity did not alter the flow pattern, but took a longer period to establish steady circulation.

Case 3: Influence of strength of forcing on meridional extent of the gyre.

In this case, the strength of the forcing, *i.e.*, the PV gradient flux due to pressure gradient, is reduced to $5 \times 10^{-10} \text{ m}^{-1} \text{ s}^{-1}$, under otherwise the same conditions as in Case 1. The results show that the extent of anticyclonic gyre is reduced from 950 km to approximately 780 km (Fig. 18a). When the forcing is $3 \times 10^{-10} \text{ m}^{-1} \text{ s}^{-1}$, the gyre is reduced to 670 km (Fig. 18b). Hence, the meridional scale of the gyre shows a strong dependence on the intensity of forcing.

Case 4: PV influx without subduction, for a no-slip eastern boundary.

Under otherwise the same conditions as in Case 1, the influence of the eastern boundary condition on the evolving circulation is tested in this case. Treating the

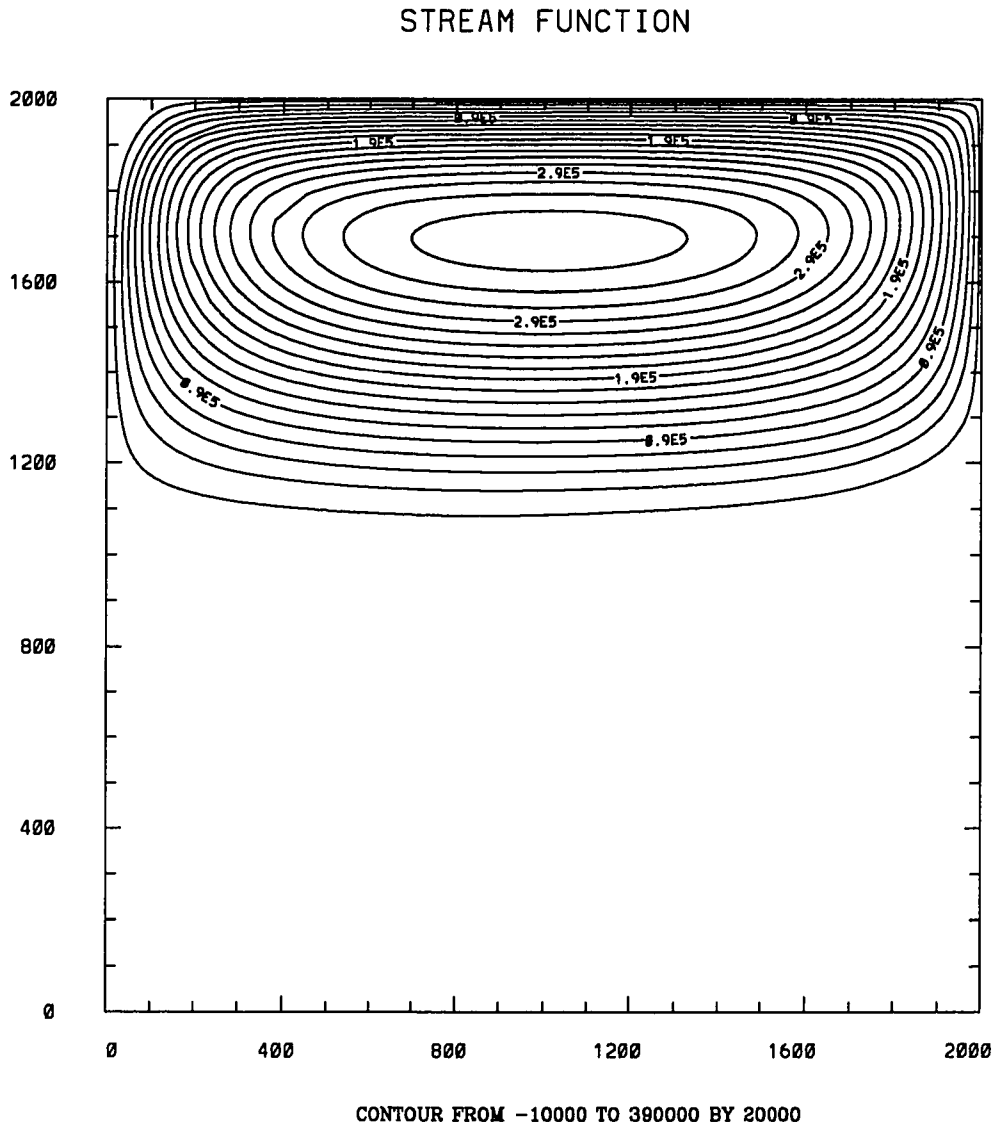


Figure 16: The distribution of streamfunction with the model domain doubled meridionally ($2000 \text{ km} \times 2000 \text{ km}$) for Case 2. The forcing and the boundary conditions used are same as in Case 1.

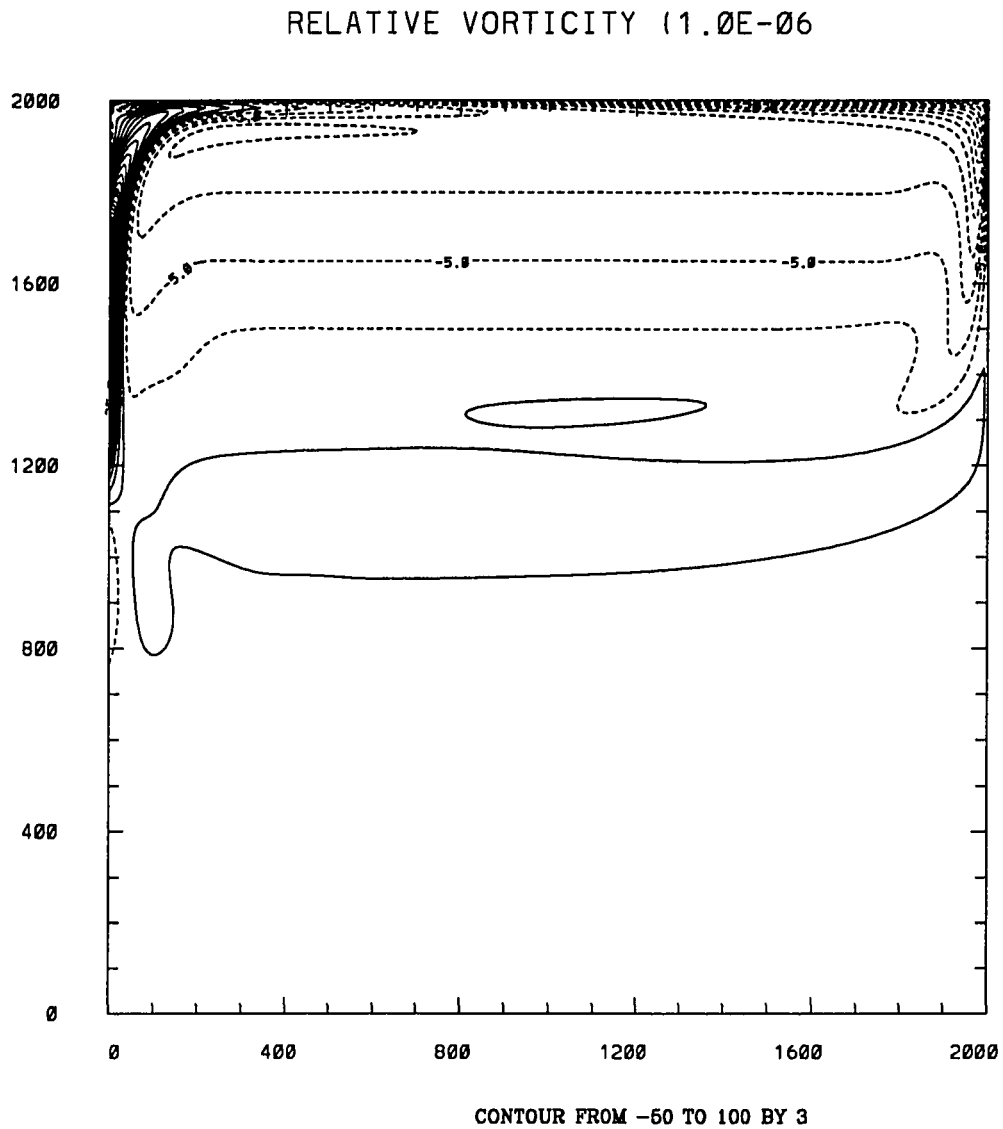


Figure 17: The relative vorticity distribution corresponding to streamfunction distribution (Fig. 16) for Case 2.

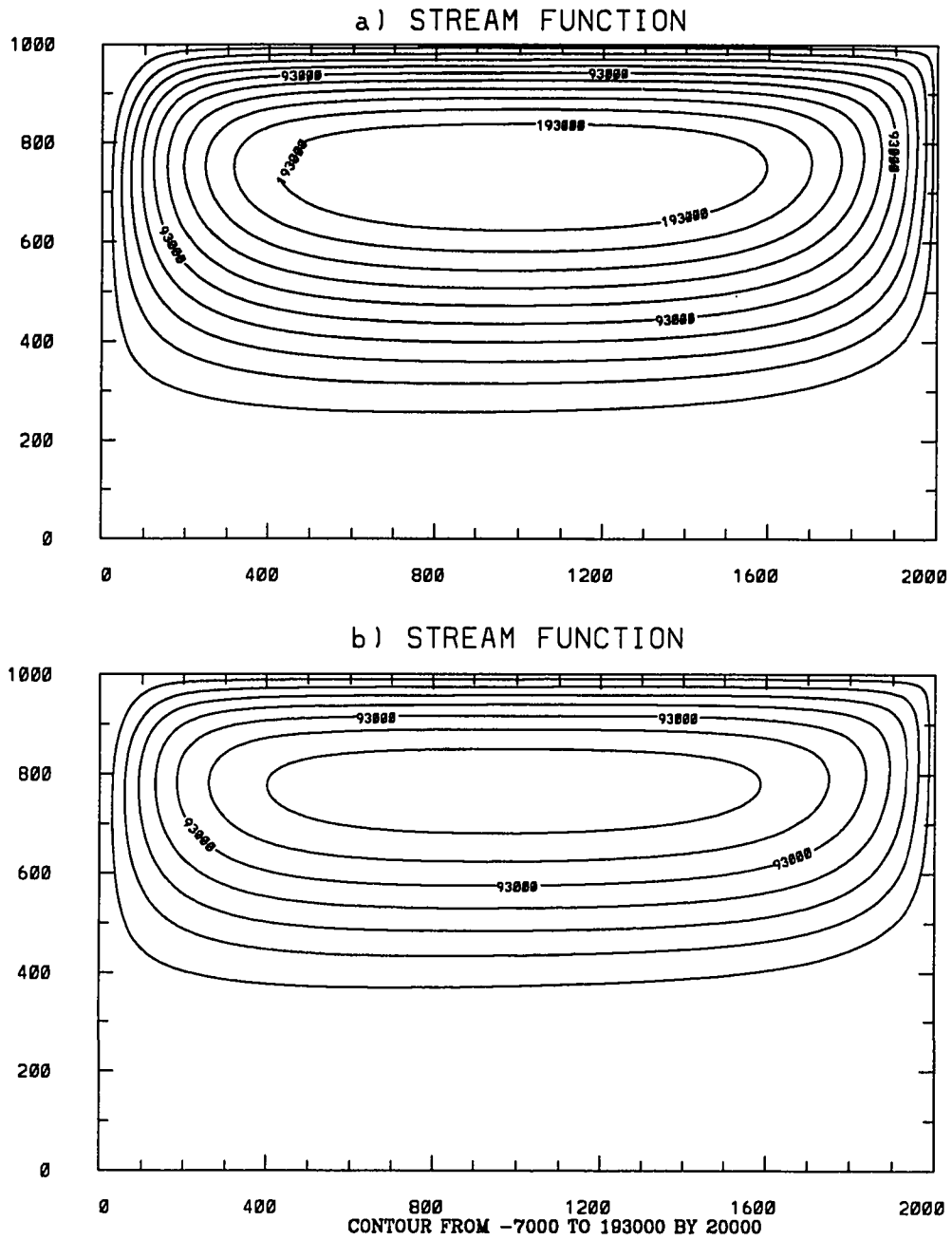


Figure 18: Case 3: The distribution of streamfunction for a prescribed vorticity gradient of (a) $5 \times 10^{-7} \text{ m}^{-1} \text{ s}^{-1}$ and (b) $3 \times 10^{-7} \text{ m}^{-1} \text{ s}^{-1}$ on the northern boundary.

eastern boundary as a solid wall, a no-slip condition is prescribed. This results in a “viscous” boundary layer on the eastern, as well as the western boundary. The change in the boundary condition alters the flow pattern dramatically. The flow takes a longer time to reach a quasi-steady state with larger fluctuations in KE and enstrophy (Fig. 19) than in the free slip eastern boundary cases. The initial spinup period of approximately one and half year is followed by a sharp drop in KE between 900 and 1200 days (Fig. 19). Later, a quasi-steady state is approached with 19 day period oscillations in the mean KE and enstrophy. The 19 day period oscillations are associated with the eddy shedding frequency from the eastern boundary layer. This is discussed further in the next chapter.

Figure 20 shows a time averaged solution of the stream function (ψ) and the relative vorticity (ζ) distribution averaged over three eddy cycles (Day 1440 to Day 1494) after it reached a quasi-steady state. In this case the anticyclonic gyre is compressed to the northern half of the basin, with a weak cyclonic gyre in the southern half of the basin. As the relative vorticity distribution illustrates, friction at the eastern boundary generates positive PV causing the eastern boundary layer to separate from the boundary, at a short distance south of the northeast corner. The strong jet separating from the eastern wall carries positive vorticity into the domain. In this case, part of the negative vorticity input along the northern boundary is balanced by positive vorticity generated at the eastern boundary. Also the contour maps of ψ and ζ are plotted for the instantaneous and eddy motions in figures 21 and 22. The instantaneous picture of the ψ shows the effect of eddies on the mean flow. Except in the western, northern and eastern boundary layers the flow is severely affected by the presence of eddies, especially in the southern half of the basin. Eddy field is obtained by subtracting the instantaneous flow field from the mean field (Fig. 22). Eddy ψ map shows vortices of basin-scale dimensions with an alternating direction of rotation (solid lines denote positive ψ means a clockwise circulation) and are propagating to

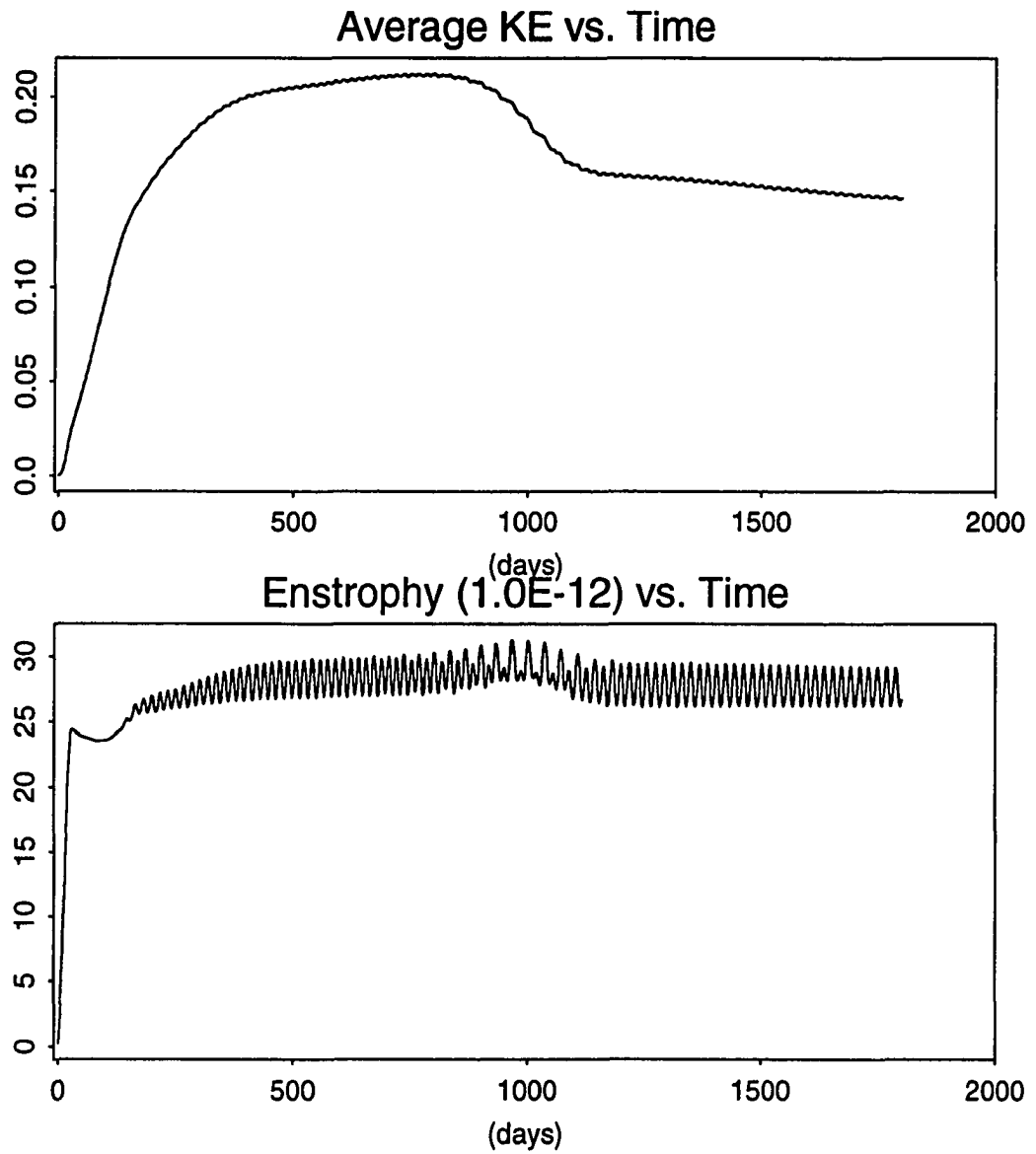


Figure 19: The basin averaged kinetic energy and the enstrophy against time for Case 4.

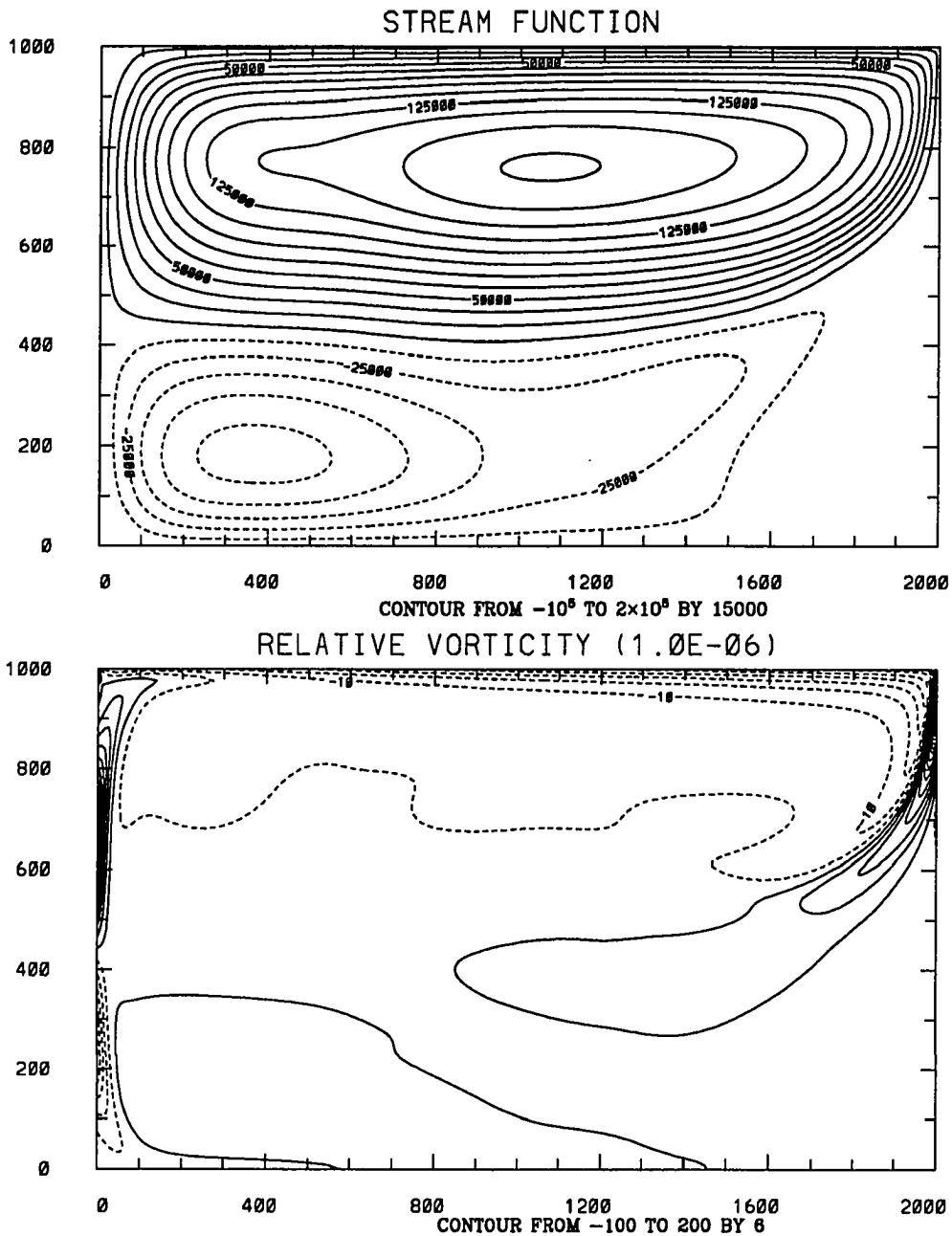


Figure 20: Case 4: Time averaged streamfunction and relative vorticity distribution under the same conditions as in Case 1, except for the no-slip condition on the eastern boundary.

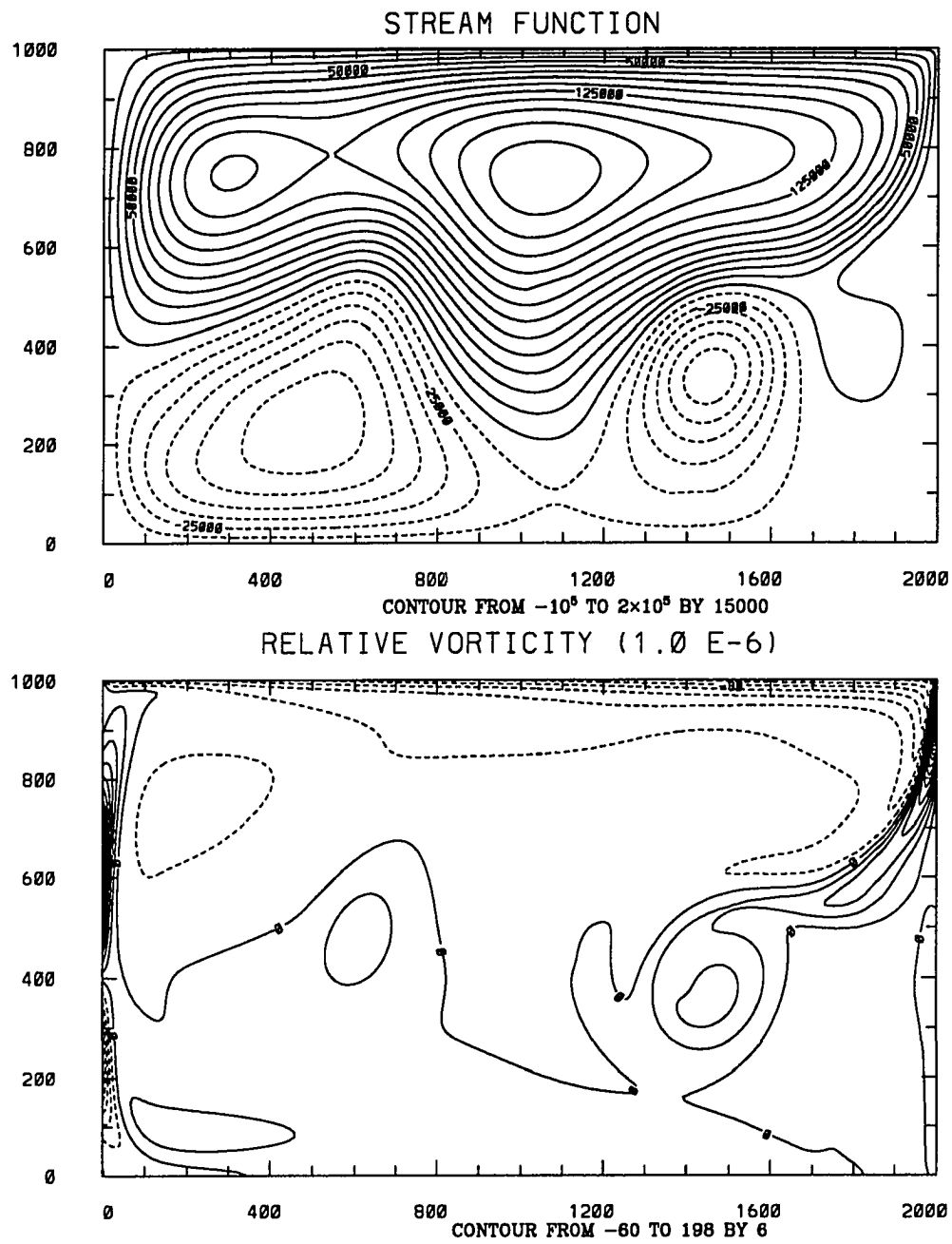


Figure 21: Case 4: Instantaneous fields of streamfunction and relative vorticity distribution at the end of four years.

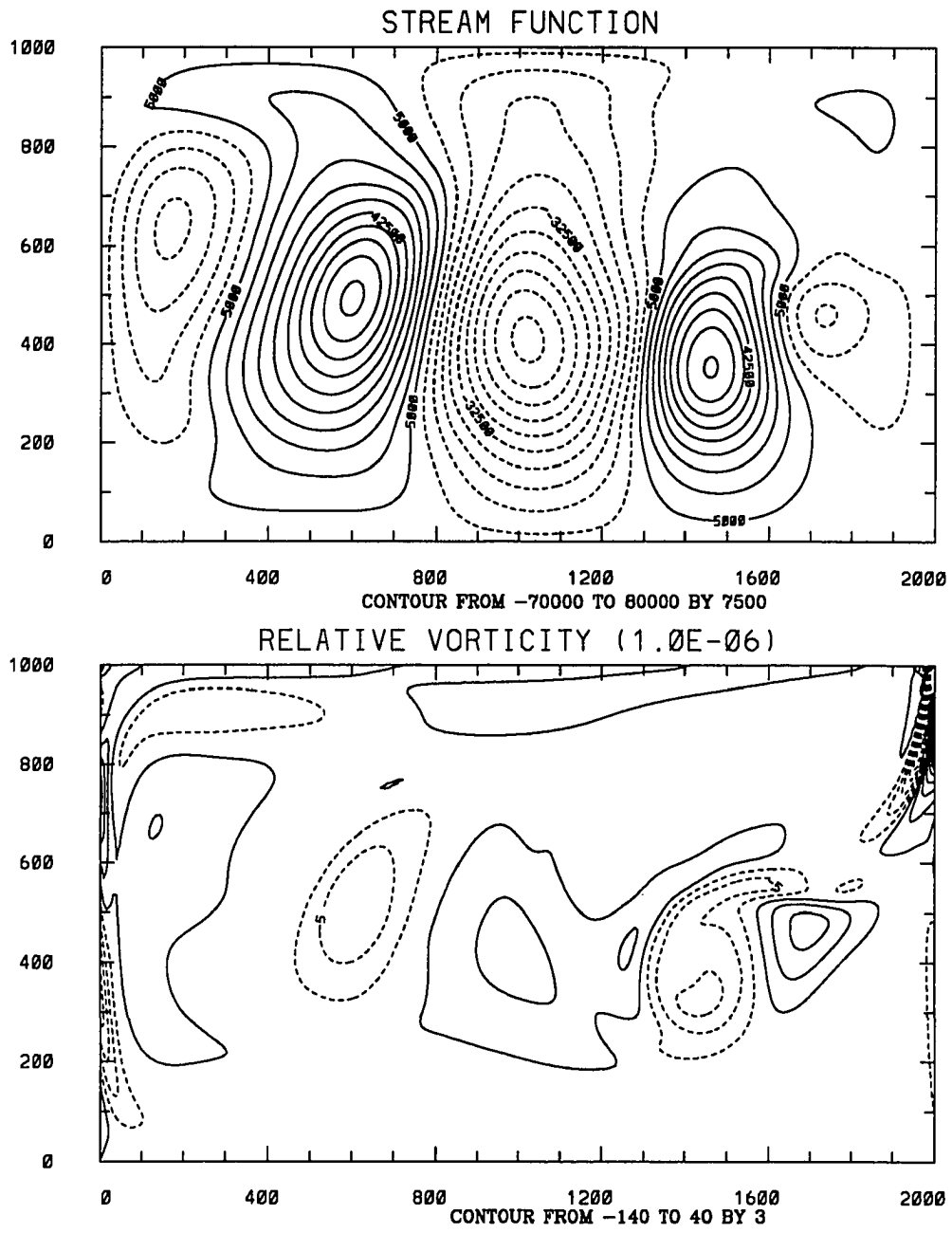


Figure 22: Eddy fields of streamfunction and relative vorticity distribution in Case 4.

the west. Eddies are of elliptic shape with the major axis in the north-south direction.

To quantify the relative importance of each term in the vorticity equation, their individual distributions are studied. Figures 23, 24 show contour lines of the four terms in the vorticity equation (Eq. 4.10), local change (“transient, $\partial\zeta/\partial t$ ”), planetary vorticity advection (“ βv ”), relative vorticity advection (“nonlinear, $J(\psi, \zeta)$ ”) and divergence of eddy flux of vorticity (“viscosity, $-A \nabla^2 \zeta$ ”). For better comparison, the maximum values for the viscous and inertial terms near the north-east corner are truncated to define same contour intervals for all the four terms in the vorticity equation. In the interior, the main balance is among transient, nonlinear and beta terms, with the former two being more dominant. However, in the boundary layers the viscous and inertial terms mainly balance each other. Though the nonlinear and transient terms are dominant in the interior, their magnitudes in the interior are much smaller than in the boundary layers.

Case 5: PV input due to subduction with a no-slip eastern boundary.

If the pressure gradient term in Eq. 4.2 vanishes, the advective PV flux due to subduction is balanced by the Reynolds flux of vorticity. The PV flux condition in this case reduces to:

$$-A \frac{\partial \bar{\zeta}}{\partial y} = -(f + \bar{\zeta}) \bar{v}$$

Subduction is incorporated into the model by specifying the following velocity distribution on the northern boundary as:

$$v(x) = v_o \sin[\pi x/a] \quad \text{for } x \leq a$$

$$v(x) = -v_i \sin[\pi(L-x)/(L-a)] \quad \text{for } a < x \leq L$$

where a is extent over which the outflow occurs and L is the basin dimension in the east-west direction. v_i and v_o are the amplitudes of the inflow and outflow sinusoidal profiles. The maximum inflow velocity v_i chosen here is $5 \times 10^{-3} \text{ m s}^{-1}$, comparable

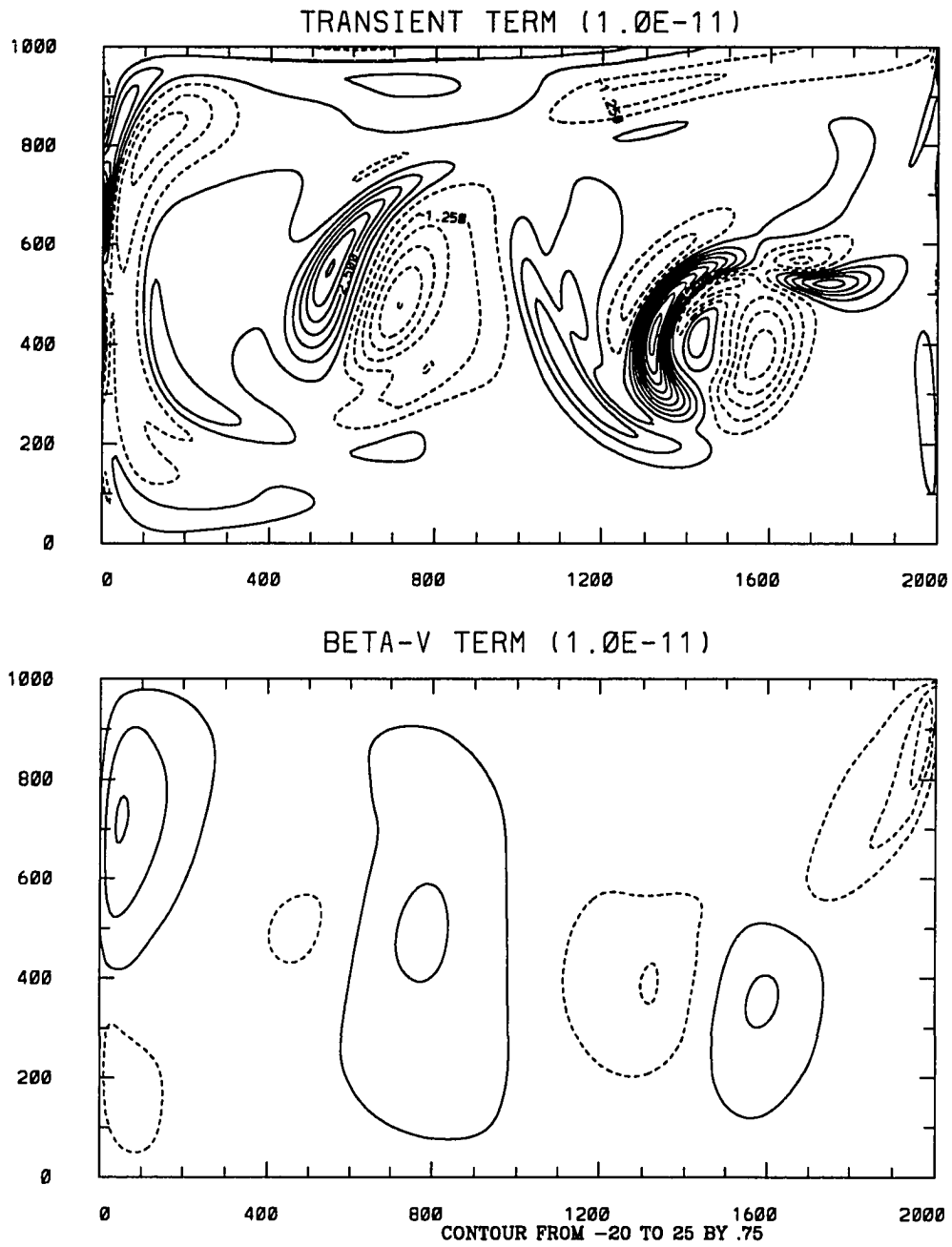


Figure 23: The distribution of transient and beta terms contributing to the relative vorticity in Fig. 21.

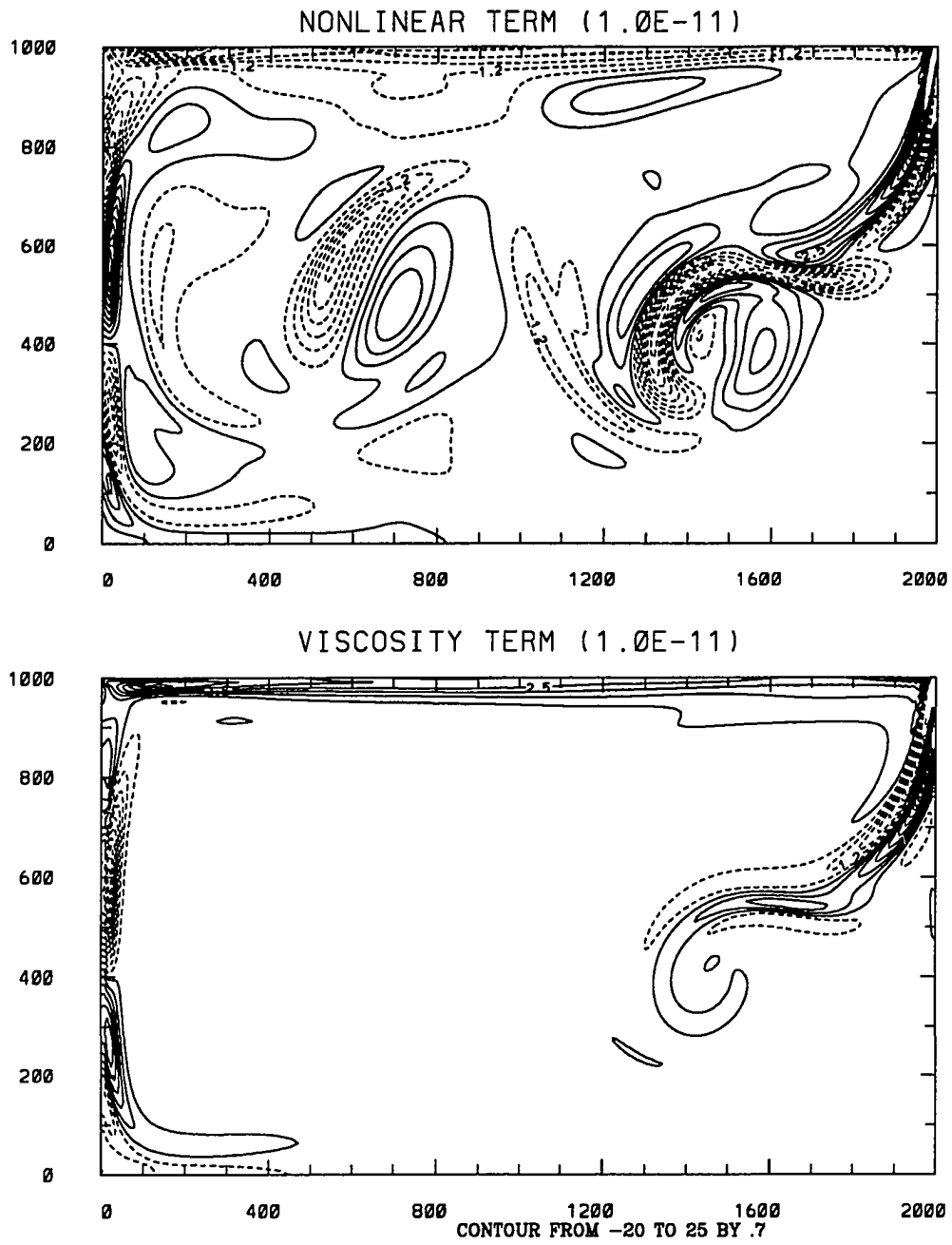


Figure 24: The distribution of nonlinear and viscosity terms contributing to the relative vorticity in Fig. 21.

to the quasi-isopycnic velocities observed in the eastern subtropical North Atlantic. The maximum outflow velocity is $v_o = v_i L/a$ balancing the mass flux.

The streamfunction on the northern boundary follows from integrating the velocity distribution with ψ set to zero at the corners. The streamfunction on all other boundaries remains zero, satisfying the no normal flow condition. In this case, the model reaches steady state in a period of one year. The streamfunction values prescribed on the boundaries are around 10 times smaller than the obtained interior maximum values. This implies that a large part of the flow recirculates and the influence of subduction in setting a new PV at the outcrop is minimal. The streamfunction distribution shows an anticyclonic gyre of a smaller meridional extent than in the previous cases (Fig. 25). The gyre extends approximately 450 km from the northern boundary. The strength of the circulation is weaker by one fifth of that in case 4. In the northwest corner, a small cyclonic gyre is present with an intensity of circulation about one third less than in the anticyclonic part (Fig. 25). The reason is that outflow on the northern boundary removes PV from the domain and is balanced by diffusive flux of positive PV into the domain, which creates a cyclonic gyre.

Case 6: PV due to mean pressure gradient and subduction.

The model is now run with both pressure gradient and subduction prescribed on the northern boundary (Eq. 4.2). The instantaneous flow field (Fig. 26) and the mean field (Fig. 27) shows a circulation pattern similar to that of Case 4 except for the flow being more unsteady and of lesser intensity. No cyclonic gyre is observed in the

streamfunction distribution, in contrast with Case 5. This simulation illustrates the dominance of the pressure gradient term over advective PV transport term due to subduction. The strength of the circulation is nearly three times that in Case 5.

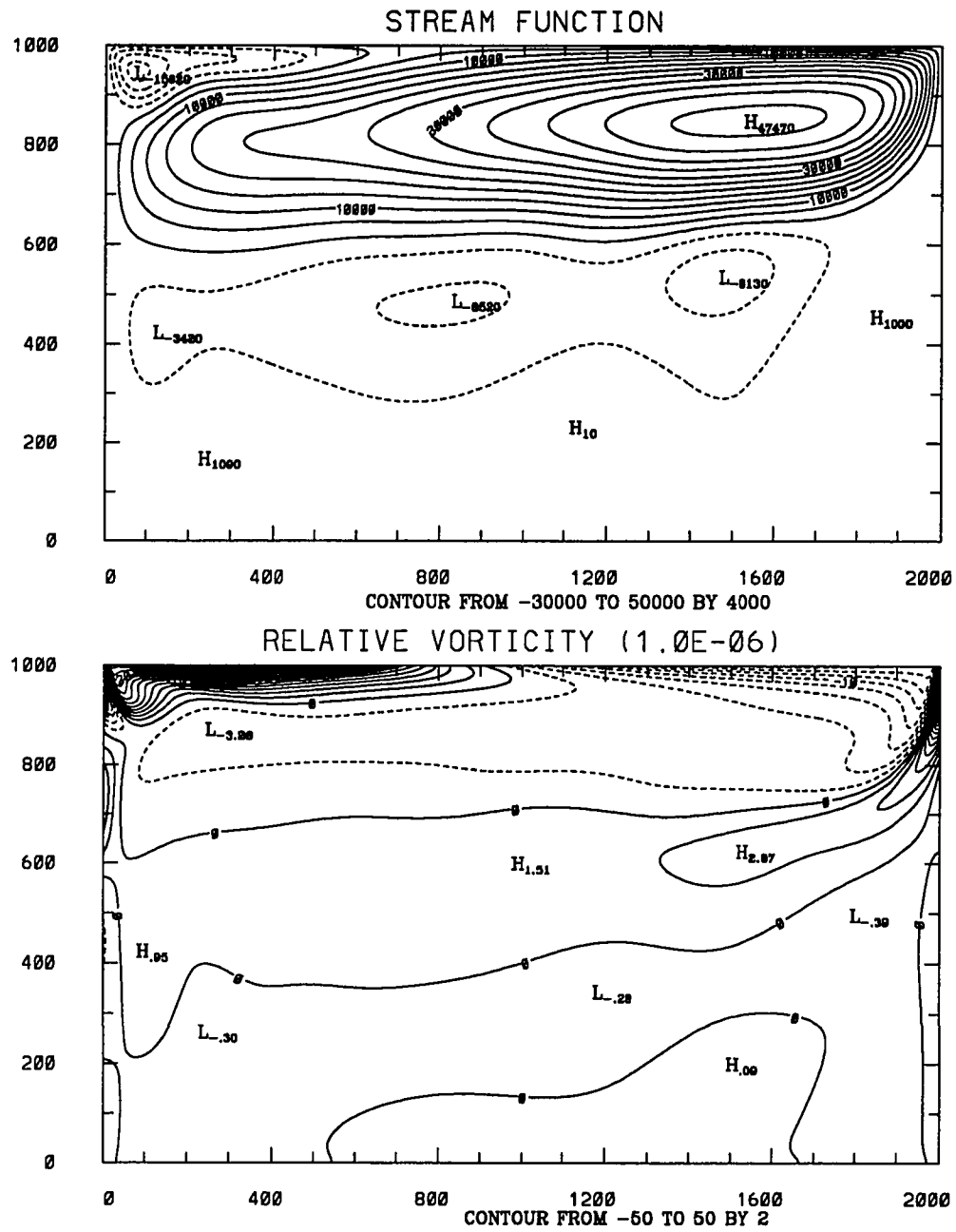


Figure 25: Case 5: The distribution of streamfunction (ψ) and relative vorticity (ζ), when the forcing is only due to subduction.

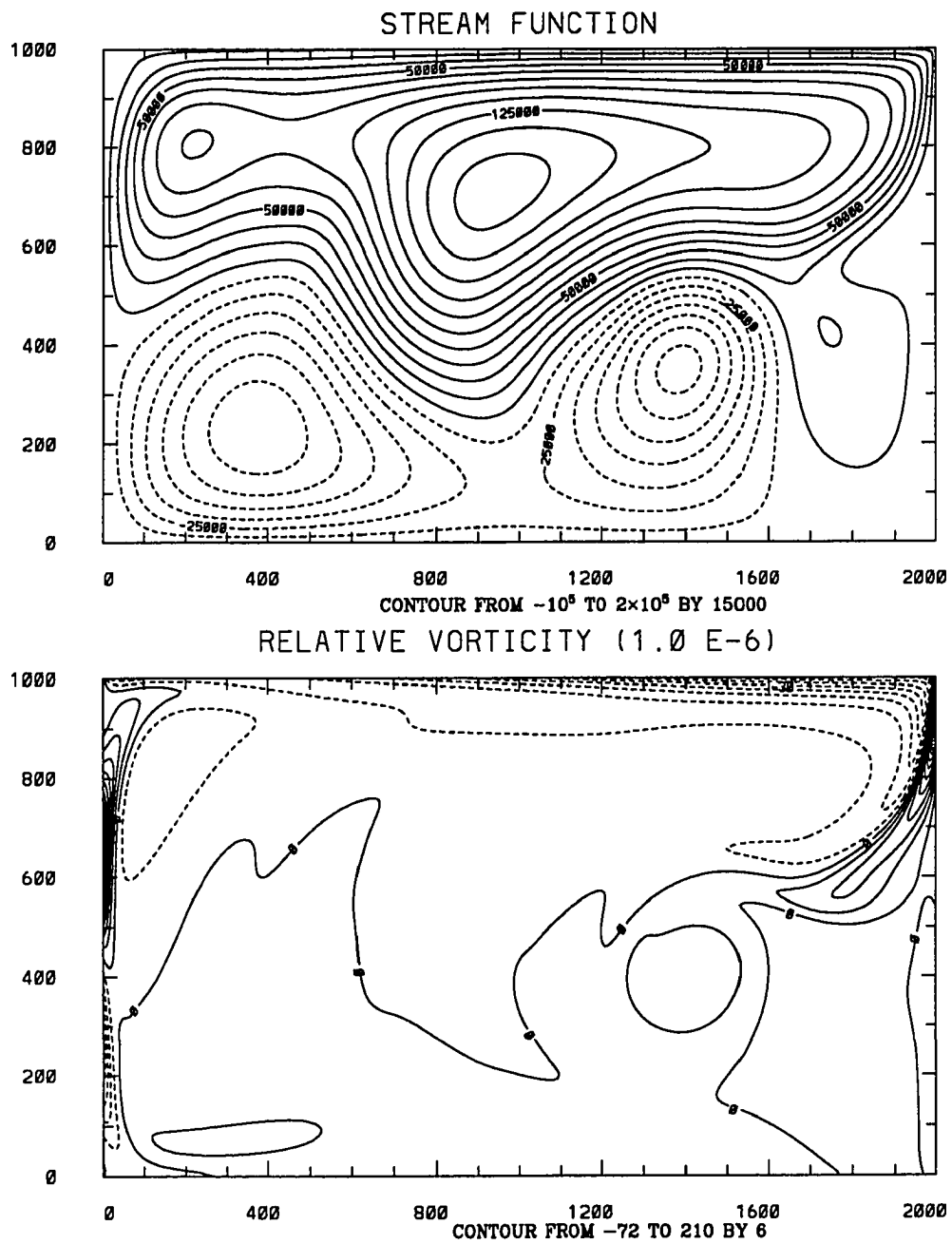


Figure 26: Case 6: Instantaneous fields of streamfunction and relative vorticity distribution at the end of four years.

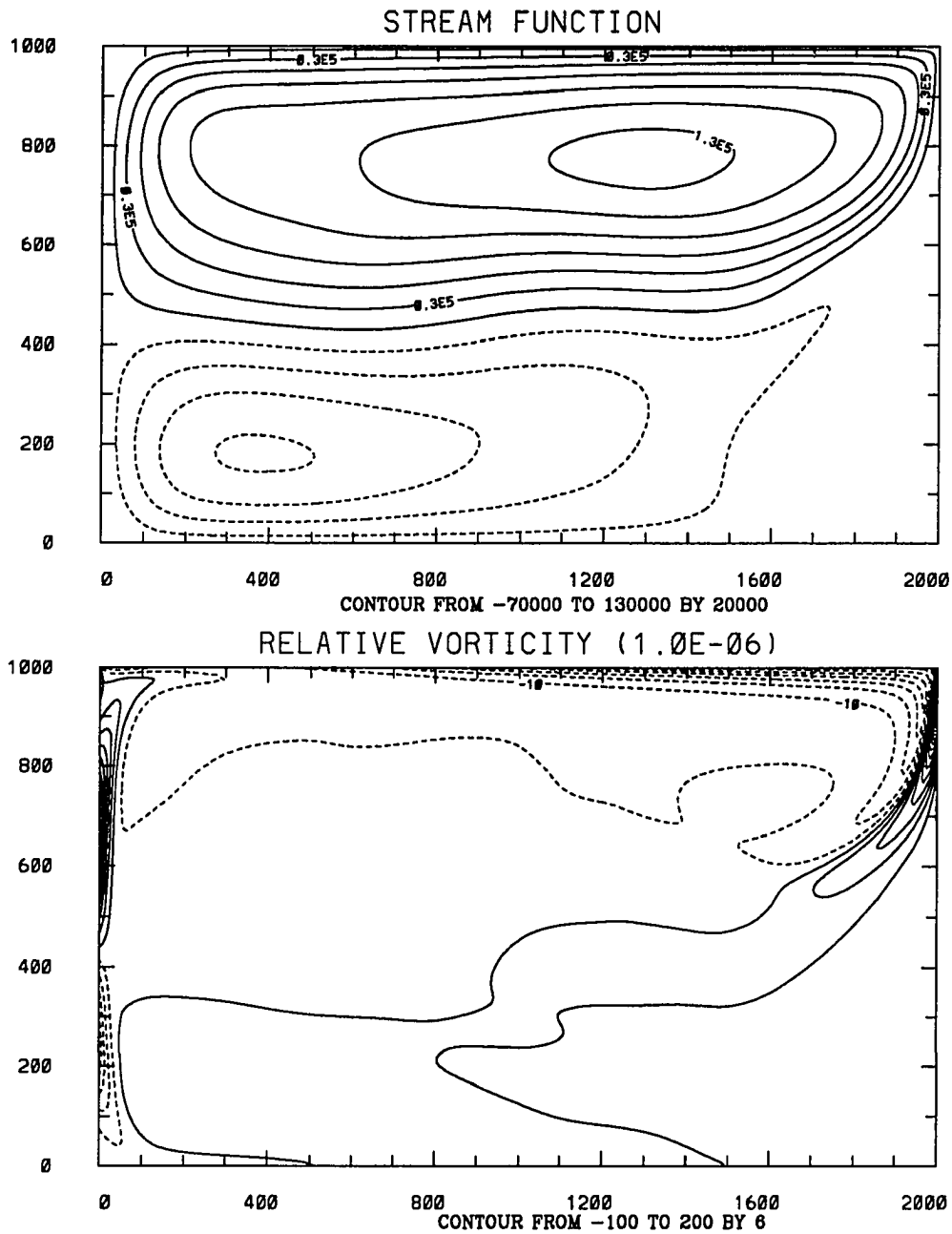


Figure 27: Case 6: Time averaged distribution of streamfunction (ψ) and relative vorticity (ζ), when the forcing is due to along-isopycnal pressure gradient and the subduction.

In the eastern part of the domain, the subduction and the pressure gradient reinforce each other, increasing the transfer of PV into the interior. On the western side, they counteract each other resulting in a smaller PV transport into the domain. The period of oscillation observed in the mean KE and enstrophy plots after spin up is also around 19 days as in Case 4 (Fig. 28) as this is associated with the eddy shedding period from the eastern boundary layer. The step that appeared in KE distribution in Case 4 (Fig. 19) is smoothed out here as the flow adjusted to the non-linear processes that are involved.

Case 7: Effect of positive vorticity on interior circulation

When the model is forced with positive vorticity input (by a negative pressure gradient), it produces very different vorticity and streamfunction fields. In a final quasi-steady state, a more or less steady cyclonic gyre develops in a narrow band along the northern boundary with a deep southward lobe along the western boundary (Fig. 29). Part of the westward flow along northern boundary turns southward along the western boundary, and penetrates farther south than the rest of the cyclonic gyre, forming a cyclonic gyre of its own small east-west extent. An anticyclonic eddy of lesser intensity adjoins the cyclonic gyre. The rest of the basin is almost devoid of any circulation. The influence of this form of forcing confines the circulation to the upper half of the domain.

Case 8: Time dependent forcing

The pressure gradient at the outcrop can vary seasonally. To account for this, a sinusoidal time dependent forcing function was applied on the northern boundary with annual period. The forcing function starts at time zero with negative vorticity

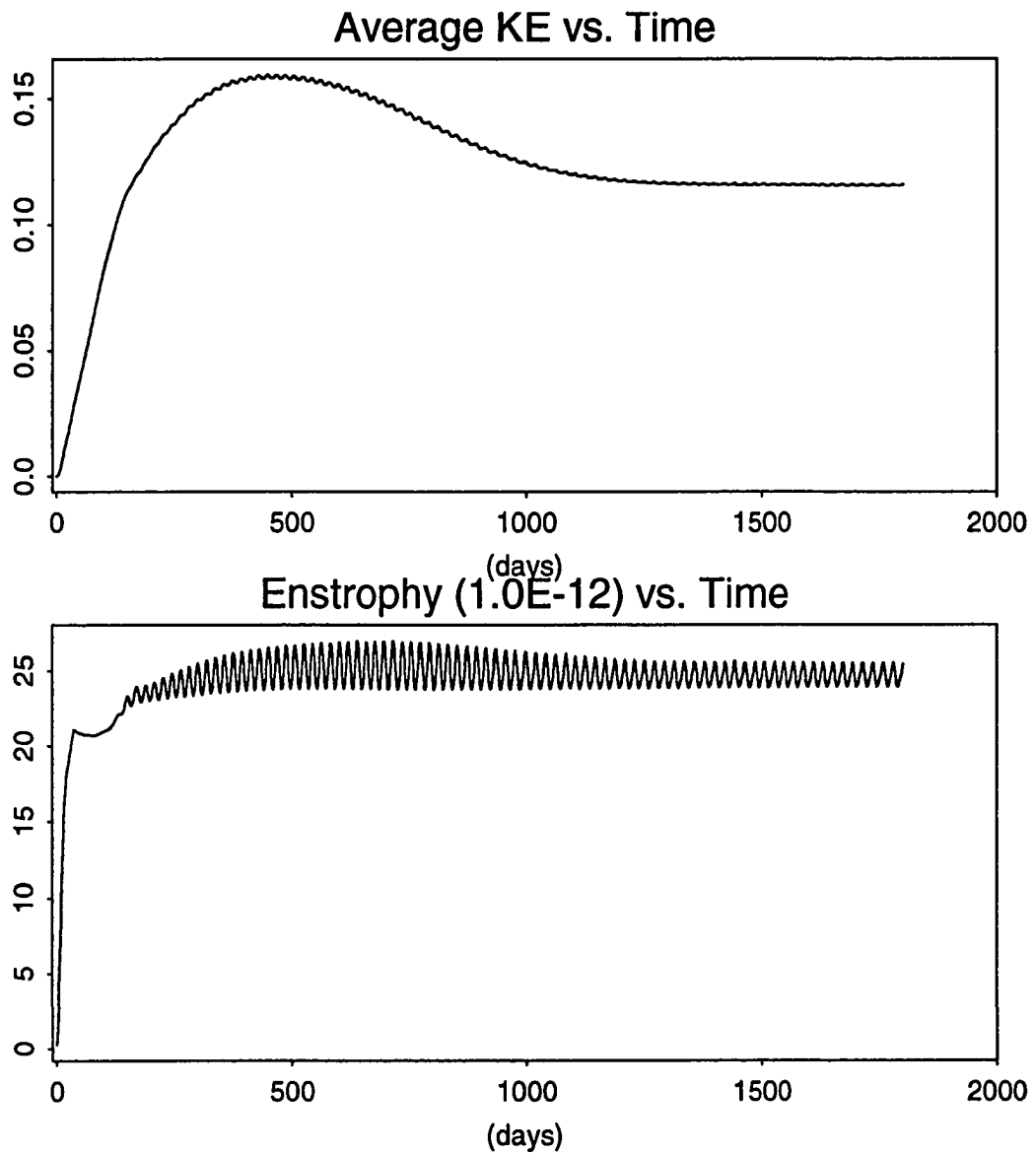


Figure 28: The basin averaged kinetic energy and the enstrophy against time for Case 6.

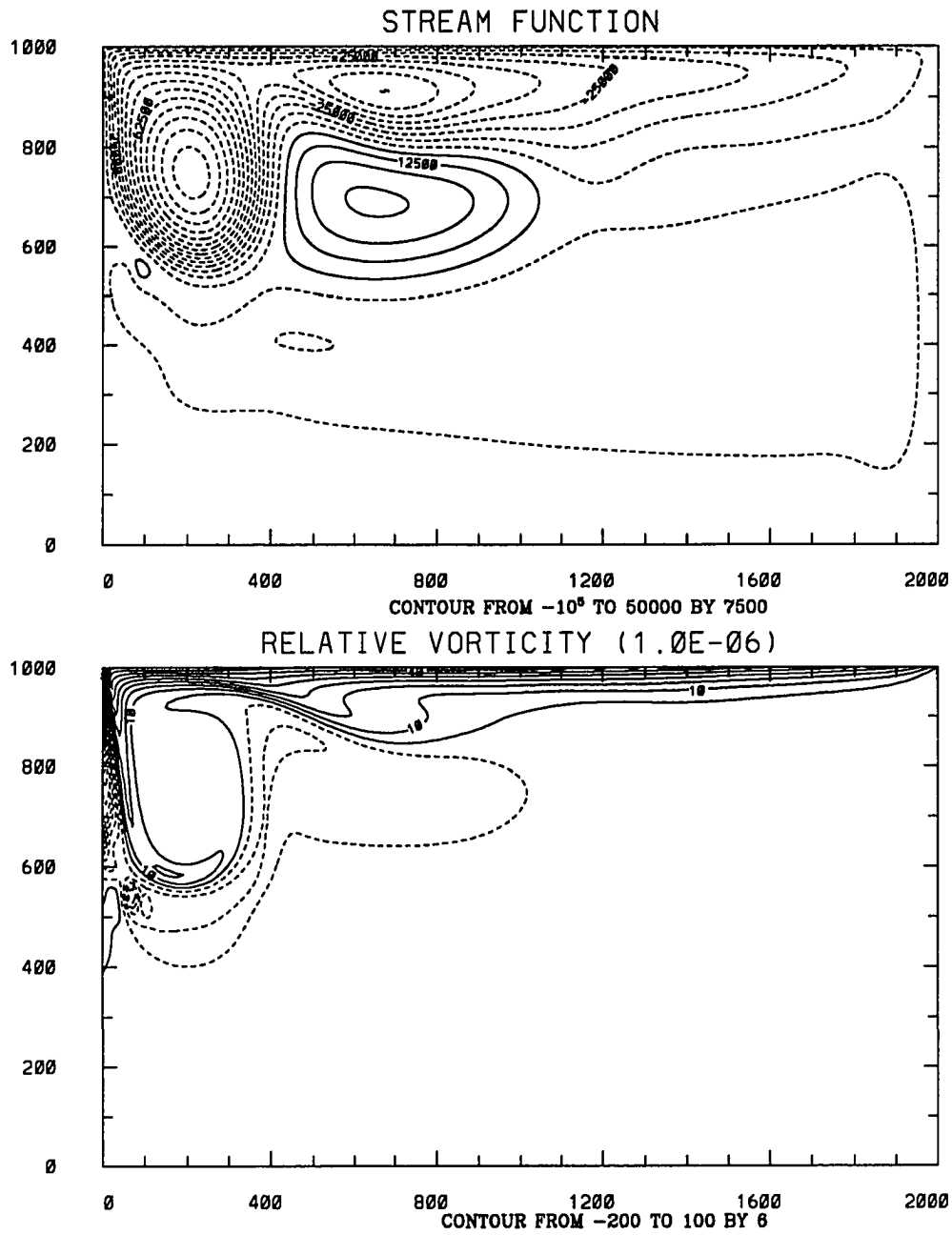


Figure 29: Case 7: The distribution of streamfunction (ψ) and relative vorticity (ζ), when model forcing is by positive vorticity input.

input rising from zero to a peak at three months, then declining and turning into positive vorticity input in the second half of the year. The PV flux due to subduction is zero and on the eastern boundary the no slip condition still holds. The average KE and enstrophy distribution shows the effect of periodic forcing on their values (Fig. 30). At the end of six months the flow and the vorticity patterns are much as in the steady forcing Case 4, albeit at smaller amplitude (Fig. 31). At the end of one year (Fig. 32), a cyclonic gyre appears, again much as in the steady forcing case, but with more vigorous unsteady motions outside the gyre. The same basic pattern is repeated year after year, with more energy and more variety in the unsteady part of the flow than in the steady cases.

Case 9: Effect of grid size

To check the influence of grid spacing on the evolution of interior circulation for our critical Cases 4 and 6 the grid size is reduced to 4 km instead of 8 km. Using a similar kind of forcing as in Case 4, where pressure gradient term is PV source, the mean KE distribution (Fig. 33) shows that the flow never reaches a steady state. After the initial spinup of the model, there is a sharp drop in KE as in Case 4. However, the KE again accumulates over a period of 1300 days followed by the 25 % drop in the KE. This cycle repeats with time. Building up and collapsing of KE in the domain is associated with the relative influence of input and dissipation of vorticity into the model domain. However, when the advective PV transport term (Eq. 4.2) is considered, such periodic building up of KE never occurred after the initial spinup (Fig. 34). The model reaches a quasi-steady state over a period of four years just as in Case 6.

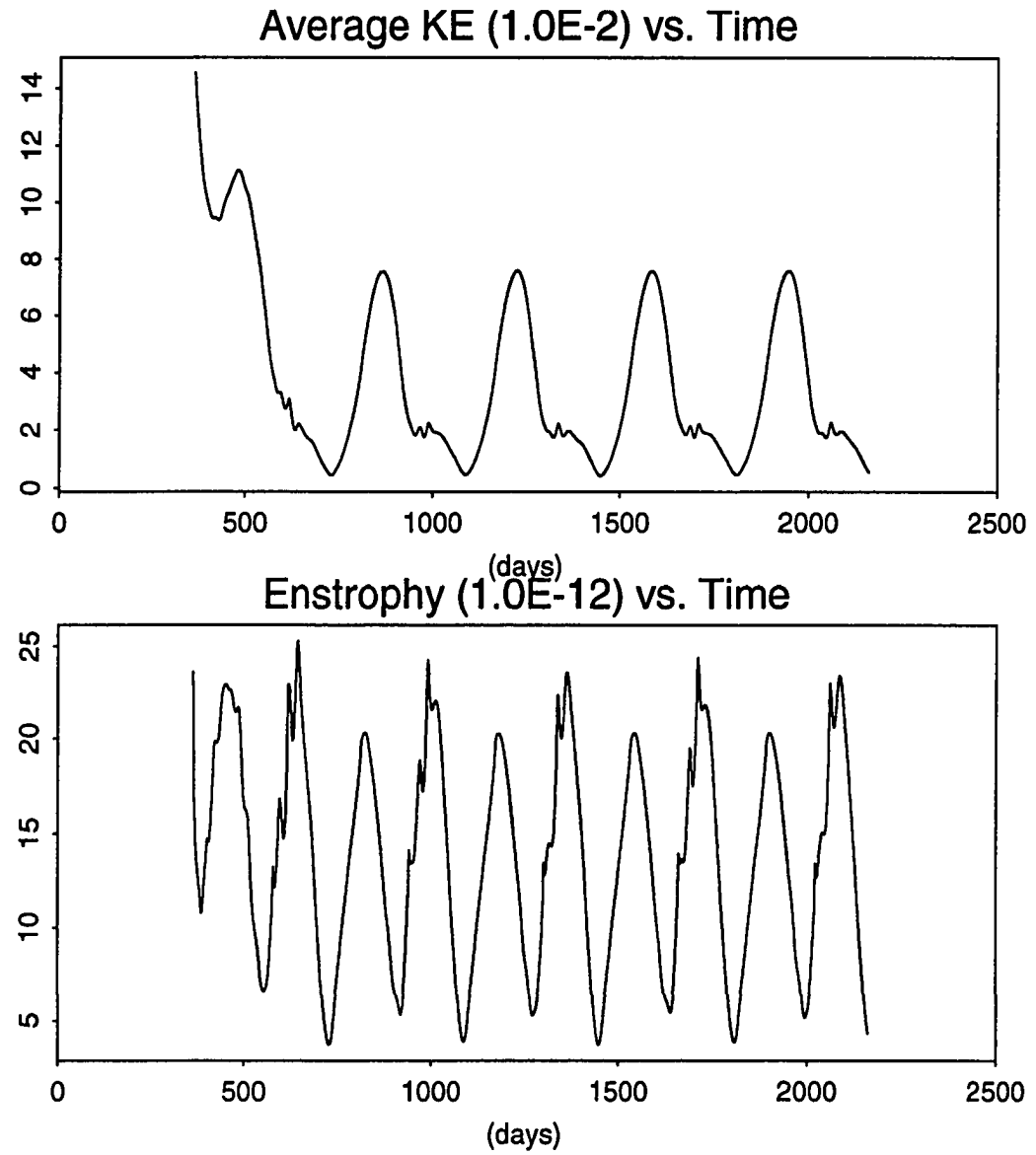


Figure 30: The distribution of kinetic energy and enstrophy for Case 8.

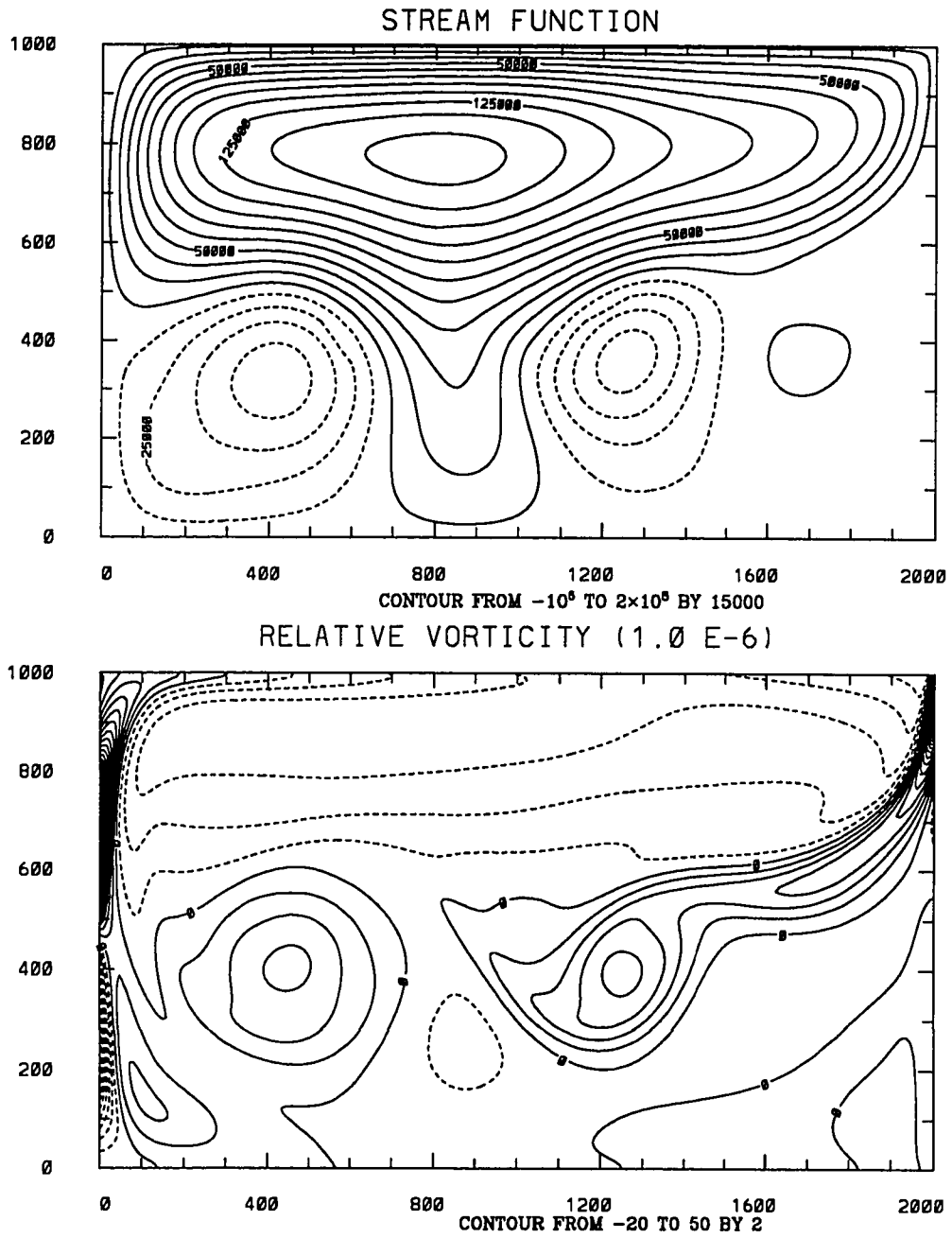


Figure 31: The distribution of streamfunction (ψ) and relative vorticity (ζ) after six months, for Case 8.

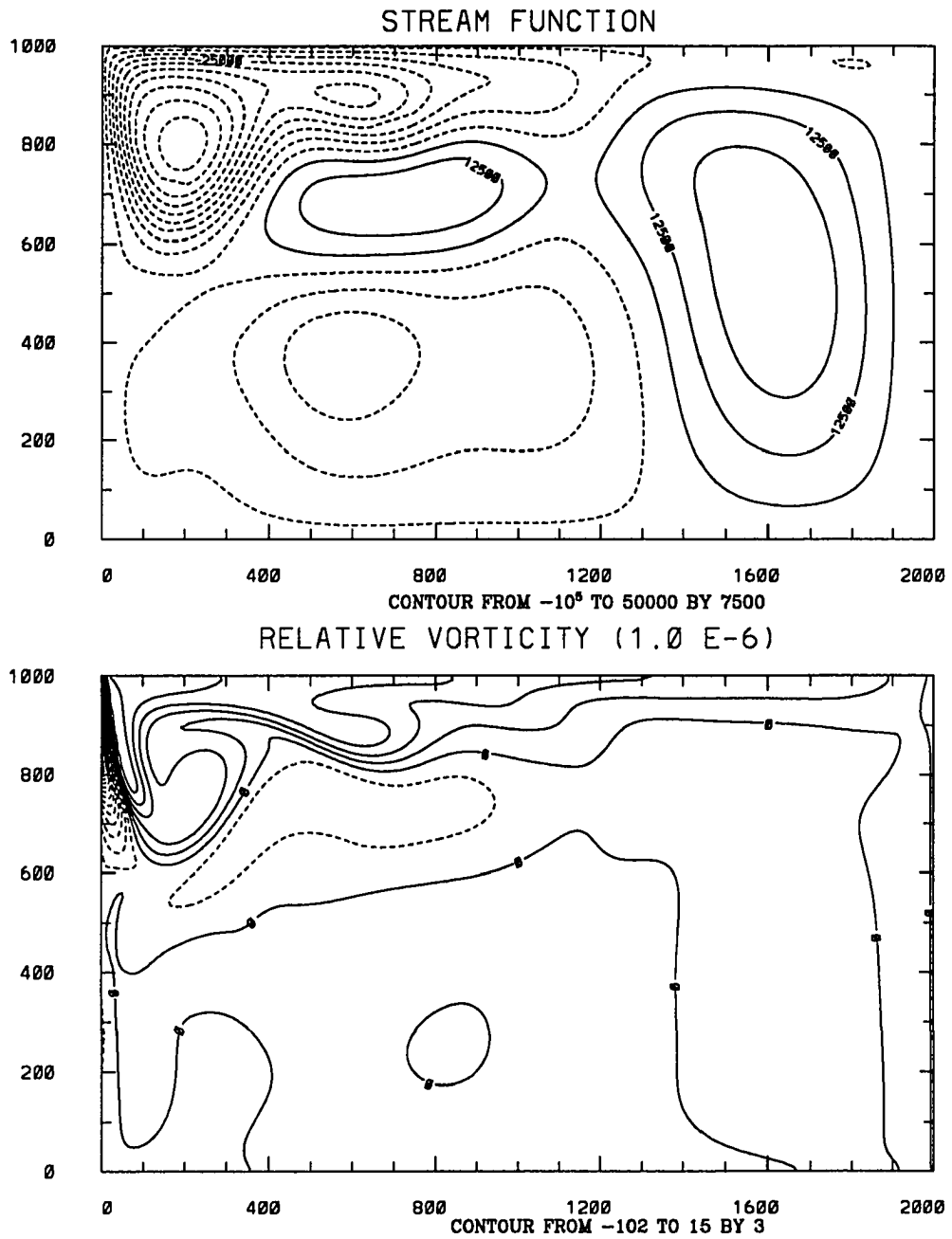


Figure 32: The distribution of streamfunction (ψ) and relative vorticity (ζ) after one year, for Case 8.

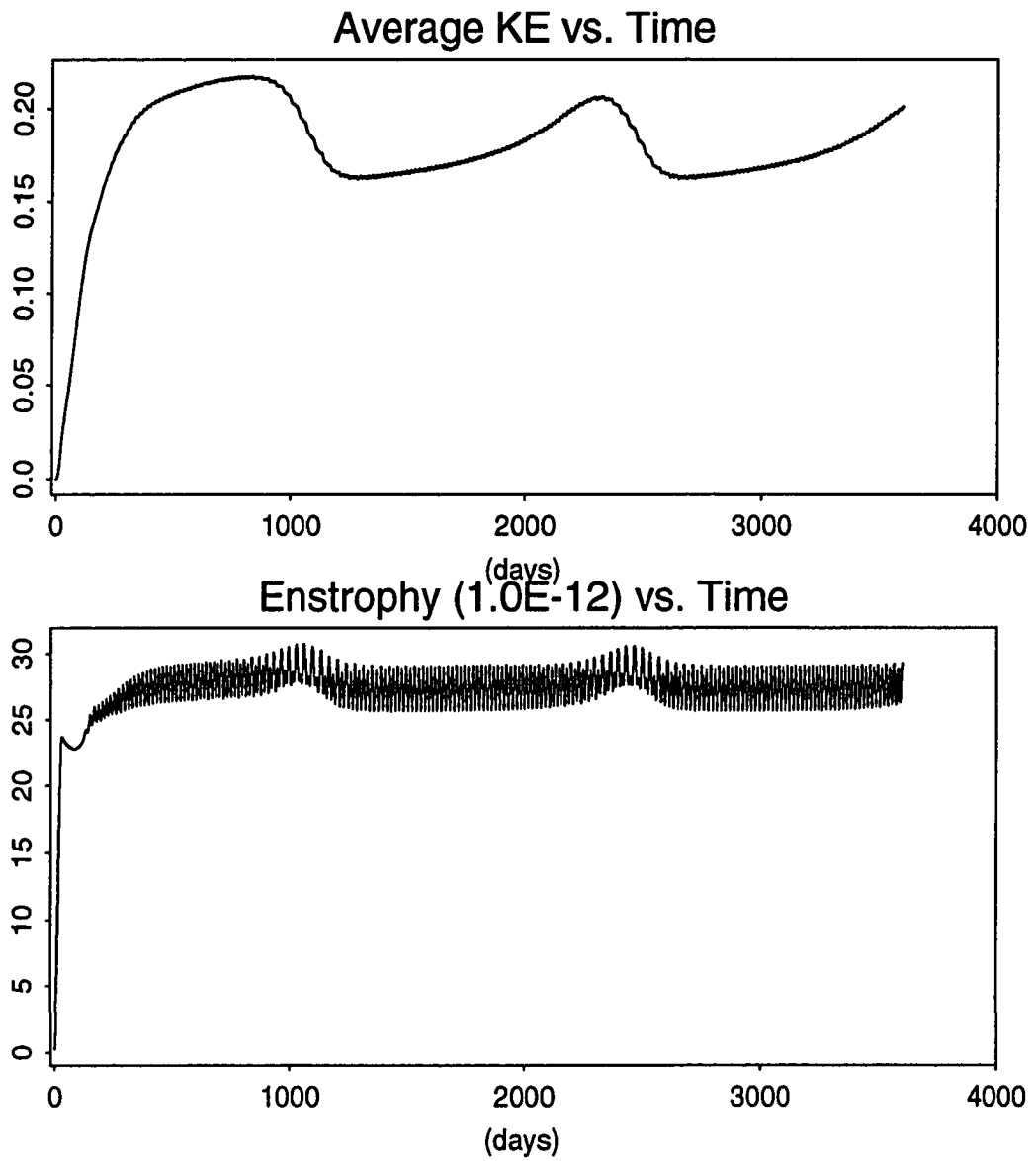


Figure 33: The distribution of kinetic energy and enstrophy for Case 9 with 4km grid. Conditions similar to Case 4.

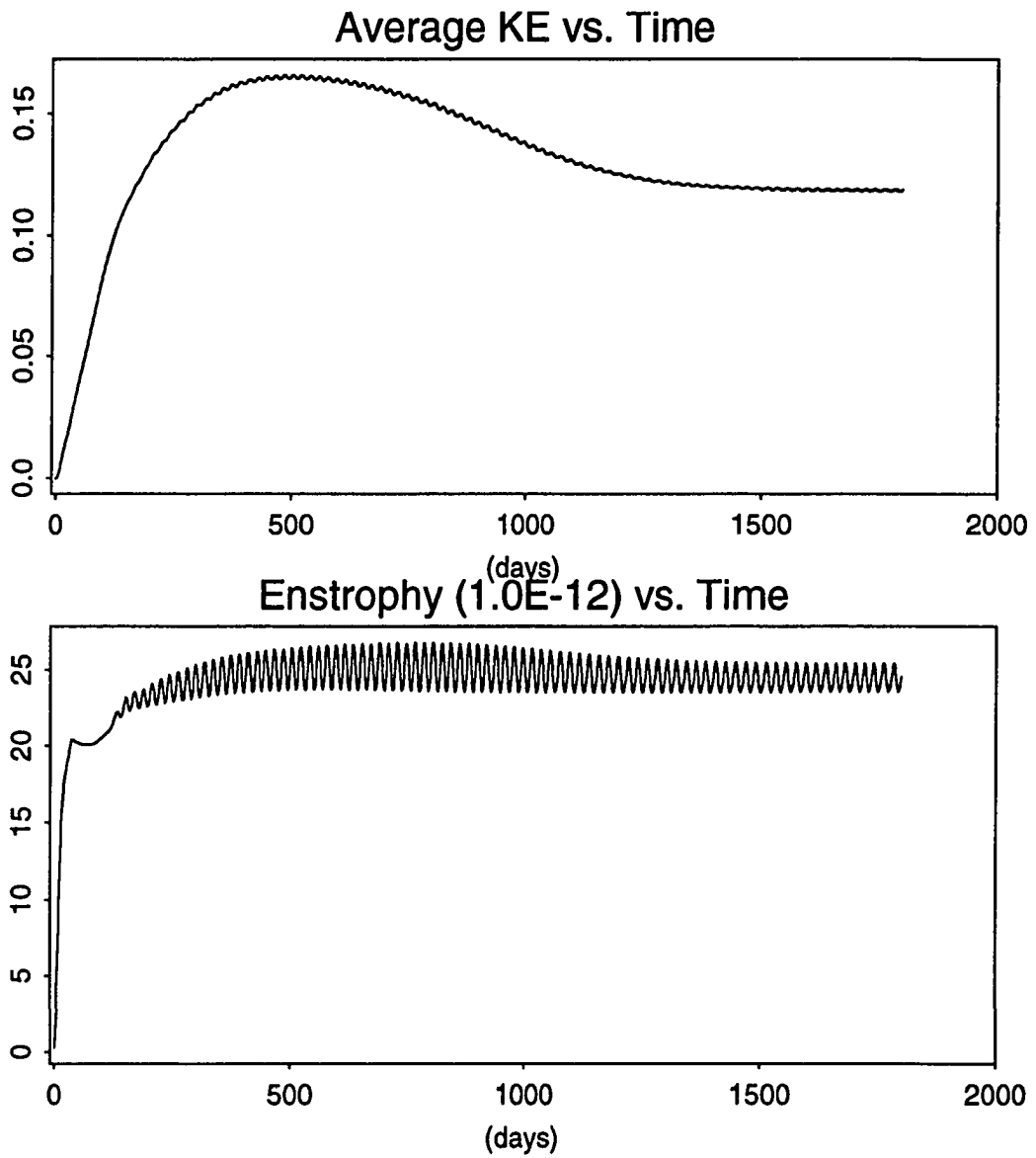


Figure 34: The distribution of kinetic energy and enstrophy for Case 9 with 4km grid. Conditions similar to Case 6.

6 Discussion

This thesis explores a recently identified mechanism of circulation in thermocline layers, forced at their surface outcrops. Instead of conventional Ekman pumping driving interior layers, the forcing function in the present study is PV input by wind stress and surface buoyancy flux, which reduces to the along-outcrop pressure gradient. The latter is balanced by a part of the wind stress force, while the other part of the wind stress balances the generalized Ekman drift $\overline{v(f + \zeta)}$. Thus the effective driving force may be thought to be lateral shear along the outcrop of an isopycnic layer.

Surface PV transport is taken over in the interior by advective PV flux (due to subduction) and Reynolds flux of vorticity sustained by geostrophic turbulence. Continuity of PV transport within a isopycnic layer is the key principle underlying the modeling effort, and was written in Eq. (3.12). In the derivation of that equation the seasonal migration of isopycnals due to buoyancy fluxes was taken into account but was cancelled by other terms. The resulting expression was not directly dependent on the surface heat flux although such heat flux is implied by geostrophic cold water advection across isopycnal outcrop (Eq. 3.8). Within the interior, Reynolds flux of vorticity dominates over advective PV transport due to subduction. But, where Reynolds flux of vorticity is negligible, subduction may carry PV flux.

The model simulations show that boundary forcing by what is effectively lateral shear generates circulation patterns quite different from the classical Ekman pumping theory. In the present study, the eastern, western and northern boundary layers are crucial in setting the pattern of circulation. In contrast, in the classical wind driven

models, the interior circulation is governed by Sverdrup dynamics and the western boundary current merely acts as a conduit to complete the circulation. But here, the eastern boundary condition, in particular, is found to be crucial for the pattern of flow.

With a free slip eastern wall, the flow results in a Fofonoff gyre with strong boundary currents on the northern, eastern and western walls. This is similar to the solution obtained by Fofonoff (1954) in a frictionless steady horizontal flow asserting the dominance of non-linear term in the vorticity balance. A similar circulation pattern is also obtained by Cessi *et al.* (1987), who analyzed a barotropic model forced on the north and south boundaries by PV anomalies. Their results showed a closed gyre and homogenized PV in the interior. The homogenized value of PV was the average of the PV values on the boundary, weighted by the corresponding velocities on the boundary. The homogenized value of PV decreased as the forcing strengthened or the dissipation weakened, while the size and strength of the gyre increased, as is the case in our study. The meridional extent of the recirculating gyre was proportional to the PV anomaly prescribed on the boundaries. However, the PV anomalies prescribed by Cessi *et al.* (1987) were arbitrary with no functional relationship to boundary layer dynamics or diabatic processes creating PV anomalies.

As observed in Cases 2 and 3 of our model simulations, the meridional extent of the anticyclonic gyre with a free slip eastern boundary decreased when the intensity of forcing (the PV input, *i.e.*, the along-outcrop pressure gradient) was reduced. On the other hand, the friction coefficient had no effect on the gyre size. A simple dimensional argument yields the functional form of relationship of gyre size to other parameters. Let meridional scale of the circulation (Y_G) depend on forcing (the pressure gradient, $\partial\Pi/\partial x$), the planetary vorticity gradient (β) and the isopycnic lateral diffusivity (A). Performing dimensional analysis yields two non-dimensional numbers:

$$\frac{Y_G \beta^{2/3}}{(\partial\Pi/\partial x)^{1/3}}, \quad \frac{\beta A}{\partial\Pi/\partial x}$$

The second non-dimensional number is the inverse of Reynolds number and its value in the present study is of the order of 2×10^{-8} , indicating the near inertial flow. For the parameter values considered in Cases 2 and 3, an average value of 7.2 was obtained for the first non-dimensional number. The plot of the meridional scale of the gyre (Cases 2 and 3) with the length scale defined by the first non-dimensional number (Fig. 35) yielded a linear empirical relationship:

$$Y_G = 6 \left(\frac{\partial \Pi / \partial x}{\beta^2} \right)^{1/3} + 1.25 \times 10^5$$

Such an empirical relationship gives an estimate of the extent to which PV at the surface outcrop (due to different surface forcing mechanisms) can drive the circulation in case of upwelled isopycnals.

In Böning's (1986) numerical model study on wind-driven circulation, the beta term (βv) and the nonlinear term ($J(\psi, \zeta)$) dominate the vorticity balance when free slip boundaries are used. But in Case 1, it is the nonlinear and the viscous terms in the boundary layers which contribute mainly to the total integrated vorticity balance in the domain.

When a no-slip condition is prescribed at the eastern wall, it totally alters the circulation by causing the eastern boundary current to separate and create eddies that propagate toward the western boundary. The cases run with the no-slip boundary condition on the eastern wall invariably produced cyclonic eddies that advected towards the western boundary. These eddies, initially approximately 300 km in diameter grew with time while their strength diminish as they dissipate their energy in the course of their westward motion. They originated from the injection of positive PV into the domain.

Figs. 36 and 37 show the variation of PV in the eastern boundary layer. The distribution of PV at a particular latitude (at $Y=1160$ km) show that the eastern boundary layer scale in the no slip case is of the order of 50 km (6 to 7 grid points). The magnitude of positive PV generated at the eastern boundary (for example at $Y=$

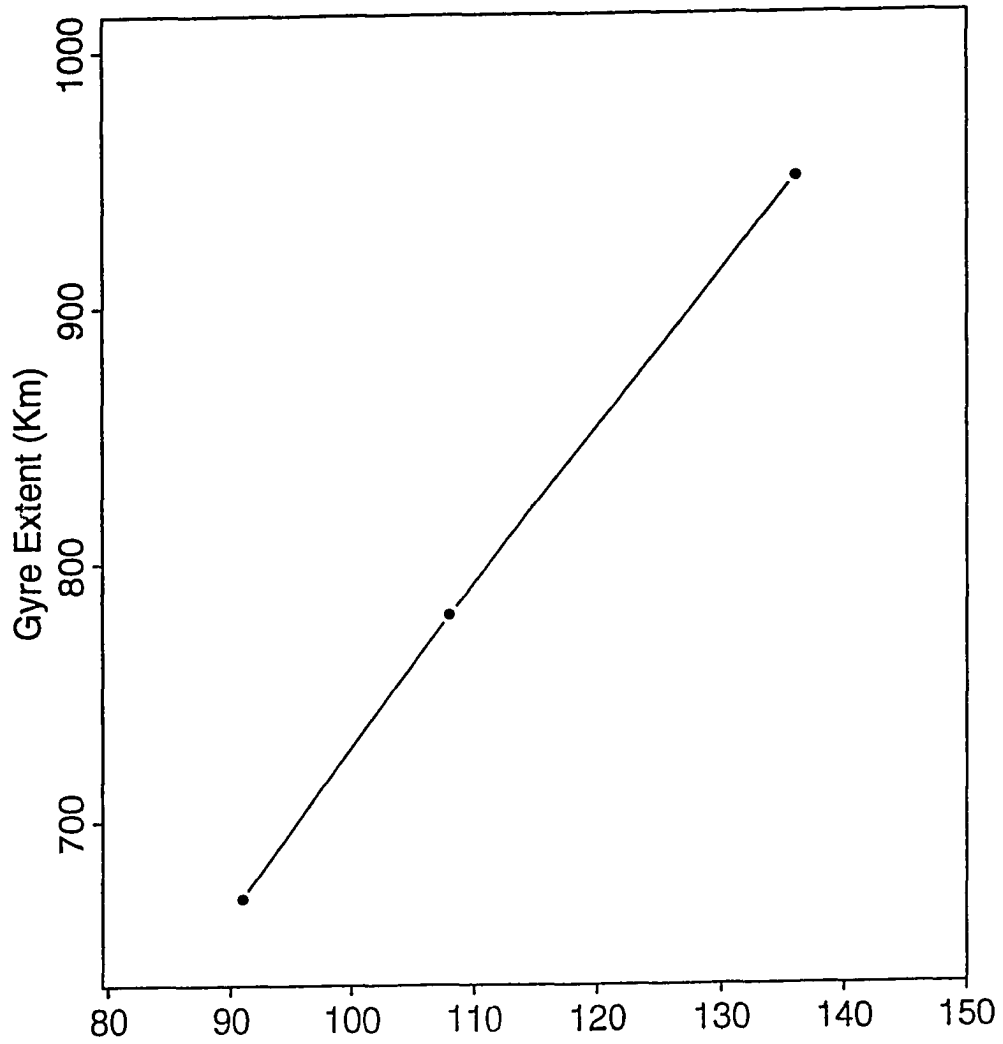


Figure 35: Variation of the meridional extent of the gyre (Y) with the non-dimensional number $(\partial\Pi/\partial x/\beta^2)^{1/3}$.

1120 km) in the no slip case is seven times that in the free slip case. In the latter case positive PV is generated only due to the planetary vorticity effect.

A marked drop in the mean KE observed after the initial spinup of the model in Fig. 19 hints at a dynamical scale problem related to large dissipation rates. The cascading of energy is lagging behind the spin up process *i.e.*, the energy is not dissipated at the rate that it is put into the domain. During this time, the animation of the relative vorticity field showed the formation of cyclonic eddies near the eastern boundary with two dominant periods of 16 and 18 days (also reflected in enstrophy plot, Fig. 19b). Eddies with longer periods were dissipated near the western boundary, while the slower ones carried the residual vorticity into the south-western corner which eventually dissipated. Finally, it adjusts to an equilibrium state where eddies are shed from the eastern boundary with a constant period of 19 days.

The 19 day period oscillations matches with the diffusion time scale that was calculated from the eastern boundary layer thickness (δ_e) and the lateral diffusivity (A) as: δ_e^2/A . Coincidentally, this is also the estimated time for the eddies, in the eastern North Atlantic, to grow from zero to their average energy level (Käse *et al.*, 1985). Böning (1986), attributed such fluctuations in mean KE to the inability of the lateral friction to dissipate the total wind input energy in his numerical model study.

Subduction is assigned considerable importance in ventilation thermocline theories. It is supposed to be the main forcing mechanism driving thermocline circulation. The results from Case 6 show by contrast, that the effect of along-isopycnal pressure gradient overshadows the effect of subduction. One important aspect shown in this study is that, even a simple barotropic model can reveal the importance of boundary layers on isopycnal surfaces as potent generators of mean flow and geostrophic turbulence. The results depend, however, on the constant layer depth idealization: they only indicate the general character of circulation arising from the vorticity input at layer outcrops. The presence of adjacent layers less vigorously forced would presum-

ably damp the response in a strongly forced layer and vice versa. Such interactions may or may not be strong, but they are unlikely to alter the general character of circulation forced in the particular way here considered.

To a limited extent, the present study mimics flow conditions observed in the eastern North Atlantic where the flow separates from the eastern boundary, and develops eddy motions. It shows also an intense jet along the northern boundary which can be reasonably related to the eastward flowing Azores current in the eastern Atlantic region. The high velocities in the model suggest that the forcing was too strong for simulating this current. The eastern part of the circulation pattern seen in Fig. 26 resembles somewhat the flow structure in the eastern North Atlantic (Stramma and Siedler, 1988; cf. Fig. 10). The model also reproduced the westward propagating eddies near the flow separating from the eastern boundary. However, the eddy sizes in the model are larger than those observed in the eastern subtropical North Atlantic.

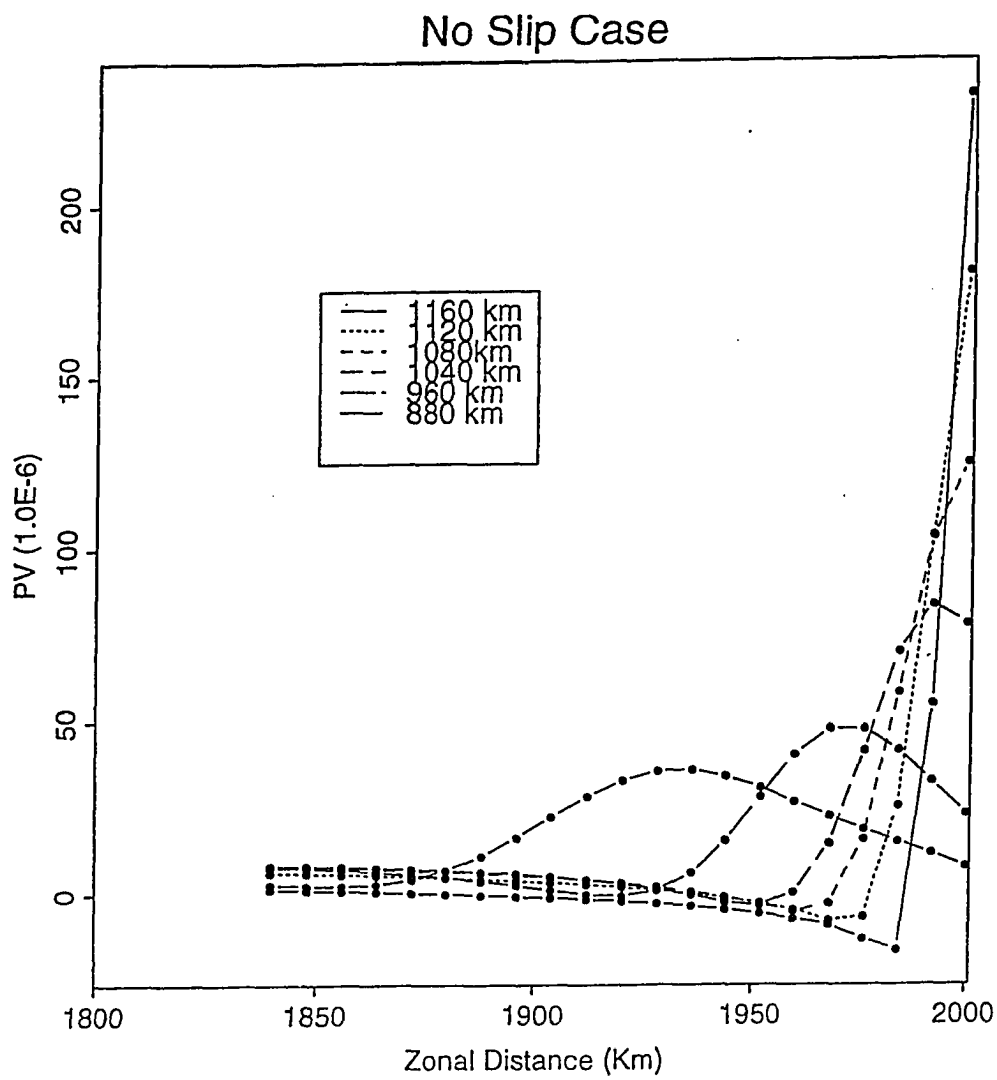


Figure 37: Variation of potential vorticity near the eastern boundary for Case 4.

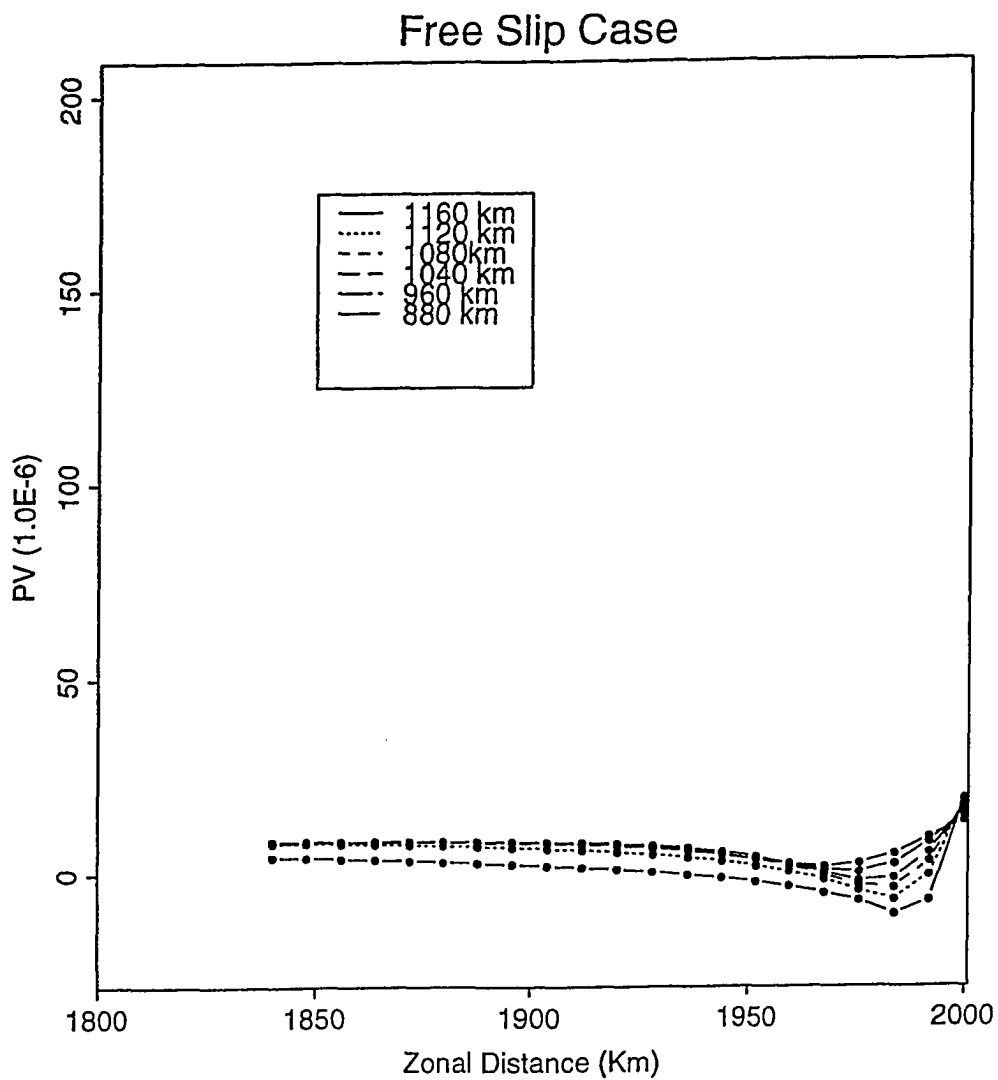


Figure 36: Variation of potential vorticity near the eastern boundary for Case 1.

7 Conclusions

The present study demonstrates the application of PV as a potential tool to understand and determine the structure of thermocline circulation. PV conservation in the ocean (viewed as a stack of constant potential density layers) makes the thermocline problem tractable. Here, we used the flux form of Ertel's theorem to determine the surface PV flux, arising from wind and buoyancy forcing, at an isopycnal layer surface outcrop. We took into account the seasonal movement of the isopycnals and geostrophic turbulence. The surface PV flux transport is taken over in the interior by advective PV flux (due to subduction) and Reynolds flux of vorticity sustained by the geostrophic turbulence. Continuity of PV transport (flux times layer thickness) from the surface to a short distance below yields the following surface boundary condition on an isopycnal layer:

$$\frac{\overline{\partial\Pi}}{\partial s} = (f + \overline{\zeta})\overline{v_n} + \overline{v'_n\zeta'}$$

where $\overline{\partial\Pi}/\partial s$ is the total pressure gradient along the surface outcrop, $\overline{v'_n\zeta'}$ Reynolds flux of vorticity, v_n , along-isopycnal velocity component (almost northward), both normal to the outcrop.

One notable feature of the above expression is the absence of a term related to surface buoyancy flux or the seasonal migration of isopycnals. The density tendency term in the flux form of Ertel's theorem is cancelled out by the seasonal movement of the isopycnals. The result shows that subduction is not tied to a specific rate of heating required to hold an isopycnal in a fixed position, a result Nurser and Marshall (1991) would seem to imply. Furthermore, Reynolds flux of vorticity should in most cases dominate PV flux into an isopycnal layer. Where Reynolds flux of vorticity is

negligible, subduction carries the PV flux, typically at small intensity.

The impermeability theorem for isopycnal surfaces allows PV input/output to occur only at boundaries. The constant layer-depth idealization leads to a minimally complex model of the circulation in an isopycnic layer in isolation. The model is forced on the northern boundary with the flux condition written down above. The results show active northern, eastern and western boundary layers governing an interior circulation pattern unlike that in classical models driven by Ekman pumping. The main feature of the circulation is an anticyclonic gyre with a strength dependent mainly on the intensity of the forcing, the sphericity of the earth, lateral diffusivity and the eastern boundary condition. Other important features are the vigorous eddies south of the anticyclonic gyre shed by an unstable eastern boundary layer in contact with a solid boundary. With free slip at the eastern boundary (upwelled isopycnic layer), the boundary layer there is relatively stable and it allows the steady circulation to penetrate a considerable distance south. The interior circulation pattern is then similar to that predicted by Rhines and Young (1982b). The western boundary is the only sink for PV in this case.

In the case of a no-slip eastern boundary condition, the eastern boundary layer separates at a short distance from the northeast corner, pumping positive vorticity into the basin. Cyclonic eddies form near the eastern boundary and propagate westward at a speed of barotropic Rossby waves. The “nonlinear” terms and the “viscous” terms dominate the area integrated PV balance, however. The model results show that vorticity input, viscous and inertial effects in boundary layers are all potent factors in determining interior circulation. They also demonstrate that PV input due to the total pressure gradient overshadows PV input due to subduction. We also suggest that the results, for the no slip eastern boundary case, reflect major circulation features in the Azores current area.

References

- Arakawa, A., 1966: Computational design for long-term numerical integrations of the equations of atmospheric motion. *J. Comput. Phys.*, **1**, 119-143.
- Armi, L., and H. Stommel, 1983: Four views of a portion of the north atlantic subtropical gyre. *J. Phys. Oceanogr.*, **13**, 828-857.
- Böning, C. W., 1986: On the influence of frictional parametrization in wind-driven ocean circulation models. *Dyn. Atmos. Oceans*, **10**, 63-92.
- Böning, C. W., and M. D. Cox, 1988: Particle dispersion and mixing of conservative properties in an eddy-resolving model. *J. Phys. Oceanogr.*, **18**, 320-338.
- Bryan, K., 1987: Potential vorticity in models of the ocean circulation. *Quart. J. Roy. Meteorol. Soc.*, **113**, 713-734.
- Cessi, P., G. R. Ierley and W. R. Young, 1987: A model of the inertial recirculation driven by potential vorticity anomalies. *J. Phys. Oceanogr.*, **17**, 1640-1652.
- Cox, M. D., 1985: An eddy resolving numerical model of the ventilated thermocline: Time dependence. *J. Phys. Oceanogr.*, **15**, 1312-1324.
- Cox, M. D. and K. Bryan., 1984: A numerical model of the ventilated thermocline: Time dependence. *J. Phys. Oceanogr.*, **14**, 674-687.
- Cushman-Roisin, B., 1987a: On the role of heat flux in the Gulf Stream-Sargasso Sea subtropical gyre system. *J. Phys. Oceanogr.*, **17**, 2189-2202.
- Cushman-Roisin, B., 1987b: Dynamics of the oceanic surface mixed layer. *Hawaii Institute of Geophysics Special Publications*, P. Muller and D. Henderson, Eds.
- Csanady, G. T., 1990: The role of the subtropical gyres in the heat balance of the Warmwassersphaere, *J. Mar. Sys.*, **1**, 13-27.
- Csanady, G. T., and J. Pelegri., 1995: Vorticity balance of boundary currents. *J. Mar Res.*, **53**, 171-187.
- Csanady, G. T., and G. V. R. K. Vittal, 1995: Vorticity balance of outcropping isopycnals. Submitted to *J. Phys. Oceanogr.*
- Dantzler, H. L., 1977: Potential energy minima in the tropical and subtropical North Atlantic. *J. Phys. Oceanogr.*, **7**, 512-519.
- Dewar, W. K., P. B. Rhines and W. R. Young, 1984: The nonlinear spinup of the ocean circulation. *Geophys. Astrophys. Fluid Dyn.*, **30**, 169-197.
- Emery, W. J., 1983: On the geographical variability of the upper level mean and eddy fields in the North Atlantic and North Pacific. *J. Phys. Oceanogr.*, **13**, 269-291.
- Ertel, H., 1942: Ein neuer hydrodynamischer Wirbelsatz. *Met. Z.*, **59**, 271-281.
- Fofonoff, N. P., 1954: Steady flow in a frictionless homogenous ocean. *J. Mar. Res.*, **13**, 254-262.
- Goldstein, S. (Ed.) 1938: *Modern developments in fluid dynamics*, 1, 2. Dover publications, New York, re-published 1965, 702 pp.
- Gould, W. J., 1985: Physical Oceanography of Azores front. *Prog. Oceanogr.*, **14**, 167-190.
- Haynes, P. H., and M. E. McIntyre, 1987: On the evolution of vorticity and potential vorticity in the presence of diabatic heating and frictional or other forces. *J. Atmos. Sci.*, **44**, No.5, 828-841.
- Haynes, P. H. and M. E. McIntyre, 1990: On the conservation and impermeability theorems for potential vorticity. *J. Atmos. Sci.*, **47**, 2021-2031.
- Holland, W. R., T. Keffer and P. B. Rhines, 1984: The general circulation of the oceans: the potential vorticity field. *Nature*, **308**, 698-705.

- Hoskins, B. J., M. E. McIntyre and A. W. Robertson, 1985: On the use and significance of isotropic potential vorticity maps. *Quart. J. Roy. Meteor. Soc.*, **111**, 877-946.
- Huang, R. X., 1988: A three-layer model for the wind driven circulation in the subtropical-subpolar basin. Part III. Potential vorticity analysis. *J. Phys. Oceanogr.*, **18**, 739-752.
- Huang, R. X., 1990: On the three-dimensional structure of the wind-driven circulation in the North Atlantic. *Dyn. Atmos. Oceans*, **15**, 117-159.
- Huang, R. X., 1994: Obduction. *J. Phys. Oceanogr.*, submitted.
- Huang, R. X., and K. Bryan, 1987: A multilayer model of the thermocline and wind-driven ocean circulation. *J. Phys. Oceanogr.*, **17**, 2294-2317.
- Ierley, G. R., and W. R. Young, 1983: Can the western boundary layer affect the potential vorticity distribution in the Sverdrup interior of a wind gyre? *J. Phys. Oceanogr.*, **13**, 1753-1763.
- Iselin, C. O' D., 1936: A study of the circulation of the western North Atlantic. *Papers in Physical Oceanography and Meteorology*, **4**, No. 4.
- Iselin, C. O' D., 1939: The influence of vertical and horizontal turbulence on the characteristics of waters at mid-depths. *Trans. Am. Geophys. Union*, **3**, 414-417.
- Isemer, H. J. and L. Hasse, 1987: *The Bunker Climate Atlas of the North Atlantic Ocean*, **2** Springer-Verlag, 252pp.
- Jacobsen, J. P., 1929: Contribution to the hydrography of the North Atlantic: The "Dana" Expedition 1920-22. Oceanographical reports edited by the Dana-committee, **1**, **3**, 98pp.
- Jenkins, W. J., 1987: ^3H and ^3He in the beta triangle: Observations of gyre ventilation and oxygen utilization rates. *J. Phys. Oceanogr.*, **17**, 763-783.
- Joyce, T. M., 1981: The influence of the mid-Atlantic ridge upon the circulation and the properties of the Mediterranean water southwest of the Azores. *J. Mar. Res.*, **39**, 31-52.
- Joyce, T. M., and W. J. Jenkins, 1993: Spatial variability of subducting water in the North Atlantic: A pilot study. *J. Geophys. Res.*, **98**, 10111-10124.
- Käse, R. H., and G. Seidler, 1982: Meandering of the subtropical front southeast of the Azores. *Nature*, **296**, 245-246.
- Käse, R. H., W. Zenk, T. B. Sanford and W. Hiller, 1985: Currents, Fronts, and eddy fluxes in the Canary basin. *Prog. Oceanogr.*, **14**, 231-257.
- Käse, R. H., J. F. Price, P. L. Richardson and W. Zenk, 1986: A quasi-synoptic survey of the thermocline circulation and water mass distributions within the Canary basin. *J. Geophys. Res.*, **91**, 9739-9748.
- Käse, R. H., A. Beckmann and H. Hinrichsen, 1989: Observational evidence of salt lens formation in the Iberian basin. *J. Geophys. Res.*, **91**, 4905-4912.
- Keffer, T., 1985: The ventilation of the world oceans: Maps of the potential vorticity field. *J. Phys. Oceanogr.*, **15**, 1414-1432.
- Kowalik, Z., and T. S. Murty, 1993: *Numerical modeling of ocean dynamics*. World Scientific, 481pp.
- Krauss, W., 1986: The North Atlantic current. *J. Geophys. Res.*, **91**, 5061-5074.
- Krauss, W., and R. H. Käse, 1984: Mean circulation and eddy kinetic energy in the eastern North Atlantic. *J. Geophys. Res.*, **89**, 3407-3415.
- Krauss, W., and J. Meincke, 1982: Drifting buoy trajectories in the North Atlantic Current. *Nature*, **296**, 737-740.
- Leetmaa, A., and A. F. Bunker, 1978: Updated charts of the mean annual wind stress, convergences in the Ekman layers, and Sverdrup transports in the North Atlantic. *J. Mar. Res.*, **36**, 311-322.
- Levitus, S., 1982: *Climatological atlas of the world ocean*. NOAA Prof. Paper, **13**, Washington D.C., 173pp.

- Luyten, J. C., J. Pedlosky and H. Stommel, 1983: The ventilated thermocline. *J. Phys. Oceanogr.*, **13**, 292-309.
- Luyten, J. C., and H. Stommel, 1986: Gyres driven by combined wind and buoyancy flux. *J. Phys. Oceanogr.*, **16**, 1551-1560.
- Maillard, C., and R. Käse, 1989: The near surface flow in the subtropical gyre south of the Azores. *J. Geophys. Res.*, **94**, 16133-16140.
- Mann, C. R., 1972: A review of the branching of the Gulf Stream system. *Proceedings of the Royal Society of Edinburgh (B)*, **72**, 234-242.
- Marshall, J. C., and A. J. G. Nurser, 1991: A continuously stratified thermocline model including a mixed layer of variable depth and density. *J. Phys. Oceanogr.*, **21**, 1780-1792.
- Marshall, J. C., and A. J. G. Nurser, 1992: Fluid dynamics of oceanic thermocline circulation. *J. Phys. Oceanogr.*, **22**, 583-595.
- Marshall, J. C., A. J. G. Nurser and R. G. Williams, 1993: Inferring the subduction rate and period over the North Atlantic. *J. Phys. Oceanogr.*, **23**, 1315-1329.
- McCartney, M. S., 1982: The subtropical recirculation of mode waters: *J. Mar. Res.*, **40**, Suppl., 427-464.
- McDowell, S., P. B. Rhines and T. Keffer, 1982: North Atlantic potential vorticity and its relation to the general circulation. *J. Phys. Oceanogr.*, **12**, 1417-1436.
- Montgomery, R. B., 1938: Circulation in upper layers of southern North Atlantic Ocean deduced with use of isentropic analysis. *Papers Phys. Oceanogr. Meteorol.*, **6**, 55 pp.
- Munk, W. H., 1950: On the wind-driven circulation. *J. Meteorology*, **7**, 79-93.
- Musgrave, D. L., 1990: Numerical studies of tritium and helium-3 in the thermocline. *J. Phys. Oceanogr.*, **20**, 344-373.
- Needler, G. T., 1967: A model of thermocline circulation in an ocean of finite depth. *J. Mar. Res.*, **25**, 329-342.
- Nurser, A. J. G., and J. C. Marshall, 1991: On the relationship between subduction rates and diabatic forcing of the mixed layer. *J. Phys. Oceanogr.*, **21**, 1793-1802.
- O'Brien, J. J., 1985: The hyperbolic problem. 165-186. In: *Advanced physical oceanographic numerical modeling*, J. J. O'Brien (ed.), D. Reidel.
- Obukhov, A. M., 1962: On the dynamics of stratified fluid. *Dokl. Akad. Nauk. USSR*, **145(6)**, 1239-1242.
- Pedlosky, J., 1986: The buoyancy and wind-driven ventilated thermocline. *J. Phys. Oceanogr.*, **16**, 1077-1087.
- Pedlosky, J., 1990: The dynamics of the oceanic subtropical gyres. *Science*, **248**, 316-322.
- Pedlosky, J., and W. R. Young, 1983: Ventilation, potential vorticity homogenization and the structure of the ocean circulation, *J. Phys. Oceanogr.*, **13**, 2020-2037.
- Pollard, R. T., and S. Pu, 1985: Structure and ventilation of the upper Atlantic ocean northeast of the Azores. *Prog. Oceanogr.*, **14**, 443-462.
- Rhines, P. B., 1986a: Lectures on ocean circulation dynamics, in *Large-Scale Transport Processes in Oceans and Atmospheres*, edited by J. Willebrand and D. L. T. Anderson, pp105-161, D. Reidel Publishing Co., Dordrecht.
- Rhines, P. B., 1986b: Vorticity dynamics of the oceanic general circulation, *Annual Review Fluid Mechanics*, **18**, 433-497.
- Rhines, P. B., 1993: Oceanic general circulation: Wave and advection dynamics. In *Modelling Oceanic Climate Interactions*, edited by J. Willebrand and D. L. T. Anderson, pp67-150, Vol. 11, NATO ASI series.
- Rhines, P. B., and W. R. Young, 1982a. Homogenization of potential vorticity in planetary gyres, *J. Fluid Mech.*, **122**, 347-367.
- Rhines, P. B., and W. R. Young, 1982b. A theory of wind-driven circulation. I. Mid-ocean gyres., *J. Mar. Res.*, **40**, Suppl., 559-596.

- Rhines, P. B., and W. R. Young, 1983: How rapidly is a passive scalar mixed within closed streamlines? *J. Fluid Mech.*, **133**, 133-145.
- Rhines, P. B., and R. Schopp, 1991: Wind driven circulation: theory and quasi-geostrophic simulations for non-symmetric winds. *J. Phys. Oceanogr.*, **21**, 1438-1469.
- Roache, P. J., 1976: *Computational Fluid Mechanics*, Hermosa Publisher, Albuquerque, N. M., 446pp.
- Robinson, A. R., and H. Stommel, 1959: The oceanic thermocline and the associated thermohaline circulation. *Tellus*, **11**, 295-308.
- Rossby, C. G., 1936: Dynamics of steady ocean currents in the light of experimental fluid mechanics. *Papers Phys. Oceanogr. Meteorol.*, **5**, 43 pp.
- Rossby, C. G., 1940: Planetary flow patterns in the atmosphere. *Quart. J. R. Met. Soc.*, **66**, Suppl., 68-87.
- Sarmiento, J. L., 1983: A tritium box model of the North Atlantic thermocline. *J. Phys. Oceanogr.*, **13**, 1269-1274.
- Sarmiento, J. L., C. G. H. Rooth and W. Roether, 1982: The North Atlantic tritium distribution in 1972. *J. Geophys. Res.*, **87**, 8047-8056.
- Saunders, P. M., 1982: Circulation in the eastern North Atlantic. *J. Mar. Res.*, **40**, 641-657.
- Schmitz, W. J., J. F. Price and P. L. Richardson, 1988: Recent moored current meter and SOFAR float observations in the eastern Atlantic near 32°N. *J. Mar. Res.*, **46**, 301-319.
- Siedler, G., W. Zenk and W. J. Emery, 1985: Strong current events related to a subtropical front in the Northeast Atlantic. *J. Phys. Oceanogr.*, **15**, 885-897.
- Spall, M. A., 1990: Circulation in the Canary basin: A model/data analysis. *J. Geophys. Res.*, **95**, 9611-9628.
- Stommel, H., 1979: Determination of watermass properties of water pumped down from the Ekman layer to the geostrophic flow below. *Proc. Natl. Acad. Sci., U.S.*, **76**, 3051-3055.
- Stommel, H., P. Niiler and D. Anati, 1978: Dynamic topography and recirculation of the North Atlantic. *J. Mar. Res.*, **36**, 449-468.
- Stramma, L., 1984: Geostrophic transport in the warm water sphere of the eastern subtropical North Atlantic. *J. Mar. Res.*, **42**, 537-558.
- Stramma, L., and G. Siedler, 1988: Seasonal changes in the North Atlantic subtropical eastern North Atlantic. *J. Geophys. Res.*, **93**, 8111-8118.
- Truesdell, C., 1951: Proof that Ertel's vorticity theorem holds in average for any medium suffering no tangential acceleration on the boundary. *Geof. pur. Appl.*, **19**, 167-169.
- Welander, P., 1971: The thermocline problem. *Philos. Trans. Royal Soc. Lond.* **A270**, 69-73.
- Williams, R. G., 1991: The role of the mixed-layer in setting the potential vorticity of the ventilated thermocline. *J. Phys. Oceanogr.*, **21**, 1803-1814.
- Woods, J. D., 1985: Physics of thermocline ventilation. *Coupled Atmosphere-Ocean models*, J.C.J.Nihoul, Ed., Elsevier.
- Woods, J. D., and W. Barkmann, 1988: A Lagrangian mixed-layer model of Atlantic 18° water formation. *Nature*, **319**, 574-576.
- Wyrtki, C., L. Maggaard and J. Hager, 1976: Eddy energy in the oceans. *J. Geophys. Res.*, **81**, 2641-2646.
- Young, W. R., 1984: The role of western boundary layers in gyre-scale ocean mixing. *J. Phys. Oceanogr.*, **14**, 478-483.
- Young, W. R., 1986: Baroclinic theories of the wind driven circulation, in *General Circulation of the Ocean*, edited by H. D. I. Abarbanel and W. R. Young, pp. 134-201, Springer-Verlag, New York.

Young, W. R., and P. B. Rhines, 1982: A theory of wind-driven circulation II. Gyres with western boundary layers, *J. Mar. Res.*, **40**, 849-872.

Curriculum Vitae

Gudavalli V. R. K. Vittal

Date of Birth : June 30, 1967

Place of Birth: Machilipatnam, AP, India.

Education

M.E., Mechanical Engineering, 1990, Indian Institute of Science, Bangalore, India.

B.E, Mechanical Engineering, 1988, Osmania University, Hyderabad, India.

Publications

Csanady, G. T. and G. V. R. K.Vittal: Vorticity balance of outcropping isopycnals. Submitted to *Journal of Physical Oceanography*.

Other Publications and Abstracts

Soundarnayagam, S., C. L. Sharma, G. V. R. K. Vittal: Aerodynamic Investigations of a Water Turbine Draft Tube. IAHR International Symposium on Fluids, Belgrade, 1990.

Vittal, G. V. R. K. and G. T. Csanady: Nonlinear model of the subduction driven circulation. AGU meeting, 5-9 December, 1994.

Professional Affiliations

Graduate Research Assistant, Indian Institute of Science, Bangalore, India, 1990-1991.

Graduate Research Assistant, Old Dominion University, Norfolk, Virginia, 1991-present.

Memberships

American Meteorological Society

American Geophysical Union